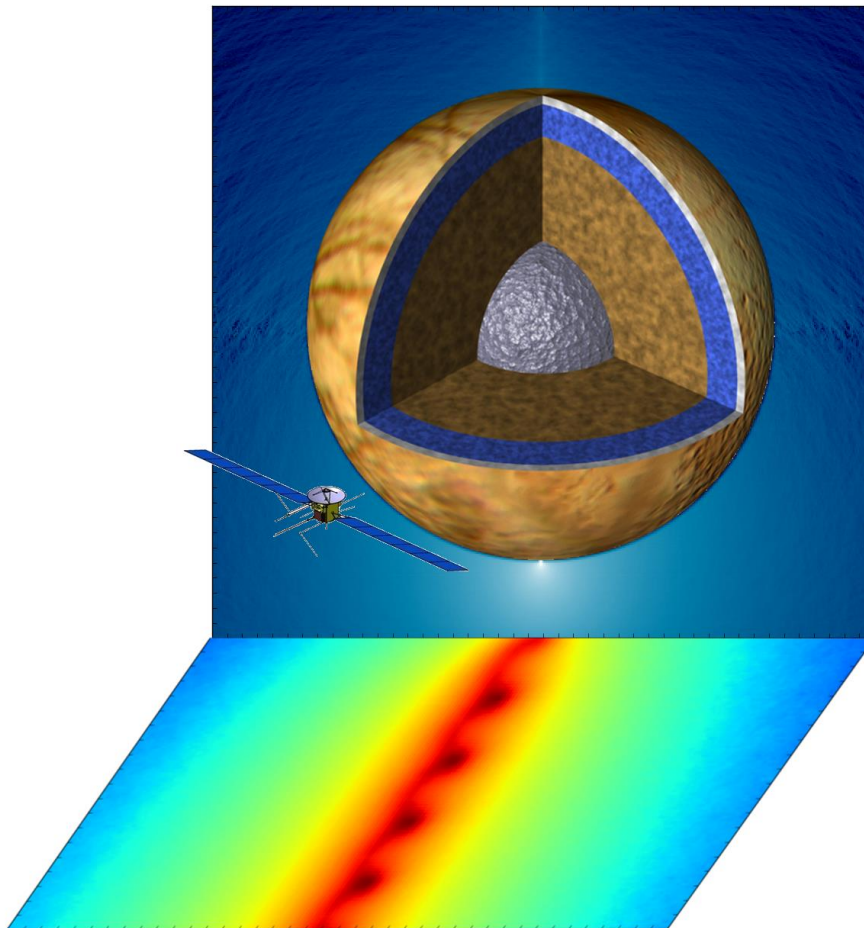


# The feasibility of in-situ observations of Europa's water vapour plumes



H.L.F. HUYBRIGHS

DELFT UNIVERSITY OF TECHNOLOGY  
SWEDISH INSTITUTE OF SPACE PHYSICS

April 2015

**Cover page:** JUICE spacecraft from: <http://sci.esa.int/juice/48350-juice-spacecraft/>, Europa model from: <http://photojournal.jpl.nasa.gov/catalog/PIA01130>.

MASTER'S THESIS

(HANS) H.L.F. HUYBRIGHS – 1542567

[hans.huybrighs@gmail.com](mailto:hans.huybrighs@gmail.com)

[h.l.f.huybrighs@student.tudelft.nl](mailto:h.l.f.huybrighs@student.tudelft.nl)

SUPERVISORS

PROF. DR. S. BARABASH (IRF)

DR. Y. FUTAANA (IRF)

PROF. DR. L.L.A. VERMEERSEN (TU DELFT)

## ACKNOWLEDGEMENTS

First and foremost, I wish to thank my supervisors Dr. Yoshifumi Futaana and Prof. Stas Barabash at IRF and Prof. Bert Vermeersen at Tu Delft, for supporting this exciting Master's thesis project. Special thanks go to Dr. Yoshifumi Futaana for countless valuable discussions and teachings by the drawing board.

Thanks go to all my friends and colleagues at IRF for advice and support, I won't list you all in case I forget someone. Special thanks go to Charles Lue and Jesper Lindkvist for helping me out regularly with many different aspects of space physics and numerical simulations. Gratitude also goes to Dr. Lorenz Roth (Kungliga Tekniska Högskolan, Stockholm) for giving some valuable feedback on the plume model; and to Prof. Peter Wurz (University of Bern) and Dr. Martin Wieser (IRF) for providing information on the performance of NIM and JDC.

I would also like to thank my family and friends back home, for having to miss me during my stay in the North.

This Master's thesis project has been partially funded by the European Commission's Erasmus+ project.

## TABLE OF CONTENTS

Acknowledgements .....	3
List of acronyms .....	8
Summary .....	10
1 Overview .....	12
2 Introduction .....	14
2.1 Europa as a planetary body.....	14
2.1.1 Europa tidal heating and stress .....	14
2.1.2 Interior and oceans .....	15
2.1.3 Geology .....	16
2.1.4 Surface composition .....	17
2.1.5 Exosphere.....	18
2.1.5.1 Exosphere composition .....	18
2.1.5.2 Ionosphere.....	19
2.1.5.3 Neutral torus .....	19
2.1.6 Europa as a potentially habitable moon.....	20
2.2 Europa’s magnetospheric environment .....	21
2.2.1 General overview of Jupiter’s magnetosphere.....	21
2.2.2 Europa’s magnetic, plasma and energetic particle environment.....	23
2.3 Europa’s interaction with Jupiter’s magnetosphere .....	25
2.3.1 Interaction, upstream perspective.....	25
2.3.2 Interaction, Europa perspective.....	25
2.3.3 Interaction, downstream perspective .....	27
2.4 Europa’s water vapour plumes .....	28
2.4.1 Discovery of the water vapour plumes .....	28
2.4.2 Findings since the first discovery of the water vapour plumes .....	29
2.4.3 Existence of plumes suggested in literature .....	30
2.4.4 Previous unsuccessful observations .....	31
2.4.5 Conclusion and open questions .....	31
2.5 JUICE Europa flybys overview .....	32
2.6 PEP: Particle Environment Package on-board JUICE.....	34
2.6.1 Jovian plasma Dynamics and Composition analyser (JDC) .....	35

2.6.2	Neutral gas and Ions Mass spectrometer (NIM) .....	37
3	Project plan, research questions and method .....	40
3.1	Research question, research objectives and sub-goals.....	40
3.2	Theoretical content and methodology .....	41
4	Neutral plume particle simulations .....	44
4.1	Method .....	44
4.1.1	Overview of the model.....	44
4.1.2	Plume source model .....	45
4.1.3	Non-collisional.....	46
4.1.4	Superparticles.....	46
4.1.5	Particle trajectories.....	46
4.1.6	Leap frog integration.....	47
4.1.7	From trajectories to density.....	47
4.1.8	Not generating new particles at each time step .....	48
4.1.9	From density to NIM count rate .....	48
4.2	Simulation inputs – plume model .....	49
4.3	Simulation inputs – grid properties.....	50
4.4	Results.....	52
4.4.1	Density in xy plane and xz plane .....	52
4.4.2	Density distribution on the scale of Europa.....	54
4.4.3	Density during flybys .....	56
4.4.4	Density variation for different plume positions.....	57
4.4.5	Results: plumes sources along a crack.....	57
4.5	Discussion.....	59
4.5.1	Flux conservation.....	59
4.5.2	Non-collisional.....	60
4.5.3	Rotation of Europa.....	62
4.5.4	Feasibility of plume observations by NIM.....	62
4.5.5	Plume source: crack instead of point.....	63
4.5.6	Background signals .....	63
4.5.7	Gravity focus effect.....	65
5	Ionized plume particle simulations.....	66
5.1	Ionized plume particle model .....	66

5.1.1	Overview.....	66
5.1.2	Ionization of neutral particles .....	67
5.1.3	ionized particle trajectories.....	67
5.1.3.1	Charged particle motion: basic theory .....	67
5.1.3.2	Charged particle motion in our model: theory .....	74
5.1.3.3	Fields in our model.....	76
5.1.3.4	Charged particle motion in our model: implementation.....	77
5.1.3.5	Ion collisions.....	78
5.1.4	Large scale simulation .....	78
5.1.4.1	Ion density .....	78
5.1.4.2	Ion bulk velocity .....	78
5.1.4.3	Thermal speed .....	79
5.1.4.4	Average flux .....	80
5.2	Feasibility of detecting the plume with JDC.....	80
5.2.1.1	Differential flux .....	80
5.2.1.2	From differential flux to count rate .....	81
5.3	Simulation inputs: physical parameters.....	82
5.3.1	Neutral density grid .....	82
5.3.2	Environment parameters.....	82
5.3.3	JDC instrument properties .....	83
5.3.4	Juice trajectory.....	83
5.4	Simulation inputs: technical .....	84
5.4.1	Time step size.....	84
5.4.2	Number of time steps.....	84
5.4.3	Grid cell size .....	85
5.4.4	Overview.....	86
5.5	Results.....	86
5.5.1	Single plume source at the south pole.....	86
5.5.2	a crack located at Europa's south pole.....	90
5.5.3	A crack located below the closest approach .....	94
5.6	Discussion.....	96
5.6.1	Plume ion density versus plasma sheet ion density .....	96
5.6.2	Single plume point source at the south pole .....	96

5.6.3	A crack at the south pole .....	98
5.6.4	A crack below the CA.....	99
5.6.5	Comparison with background signal of water ions.....	99
5.6.6	Depletion of electrons.....	99
6	Conclusions and recommendations.....	102
6.1	Neutral plume particle simulation .....	102
6.2	Ionized plume particle simulation.....	102
6.3	Recommendations for future work.....	103
	Bibliography .....	104

## LIST OF ACRONYMS

CA: Closest approach  
CEM: Channel Electron Multiplier  
CCEM : Ceramic CEM  
ENA: Energetic Neutral Atom  
ESA: European Space Agency  
ESA: Electrostatic Analyser (depending on the context)  
FAC: Field Aligned Current  
IAU: International Astronomical Union  
INCA: Ion and Neutral Camera  
IRF: Institutet för rymdfysik: the Swedish Institute of Space Physics  
JDC: Jovian plasma Dynamics and Composition analyser  
JNA: Jovian Neutrals Analyser  
JUICE: JUpiter ICy moons Explorer  
MCP: Micro-Channel Plate  
MHD: Magnetohydrodynamics  
NASA: National Aeronautics and Space Administration  
NIM: Neutral gas and Ion Mass Spectrometer  
PEP: Particle Environment Package  
PLS: Plasma instrumentation  
PWS: plasma wave instrumentation  
ToF: Time of Flight



## SUMMARY

Europa, the second of Jupiter's Galilean moons, has attracted strong interest from the scientific community. This is because it could harbour a sub-surface ocean of liquid water beneath its icy surface, which could be habitable. Recent observations indicate the existence of water vapour plumes at Europa's south pole. The in-situ measurements of the plume particles (both neutral and ionized) may allow the direct sampling of Europa's (potentially habitable) sub-surface ocean environment, without the need of an expensive landing or surface-ice penetrating mission.

The instrument that could be able to perform in-situ sampling of the plumes is PEP (Particle Environment Package). PEP has been selected to fly on-board the European Space Agency's JUICE mission (JUper ICy moons Explorer) to be launched in 2022. PEP is under development now at the Swedish Institute of Space Physics (Institutet för rymdfysik or IRF) in Kiruna, Sweden. PEP is an instrument suite with six sensors to characterize the plasma and neutral environment in the Jovian system in-situ and remotely (via fast neutral imaging). The JUICE mission will perform two flybys of Europa.

Related to the development of PEP and future observations of Europa's plumes a Master's thesis project with the following goal has been proposed:

*“Determine if PEP can observe Europa's water vapour plume by modelling: (a) the trajectories of neutral and ionized particles from Europa's water vapour plumes with test-particle simulations and (b) the respective instrument observation.”*

In the test-particle simulations method the trajectories of particles through background electric and magnetic fields are determined by treating each particle as an isolated test particle. The project focusses on the JDC (Jovian plasma Dynamics and Composition analyser) and NIM (Neutral and Ion Mass Spectrometer) sensors that are part of PEP.

We developed a model of the neutral and ionized plume particle environment. We simulated observations of these particles with respectively the NIM and JDC sensor, and demonstrated observations of plume particles is possible even for plumes that have lower mass flux ( $\lesssim 1$  kg/s) than what has been observed (7000 kg/s).

The developed neutral plume particle model is applicable when the particles in the plume are non-collisional. The ionized plume particle model is applicable to the case where the plume ion density is lower than the typical ion density at Europa. This limits the applicability to plumes with a mass flux  $\lesssim 1$  kg/s. We argue that future Europa plume models should consider the collisions between plume particles. Furthermore the expected high ion density will strongly influence the electric fields at Europa, this effect should be taken into account.



# 1 OVERVIEW

Europa, the second of Jupiter's Galilean moons, has attracted strong interest from the scientific community. This is because it could harbour a sub-surface ocean of liquid water beneath its icy surface, which could form a habitable environment [JUICE Yellow book, 2012]. Recent observations by the Hubble Space Telescope indicate the existence of water vapour plumes at Europa's south pole [Roth et al., 2014a]. In-situ observations of such plumes could offer the possibility to directly sample Europa's sub-surface environment without the need of an extremely expensive lander or a mission to penetrate through the ice-layer.

The instrument that could be able to perform in-situ sampling of the plumes is PEP (Particle Environment Package). PEP has been selected to fly on-board the European Space Agency's JUICE mission (JUper ICy moons Explorer) to be launched in 2022. PEP is under development now at the Swedish Institute of Space Physics (Institutet för rymdfysik or IRF) in Kiruna, Sweden. PEP is an instrument suite with six sensors to characterize the plasma and neutral environment in the Jovian system in-situ and remotely (via fast neutral imaging) [PEP Scientific and Technical Plan, 2012]. The project will focus on the JDC (Jovian plasma Dynamics and Composition analyser) and the NIM (Neutral and Ion Mass Spectrometer) sensors. JDC is an ion mass spectrometer, and NIM is a high mass resolution neutral gas and thermal plasma mass spectrometer. The JUICE mission will perform two flybys of Europa [Grasset et al., 2013].

Related to the development of PEP and future observations of Europa's plasma environment a Master's thesis project with the following goal has been proposed:

*“Determine if PEP (specifically the JDC and NIM sensors) can observe Europa's water vapour plume by modelling: (a) the trajectories of neutral and ionized particles from Europa's water vapour plumes with test-particle simulations and (b) the respective instrument observation.”*

In the test-particle simulations method the trajectories of particles through gravitational, and electric and magnetic fields (for ions only) are calculated by tracing each particle as an isolated test particle.

In Chapter 2 the scientific background to this project will be given. Subsequently in Chapter 3 the project plan is discussed. This includes the formulation of the research questions and the method. In Chapter 4 and Chapter 5 we discuss, respectively, the neutral particle simulation and the ionized particle simulation. These chapters contain the following sections: method, results and discussion. The overarching conclusions of the Master's thesis project are formulated in Chapter 6.



## 2 INTRODUCTION

In this chapter the scientific background to the Master's thesis project is given. First, in Section 2.1 we introduce Europa as a planetary body. Next, in Section 2.2 we introduce Europa's magnetospheric environment. Subsequently in Section 2.3 we discuss the interaction of Europa with its magnetospheric environment. After this we introduce the topic of Europa's water vapour plumes in Section 2.4. Finally we introduce the JUICE mission and the PEP instrument in Sections 2.5 and 2.6.

### 2.1 EUROPA AS A PLANETARY BODY

Table 2-1 lists several general properties of Europa.

Property	Value
Mean radius	1562.09 km
Mass	$4.79982 \times 10^{22}$ kg
Escape velocity	2.025 km/s [ <i>Singer et al., 2013</i> ]
Orbital eccentricity	0.0101
Semi-major axis	670900 km (~9.38 Jupiter radii $R_J$ , Jupiter's equatorial radius is 71492 km)
Orbital period	3.551810 days
Rotation period	Synchronous (approximately): one rotation about rotation axis per revolution
Surface temperature	Average: ~100K. Equator: ~110 K. Poles: ~52 K. [ <i>Ojakangas et al., 1989</i> ]

**Table 2-1:** general properties of Europa. From *Schubert et al. [2009]* unless specified otherwise.

#### 2.1.1 EUROPA TIDAL HEATING AND STRESS

Io, Europa and Ganymede are in a Laplace orbital resonance. Such a resonance occurs when there is a simple integer relation between the orbital period of three or more bodies. For four Jupiter orbits of Io, Europa orbits Jupiter twice and Ganymede orbits Jupiter once [*Alexander et al., 2009*]. This resonance causes a periodic gravitational pull on Europa that forces the eccentricity of Europa's orbit around Jupiter to a value of 0.0101. [*Alexander et al., 2009; Greeley et al., 2004*] During the rotation of Europa about Jupiter the eccentricity of the orbit causes the tidal potential to vary. This variation is in turn is related to deformations of Europa occurring during each orbit, as is illustrated in Figure 2-1. Dissipation of the strain energy creates heat in the interior. Furthermore the stresses alter the surface of Europa [*Greeley et al., 2004*].

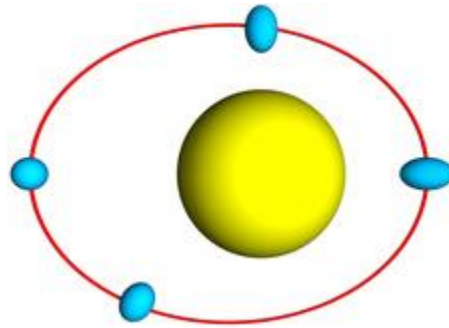


**Figure 2-1:** Variation of the distortion of Europa's shape in its eccentric orbit about Jupiter (not to scale). [<http://www.astro.washington.edu/users/smith/Astro150/Tutorials/TidalHeat/>]

### 2.1.2 INTERIOR AND OCEANS

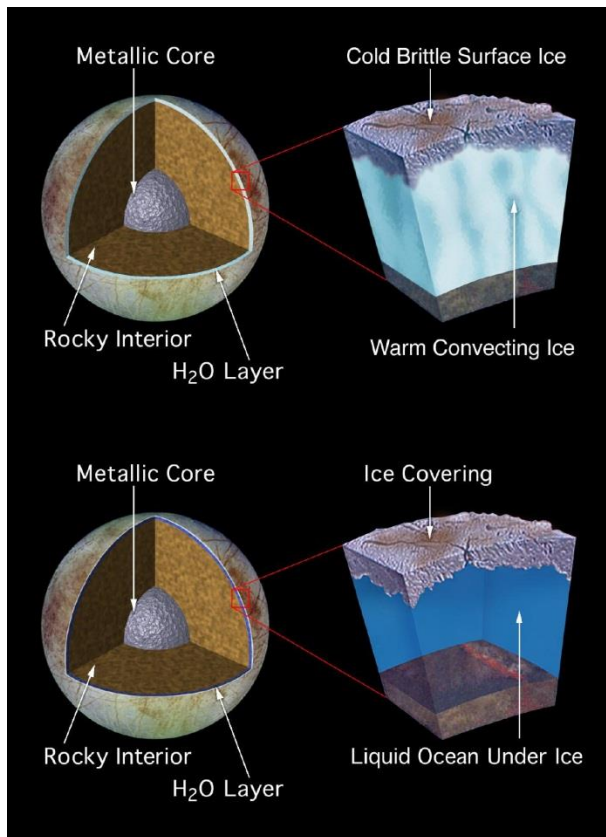


**Figure 2-2:** Two interior models for Europa, artist impression. [NASA <http://photojournal.jpl.nasa.gov/catalog/PIA01669>]

Gravity field data obtained during Galileo flyby's from radio Doppler measurements strongly suggest Europa has a differentiated interior [Schubert *et al.*, 2004]. The interior is expected to consist out of a metal (mostly iron) core, a silicate mantle and water (ice and liquid) outer layer [Anderson *et al.*, 1997; Anderson *et al.*, 1998]. The total volume of water is expected to be  $3 \times 10^9 \text{ km}^3$  (twice the amount on Earth) [Greeley *et al.*, 2004].

Multiple indirect geological indications of a sub-surface ocean Jara-Oru e *et al.* [2011] or a warm, ductile, possibly partially melted ice layer are present [Schubert *et al.*, 2004]. An induced magnetic field has been observed by the magnetometer on board of Galileo. Because Jupiter's magnetic field axis is tilted relative to its rotation axis, Europa experiences a time-varying magnetic field. The time varying magnetic field induces electrical currents inside Europa. These

currents on their turn create an induced magnetic field [Schubert *et al.*, 2004]. No significant intrinsic internal magnetic field has been detected by Galileo at Europa [Schilling *et*

*al.*, 2004]. The measurements of the induced magnetic field by Galileo put constraints on the properties and location of the conductive layer. They provide strong (indirect) evidence of a sub-surface liquid salty water ocean in Europa's outer shell [Schubert *et al.*, 2004; Zimmer *et al.*, 2000].

The thickness of the ocean layer is unknown. It is estimated from the gravity field measurements that the ice-ocean shell is from 80 to 170 km thick [Anderson *et al.*, 1998]. Galileo magnetometer data have been used to constrain the thickness of the ice layer. Depending on the assumed composition the ice layer should be less than 7-15 km thick [Schubert *et al.*, 2009].

The ocean is most likely kept in a liquid state due to tidal heating and the presence of ammonia or salts or other volatiles in the liquid water ocean. These volatiles influence the properties of the ice and liquid water in such a way that the liquid state can be preserved, for example by lowering the freezing temperature or limiting convection in the ice layer [Schubert *et al.*, 2004]. Though arguments are still being made that a liquid ocean could exist just because of radiogenic heating alone [Travis *et al.*, 2012].

It is possible that Europa currently has a volcanically active rock mantle [Greeley *et al.*, 2004]. It is expected the ocean layer and the rock layers have a direct interface Kargel *et al.* [2000] (unlike Ganymede and Callisto), with the presence of possible hydrothermal plumes [Vance *et al.*, 2009].

### 2.1.3 Geology

Europa has a surface composed of water ice with considerable amounts of hydrated minerals [Greeley *et al.*, 2004]. The surface consists of bright terrain and darker terrain, mostly on the trailing hemisphere. The trailing and leading side are defined in this document with respect to the orbital motion of Europa. Many complex surface features of different scales are present. The surface of Europa is young, on average 40 to 90 million years from crater data [Bierhaus *et al.*, 2009]. It is suggested that this young age is caused by estimated resurfacing by liquid water escaping from the interior [Greeley *et al.*, 2004]. More recently it has been suggested plate tectonics in Europa's icy outer layer could explain Europa's young surface age [Kattenhorn *et al.*, 2014]. Hydrated deposits are associated with regions of most recent disruption. Suggesting they are related to endogenic processes, possibly related to a salty subsurface ocean [McCord *et al.*, 1998; McCord *et al.*, 1999; Fanale *et al.*, 2000; McCord *et al.*, 2010].

A number of different features have been observed on the surface of Europa. Seven types of surface areas have been defined by the IAU (International Astronomical Union): regiones, chaos, craters, large ringed features, flexūs, linea, maculae and lenticulae [Doggett *et al.*, 2009].

### 2.1.4 Surface composition

The surface of Europa is composed of water ice with considerable amounts of hydrated minerals and multiple other components [Greeley *et al.*, 2004]. The surface is continuously bombarded by high-energy radiation, originating from Jupiter's magnetosphere. This causes albedo and colour changes of the surface material, but also chemical alterations [Carlson *et al.*, 2009].

Europa has a hemisphere dichotomy: the leading hemisphere is bright, while the trailing hemisphere is brownish (this is shown in Figure 2-3). It is suggested the trailing side is darkened by particle bombardment [Hendrix *et al.* 1998]. Micrometeorite deposition and impact gardening (stirring of the surface by impacts) occur mostly on the leading edge, while bombardment by high energy electrons and plasma deposition are strongest on the trailing side [Carlson *et al.*, 2009].

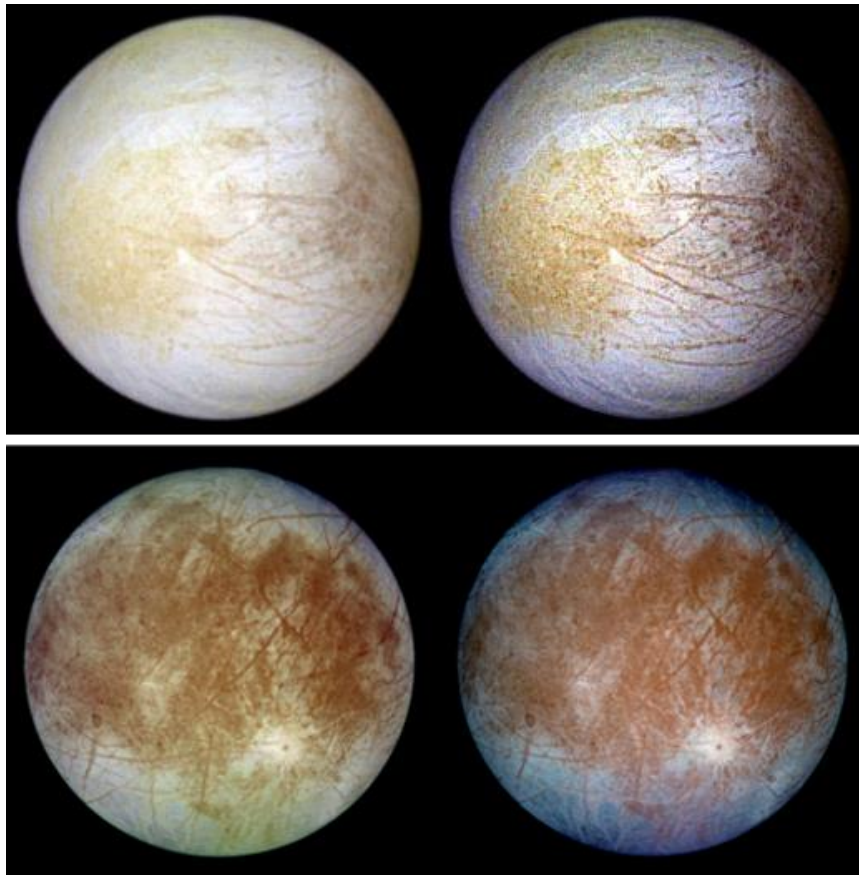


**Figure 2-3:** Europa surface dichotomy observed by the Galileo spacecraft. Top: leading hemisphere, bottom: trailing hemisphere. Left: natural color, right: enhanced color to show structural details. [NASA <http://photojournal.jpl.nasa.gov/target/Europa>]

Several sources of the surface material can be identified [Carlson *et al.*, 2009]:

- the sub-surface ocean, cryovolcanic activity or effusive flows can bring material to the surface
- impact ejecta from Io
- ion implantation of sulphur, oxygen, sodium, potassium and chlorine ions from Io
- impacts of meteorites, comets and ejecta from the outer moons

With ion implantation the impacting ions have sufficient energy to penetrate tens of Å in the surface before they are stopped. While propagating they break molecular bonds and new species can be formed.

Several species are known to be present on the surface: H<sub>2</sub>O, an unidentified hydrate, SO<sub>2</sub>, elemental sulphur, O<sub>2</sub>, H<sub>2</sub>O<sub>2</sub>, CO<sub>2</sub>, Na and K. The presence of some other species has also been suggested: carbon compounds (carbon oxygen compounds, hydrocarbons), nitrogen compounds (nitriles, ammonia, amides), ozone and oxygen compounds, sulphur compounds (hydrosulphides, sulphanes, polysulphur oxides and sulphurous acid) and iron compounds [Carlson *et al.*, 2009].

### 2.1.5 Exosphere

Sputtering of Europa's surface by ionized particles from Jupiter's magnetosphere creates a tenuous exosphere that is marginally collisional. Sputtering caused by bombardment of high-energy sulphur and oxygen ions components is the primary cause for sputtering the surface and producing the exosphere. From this exosphere a neutral gas cloud and an ionosphere also originate [Johnson *et al.*, 2009].

#### 2.1.5.1 Exosphere composition

The primary component of the exosphere is O<sub>2</sub>, a product of radiolysis on Europa's surface. Though H<sub>2</sub>O is the principle ejecta by sputtering, O<sub>2</sub> is the primary component. This is because H<sub>2</sub>O, sticks (freezes) much better to the surface at the ambient temperatures (see Table 2-1) than O<sub>2</sub> or H<sub>2</sub>. These H<sub>2</sub> and O<sub>2</sub> molecules originate from the radiolysis of H<sub>2</sub>O. For every O<sub>2</sub> particle created by radiolysis at the surface of Europa, two H<sub>2</sub> molecules are created. [Johnson *et al.*, 2009; McGrath *et al.*, 2009]

Minor constituents that have been observed are Hydrogen, Oxygen, Potassium (K) and Sodium (Na). Of these Potassium has only been observed once [Brown *et al.*, 2001]. All of these constituents (except atomic oxygen) have been observed further away from Europa, interference of O<sub>2</sub> is negligible. Sodium and Potassium are likely sputtered from the surface [Johnson *et al.*, 2009]. An endogenic source for Sodium has been proposed, rather than Sodium originating from Io being implanted in the surface of Europa. The endogenic sodium could be an indication of a sub-surface salty ocean [Johnson 2000].

The lifetime of the exospheric constituents is short, in hours to days the components of the exosphere are lost (they are either lost to space or to the surface of Europa) [Johnson *et al.*, 2009]. The exospheric sinks include: collisional ejection by low energy plasma, ionization followed by pickup by the magnetosphere, dissociation and ionization by low-energy electrons, photodissociation, gravitational escape and interaction with the surface (sticking or freezing to the surface) [Johnson *et al.*, 2009; Saur *et al.*, 1998; Smyth *et al.*, 2006; Shematovich *et al.*, 2005].

### 2.1.5.2 Ionosphere

An ionosphere, sometimes called exo-ionosphere, around Europa has been observed from radio occultations by the Galileo spacecraft [Kliore *et al.*, 1997]. The ionospheric density varies with longitude and orbital position of Europa with relation to the sun. Measurements indicate the trailing hemisphere should be illuminated for a measurable ionosphere to be present, though electron impact ionization should be larger than photoionization. The origin and characteristics of the ionosphere are not well understood [McGrath *et al.*, 2009; Johnson *et al.*, 2009].

### 2.1.5.3 Neutral torus

The neutrals in Europa's exosphere partially escape Europa's gravity and become gravitationally bound to Jupiter. They form a torus of neutral particles with peak density along Europa's orbit around Jupiter [Johnson *et al.*, 2009]. The torus has been observed (indirectly) with the INCA instrument (Ion and Neutral Camera) on-board Cassini, during Cassini's flyby of Jupiter in late 2000, early 2001. With this instrument energetic neutral atoms (ENAs) were observed that originate from the charge-exchange of the cold neutral atoms and energetic ions trapped in Jupiter's magnetosphere, see also Figure 2-4 [Mauk *et al.*, 2003; Mauk *et al.*, 2004]. Based on Galileo plasma measurements, these results have been further consolidated by [Lagg 2003; Mauk *et al.*, 2004].

The most likely constituents are the following products of sputtered water ice from the surface and sputtered O<sub>2</sub> from the exosphere: H<sub>2</sub>O, H, H<sub>2</sub>, O, OH and O<sub>2</sub> [McGrath *et al.*, 2009].

It is thought that there are three times as much atoms and molecules in Europa's neutral torus than that of Io and ten times as much as in Europa's lower exosphere. The Europa torus forms the main source of protons in Jupiter's magnetosphere and forms a boundary for plasma migrating radially inward by neutralizing it [Johnson *et al.*, 2009; Smyth *et al.*, 2006].

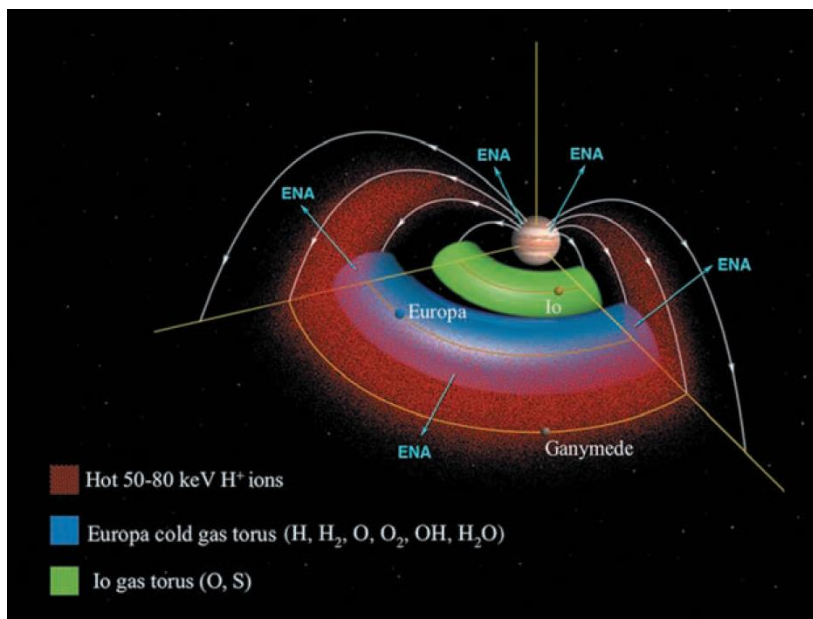


**Figure 2-4:** Schematic interpretation of the Cassini ENA image of Jupiter's magnetosphere. Two sources of ENA's can be identified: Jupiter's upper atmosphere and the Europa neutral torus (blue region). Hot protons of 50–80 keV (red region) diffuse from the regions outside Europa's orbit towards the planet and exchange charge with Europa's neutral torus, causing ENA's. Also indicated is the Io torus (green region). From Mauk *et al.* [2004].

## 2.1.6 EUROPA AS A POTENTIALLY HABITABLE MOON

Europa is a planetary body that has attracted strong attention in the search for extraterrestrial habitats and life, because it likely harbours a global sub-surface water ocean that could be habitable. The surface of Europa, on the other hand, is considered inhospitable because of the temperature, pressure and radiation environment.

	SURFACE HABITATS		DEEP HABITATS				
	Shallow water		Trapped oceans		Top oceans		
	The Earth	Mars	Ganymede	Callisto	Titan	Europa	Enceladus
Liquid Water	●	●	●	●	●	●	●
Stable Environment	●	●	●	●	●	●	●
Essential elements	●	●	●	●	●	●	●
Chemical Energy	●	●	●	●	●	●	●

**Figure 2-5:** Present state of the existing and past habitable worlds in the solar system. For each object the status of the four pre-requisites for a habitable environment is ranked from red (not possible), to yellow (likely but not yet demonstrated) and to green (demonstrated or very likely). Adapted from [JUICE Yellow book, 2012].

Based on terrestrial life four essential pre-requisites for (terrestrial-like) life are identified: the presence of (a stable) water environment, essential elements and chemical energy. These requirements are likely met on Europa. In Figure 2-5 Europa is compared, for each of these pre-requisites, to several other objects of astrobiological interest in the solar system [JUICE Yellow book, 2012]. A more detailed overview of Europa's compliance to each of these requirements follows.

1. Water: life as we know it requires water, it was identified in Section 2.1.2 that Europa could harbour a sub-surface ocean of liquid water.
2. Stable environment: the habitable environment should stay stable for a longer time to give life the opportunity to develop [JUICE Yellow book, 2012] Europa's ocean is thought to have been present for a large part of the history of the moon.
3. Essential elements: the habitable environment should contain several essential elements that are required to drive biochemical reactions (C, H, O, N, P, S). C, H, O and S have been observed on the surface of Europa (see Section 2.1.4). N has not been observed on Europa yet, but is expected to be present. It has been detected on Callisto and Ganymede. [Hand et al., 2009] Phosphorous has not been detected on any of the Galilean moons, but is present in Jupiter's atmosphere (Taylor et al. [2004]) and is expected to have been incorporated in Europa during its formation [Hand et al., 2009].

4. Chemical energy: the availability of energy might be a critical limiting factor for life on Europa. Photosynthesis is not likely to be of major importance in the sub-surface ocean, chemosynthetic metabolism is more likely. For such metabolism the presence of reducing material from the mantle on Europa's seafloor and addition of oxidizing material produced radiolytically on the surface is important [Hand et al., 2009]. Europa's ocean could be in direct contact with the crust beneath (in contrast to Callisto and Ganymede where the ocean could contact another ice layer). This crust could be geologically active and allow for hydrothermal processes, such that it could contribute to Europa's habitability by releasing elements and energy into the ocean. The crust could represent an environment that is similar to the Earth's biologically rich seafloor. [JUICE Yellow book, 2012; Kargel et al., 2000]

Furthermore Europa's ocean layer is not recognized as a particularly extreme environment, considering pressure and temperature. The pressure in the ocean layer is limited by Europa's low gravity, compared to Earth. The pressure at the bottom of the 11 km deep Mariana Trench (where life is present) is comparable to the pressure on a Europa's seafloor covered by a 100 km thick water layer [Hand et al., 2009].

## 2.2 EUROPA'S MAGNETOSPHERIC ENVIRONMENT

### 2.2.1 GENERAL OVERVIEW OF JUPITER'S MAGNETOSPHERE

Jupiter has a strong magnetic field with a field strength of  $\sim 4.3 \cdot 10^5$  Tesla  $m^3$  at the equatorial surface, opposite in polarity to that of the Earth and tilted approximately 10 degree from the spin axis [Acuna et al., 1983; Khurana et al., 2004]. The magnetic field is internally generated by a dynamo. This magnetic field creates a region around Jupiter where the planet's magnetic field dominates over all other magnetic fields: the magnetosphere [Khurana et al., 2004]. The magnetosphere of Jupiter is typically divided in three regions: inner ( $< 10 R_J$ ), middle ( $10-40 R_J$ ) and outer ( $> 40 R_J$ ). Europa is located in the inner magnetosphere. A schematic overview of Jupiter's magnetosphere can be seen in Figure 2-6 a more detailed overview showing magnetospheric dynamics can be seen in Figure 2-7.

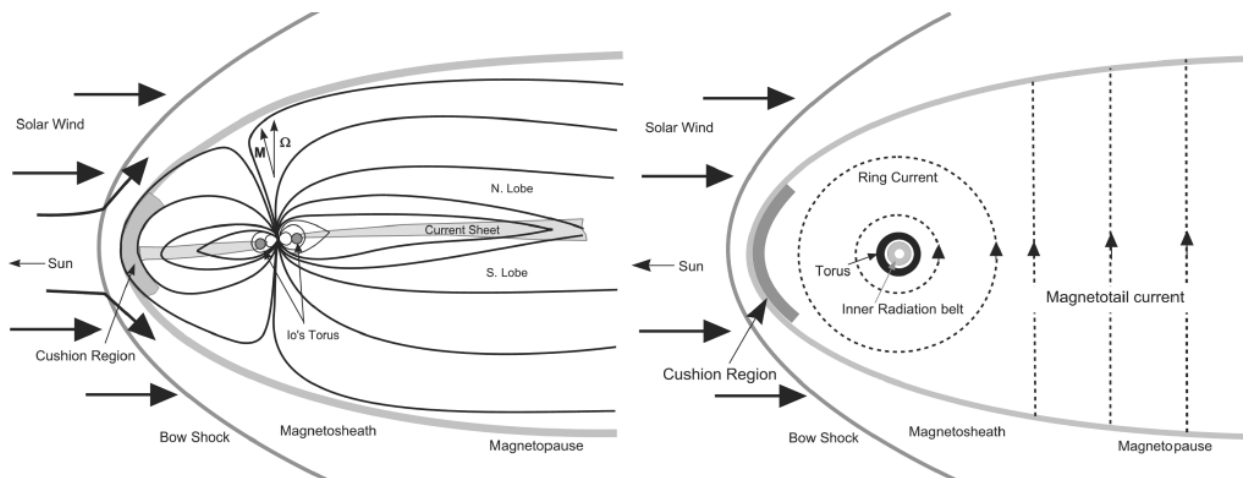


**Figure 2-6:** Overview of Jupiter's magnetosphere. Top: noon-midnight meridian. Bottom: equatorial plane. [Khurana et al., 2004]

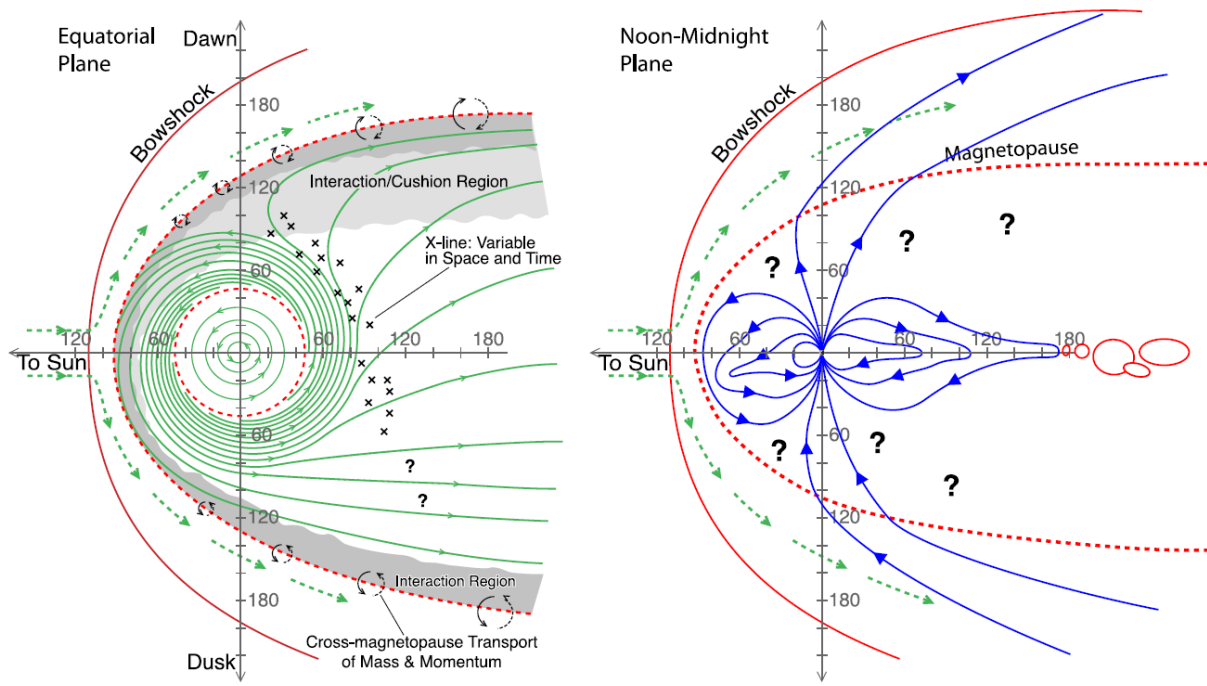


**Figure 2-7:** Structure and dynamics of Jupiter's magnetosphere. Left: equatorial plane. Right: noon-midnight plane. Blue lines: magnetic field. Green lines: flow directions, on the left: average material motion, the motion changes from corotation (within 50 R<sub>J</sub>), spiraling outward beyond this and eventually the material is lost to the magnetopause or magnetotail. Red lines: boundaries between plasma regions. Question marks indicate regions that have not been explored well. The equatorial regions have been explored more extensively than the polar regions. Adapted from *Vasyliunas et al.* [1983] and *[Delamere et al. [2010] by Bagenal et al. [2014].*

Jupiter's magnetic field diverts the incoming solar wind and creates a cavity in the solar wind of low-density hot plasma [*Khurana et al., 2004*]. The incoming solar wind is abruptly slowed down to subsonic speed by a standing shock, called the 'bow shock'. The region with sub-sonic solar wind behind the bow shock is referred to as the 'magnetosheath' [*Burgess 1995*]. The boundary between the magnetosphere and the shocked solar wind is referred to as the 'magnetopause', strong currents are present in this layer [*Khurana et al., 2004*].

Jupiter's magnetosphere is extremely large, reaching directions towards the Sun of 63-92 R<sub>J</sub> (where 1 R<sub>J</sub> = 71492 km). This makes Jupiter's magnetosphere the largest object in the heliosphere [*Bagenal et al., 2014*]. Heavy plasma (mostly various charge states of S and O) inflates the magnetosphere because of centrifugal force and thermal pressure. That is why the Chapman-Ferraro distance, the point where the solar dynamical pressure is in balance with the magnetic pressure, is smaller than the observed magnetopause distance. Heavy plasma also causes the generation of an azimuthal current sheet in the equatorial region of Jupiter's magnetosphere, the current can exceed 160 MA [*Khurana et al., 2004*].

Jupiter's magnetosphere is rotationally driven, meaning the plasma energy is transferred from Jupiter's fast rotation (rotation period = ~ 9h 55 min) and that the plasma source is not mostly the solar wind, but the moon Io [*Khurana et al., 2004; Bagenal et al., 1981; Broadfoot et al., 1981; Hill et*

*al.*, 1983]. Io is located in the inner magnetosphere. More than a ton per second of SO<sub>2</sub> escapes from Io's atmosphere. The escaping neutral particles are dissociated, ionized and trapped by the magnetic field [*Bagenal et al.*, 2014]. Ionization occurs by photionization, electron impact ionization or charge exchange. The initial velocity of the ionized particles is the speed of the original neutral particle (approximately the orbital speed at that distance) and is subsequently increased by the electric fields in the magnetosphere up to the plasma corotation velocity (approximately 75 km/s, roughly corotation velocity) [*Khurana et al.*, 2004]. Plasma acceleration to approximately the corotation velocity is caused by JxB forces related to radially outflowing currents [*Kivelson* 2000]. These currents are referred to as 'Corotation Enforcement Currents' (CEC) [*Khurana et al.*, 2004].

The plasma density in Jupiter's magnetosphere is highest in the thin plasma sheet close the magnetic dipole equator. The sheet originates near Io's orbit. The confinement is a consequence of the combined effect of centrifugal forces, thermal pressure forces and Lorentz forces. The position of the sheet can deviate from the magnetic dipole equator. In the inner magnetosphere its position is close to the centrifugal equator (the location on the field line furthest away from the spin axis), in the middle magnetosphere it moves closer to the dipole magnetic equator and it becomes parallel to the solar wind flow in the magnetotail. The plasma sheet is not planar and does not have a constant thickness. The term current sheet is often used interchangeably with the term plasma sheet, because they occur in approximately the same region [*Khurana et al.*, 2004].

### 2.2.2 EUROPA'S MAGNETIC, PLASMA AND ENERGETIC PARTICLE ENVIRONMENT

Europa is positioned at 9.38 R<sub>J</sub>, in the inner magnetosphere at the outer edge of Io's plasma torus [*Kivelson et al.*, 2009]. Because the axis of Jupiter's magnetic dipole field is tilted 10 degrees with respect to the rotation axis, the magnetic equator moves up and down over Europa every 11.23 hours (Jupiter's synodic period with respect to Europa). This creates a varying magnetic field environment at Europa. The varying magnetic field conditions at Europa induce electric currents in Europa's interior conductive layer (the salty ocean) and strongly influence the local plasma properties. These currents on their turn create an induced magnetic field [*Schubert et al.*, 2004; *Kivelson et al.*, 2009]. Table 2-2 presents an overview of plasma and field parameters at Europa.

The velocity of the approximately corotating plasma at Europa's orbit is higher than that of Europa's orbital velocity around Jupiter, the relative velocity is approximately 76 km/s (see Table 2-2). Because of this the plasma is continuously flowing over Europa from the trailing side to the leading side [*Kivelson et al.*, 2009].

The dominant plasma ions in the Io plasma torus are mostly single and double charged iogenic sulphur and oxygen with a mean ion mass of 78.5 mp (proton mass) and a mean charge of 1.5 e [*Kivelson et al.*, 2009]. Electron density at Europa's orbit is considerably lower than what it is closer to the center of the Io torus. Models based on Voyager 1 plasma data at Io's orbit predict values of 35-40 cm<sup>-3</sup> away from Europa's equator and 80-110 cm<sup>-3</sup> close to the equator (depending on the equatorial current) [*Bagenal* 1994]. Galileo flybys indicate variations in electron density for a range of 18 to 250 cm<sup>-3</sup> [*Gurnett et al.*, 1998; *Kurth et al.*, 2001]. Ambient density varies sinusoidally

(because of exponential variation of density with latitude) in combination with a variability factor of approximately 2 [Kivelson *et al.*, 2004].

The number density of energetic particles (plasma with an energy > 10 keV) in Jupiter's magnetosphere is significantly lower than the lower energy plasma density, and decreases with increasing energy [Kivelson *et al.*, 2004]. The number of protons at Europa between 50-200 keV is approximately a thousand times lower than the total plasma density [Paterson *et al.*, 1999; Paranicas *et al.*, 2002]. Though the number density of energetic particles is lower than that of the other plasma, the energy density is of significant influence to the structure of the magnetosphere and to moon-magnetosphere interaction. The trajectories of energetic particles in Jupiter's magnetosphere can differ significantly from those of the cold plasma [Kivelson *et al.*, 2004].

Property	Value	Source
$B_o$ , jovian magnetic field average min (maximum) [nT]	370 (460)	1
$n_e$ electron density equatorial average (range) [electrons $\text{cm}^{-3}$ ]	200 (18-250)	2
$\langle Z \rangle$ , ion charge, equatorial average (lobe) [qe]	1.5 (1.5)	3
$\langle A \rangle$ , ion mass, equatorial average (lobe) [ $m_p$ ]	18.5	3
$n_i$ , ion number density, average (range) [ions $\text{cm}^{-3}$ ]	130 (12-170)	3
$\rho_m$ ion mass density, average [ $\text{amu cm}^{-3}$ ]	2500 (200-3000)	3
$kT_i$ ion temperature, equator (range) [eV]	100 (50-400)	3
$kT_e$ electron temperature [eV]	100	4
$p_{i,th}$ pressure thermal plasma, equatorial (range) [nPa]	2.1 (0.10-11)	3
$p_{i,en}$ pressure of 20 keV-100 MeV ions [nPa]	12	5
$p_e$ pressure of "cold" and "hot" electrons [nPa]	3.2	
$p$ total pressure, equatorial (max) [nPa]	17 (26)	3,5
$v_{cr}$ local corotation velocity [ $\text{km s}^{-1}$ ]	117	6
$v_s$ satellite orbital velocity [ $\text{km s}^{-1}$ ]	14	6
$v_\phi$ plasma azimuthal velocity (range) [ $\text{km s}^{-1}$ ]	90 (70-100)	7
$u$ plasma velocity relative to Europa, average (range) [ $\text{km s}^{-1}$ ]	76 (56-86)	
$v_A$ Alfvén speed, equatorial (range) [ $\text{km s}^{-1}$ ]	160 (145-700)	8
$c_s$ sound speed, equatorial (range) [ $\text{km s}^{-1}$ ]	92 (76-330)	9
$B_o^2/2\mu_o$ magnetic pressure, equatorial (lobe) [nPa]	54 (84)	1
$\rho u^2$ ram pressure, equatorial, average (max) [nPa]	24 (38)	
$\rho u^2$ lobe ram pressure [nPa]	2.5	

**Table 2-2:** Plasma and field properties of the ambient magnetospheric plasma at Europa. Table from Kivelson *et al.* [2004] and Kivelson *et al.* [2009] Detailed overview of original sources: 1: Khurana [1997] 2: in-situ Galileo Kurth *et al.* [2001] 3: Voyager in-situ McNutt *et al.* [1981; Bagenal [1994] Galileo measurements: Crary *et al.* [1998]; Frank *et al.* [2001]; Paterson *et al.* [1999] 4: interpolated from Scudder *et al.* [1981], consistent with Paterson *et al.* [1999] and Frank *et al.* [2000]; Frank *et al.* [2001] 5: Paranicas *et al.* [2002] pressure estimates assume energetic particle composition of: proton + oxygen + sulphur over the energy range 20 keV to 100 MeV. 6: Morrison *et al.* [1980] 7: Paranicas *et al.* [2000] at Europa's orbit the flow speed is 20-80% of rigid corotation with large local time variations [Krupp *et al.*, 2001] 8: density values from 3, B estimates from 1 9:  $c_s$  depends on  $p$ ,  $p$  is total pressure and average ion mass from 3. Sources not included in the last column were not mentioned specifically in Kivelson *et al.* [2004].

$v_a \approx B(\mu_o m_i n_i)^{-1/2}$  and  $c_s = (\gamma p / m_i n_i)^{1/2}$  where  $B$  is the magnetic field,  $m_i$  is the average ion mass,  $n_i$  is the ion number density,  $p$  is the thermal pressure and  $\gamma$  is the ratio of specific heats.

## 2.3 EUROPA'S INTERACTION WITH JUPITER'S MAGNETOSPHERE

Before the flybys of the Galileo spacecraft the expectations were low that interesting interactions with Jupiter's magnetosphere would occur at Europa. However, the interaction turned out to be far more complex than expected [Kivelson *et al.*, 2004]. This Section provides an overview of different aspects of Europa's interaction with Jupiter's magnetosphere. We consider the interaction from three points of perspective: upstream of Europa, close to Europa and downstream of Europa.

### 2.3.1 INTERACTION, UPSTREAM PERSPECTIVE

Magnetic field measurements, obtained during the upstream Galileo flybys E12, E14 and E19, show that the plasma flow near Europa is slowed down. This slowing down is related to the addition of ionized neutrals, sputtered off from Europa's surface before ionization. These particles 'mass load' the moving plasma and extract momentum from the flow that is converted into thermal motion [Kivelson *et al.*, 1999]. No shockwave is present in front of Europa, the incident flow is slowed down by fast magnetosonic waves [Kivelson *et al.*, 2009].

### 2.3.2 INTERACTION, EUROPA PERSPECTIVE

The time varying magnetic field mentioned in Section 2.1.2 induces a periodically varying dipole magnetic field in Europa [Zimmer *et al.*, 2000; Schilling *et al.*, 2008]. The axis of the dipole is located in Europa's equatorial plane. The influence of the variable internal magnetic field is of significant influence to the total field near Europa [Neubauer 1999].

In Figure 2-8 it is sketched how the impinging plasma flow interacts with Europa. The slowing of the flow creates a region of magnetic and thermal pressure upstream of Europa that diverts some of the flow. The magnetic field is frozen into the plasma, the part of the magnetic flux tube at Europa is slowed down more than parts further away from Europa. This creates a kink in the magnetic field lines that propagates in the north and south directions. The kink (or bendback) in the magnetic field implies the presence of currents (from Ampère's circuit law:  $\nabla \times \mathbf{B} = \mu_0 \mathbf{j}$ , in which  $\mathbf{B}$  is the magnetic field,  $\mathbf{j}$  the current density and  $\mu_0$  the permeability of vacuum).

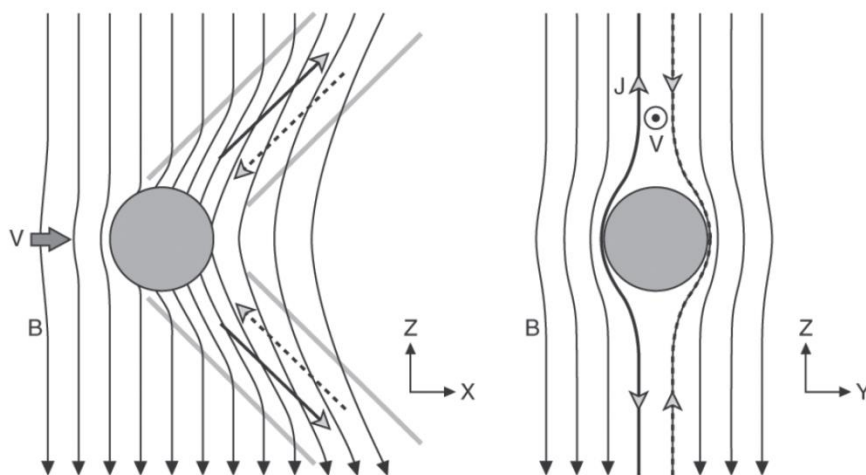


**Figure 2-8:** Alfvén wings of Europa. Left: plane parallel with magnetic field lines and unperturbed flow. Right: plane through the middle of the moon and perpendicular to the unperturbed flow (Jupiter is to the right), only the flux tubes lying between the two middle ones interact with Europa. The grey arrows indicate the direction of the field aligned currents. Adapted from Southwood *et al.* [1980] by Kivelson *et al.* [2009]

The perturbation of the magnetic field by Europa can be visualized by two tilted cylindrical regions of disturbance propagating in North and South directions (see Figure 2-9). The disturbance is propagated by Alfvén waves (a type of electromagnetic wave that can carry current along the magnetic field line *Kivelson et al. [2004]*) and travels at the Alfvén speed. The regions of disturbance are referred to as 'Alfvén wings' [*Kivelson et al., 2009*]. This description of the 'Alfvén wings' is from a MHD point of view. In MHD theory the ionized gas is treated as a fluid and modelled by mechanical laws that are complemented to take into account electromagnetic properties [*Kivelson 1995*]. In the presence of an internal magnetic field the symmetry of the Alfvén wings in the radial direction to Jupiter is disturbed, inward in one hemisphere outward in the other. Furthermore the cross-section of the wing is shrunk [*Neubauer 1999*]. This can be seen in Figure 2-10.

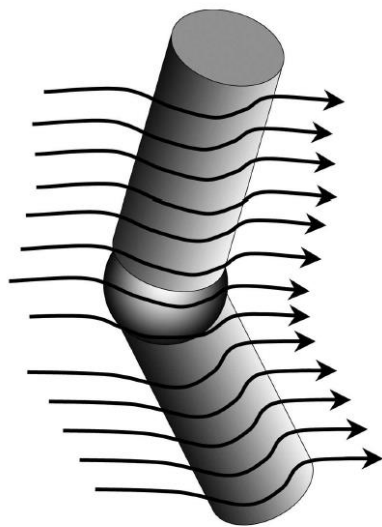


**Figure 2-9:** 3D schematic of Alfvén wings [*Kivelson et al., 2004*] The plasma flow is shown by the stream lines.

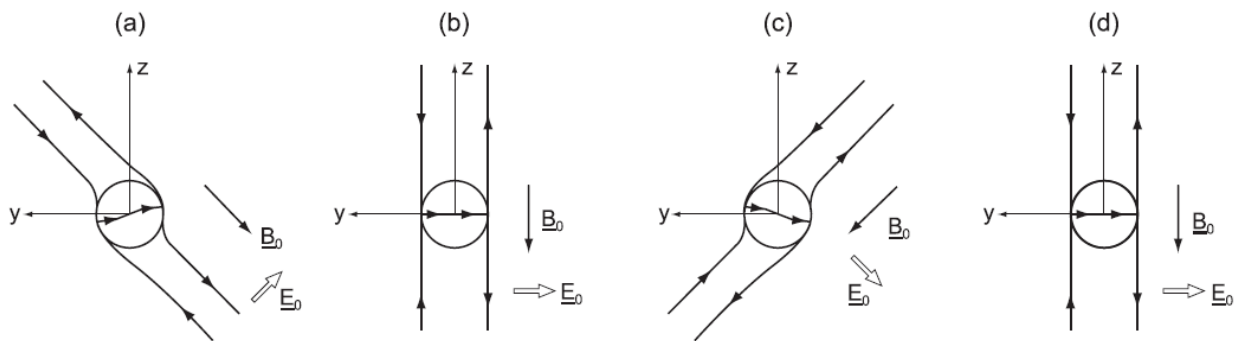


**Figure 2-10:** Influence of the induced magnetic field on the Alfvén wings and associated current systems, the induction effect diverts the northern and southern wings in different directions and changes the cross section. (a): maximum northern magnetic latitude, (b) southbound current sheet crossing, (c) maximum southern magnetic latitude (d) northbound crossing.  $B_0$  is the background magnetic field,  $E_0$  the induced electric field driving currents. From *Neubauer [1999]*

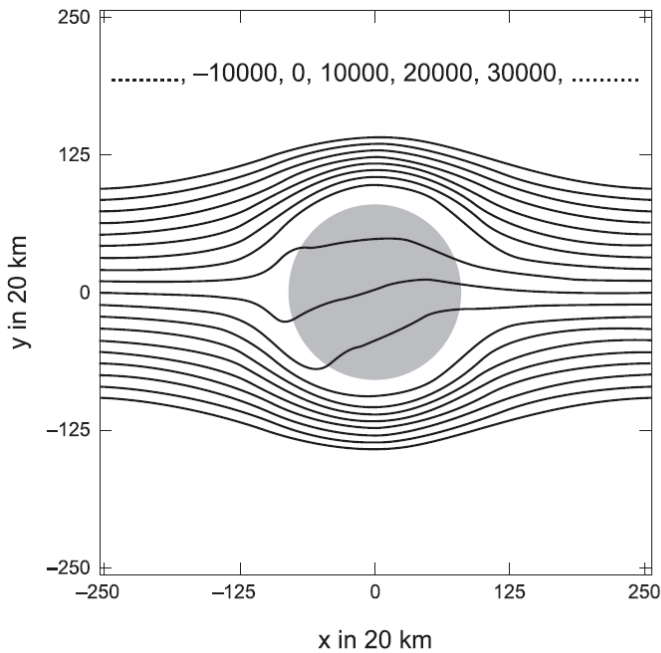


**Figure 2-11:** Streamlines of electron flow. Approximately 20% of the undisturbed upstream flow encounters Europa. The spacing between the lines is proportional to flow speed. The flow speed drops to approximately 25% of the incident flow. [Saur et al., 1998; Kivelson et al., 2009]

diversion was observed by Galileo on several occasions [Paterson et al., 1999]. The model of Saur et al. [1998] also indicates how flow streamlines turn inward, towards Jupiter. This is caused by ionospheric conductivities [Saur et al., 1998].

More particles impact on the trailing edge than on the leading edge. This is because the plasma overtakes Europa from the trailing edge. The particles thus have a high chance of interacting with the trailing edge before they arrive at the leading edge.

Particles interacting directly with Europa have a strong influence on the surface and sputter material from the surface that can contribute to the formation of Europa's exosphere (see Chapter 2.1.5).

### 2.3.3 INTERACTION, DOWNSTREAM PERSPECTIVE

The plasma flowing past Europa creates a wake, that can be found at the leading side (from the sense of direction of the orbit) of Europa.

Pick-up ions measured by Galileo's PLS (Plasma instrumentation, Frank et al., 1992) instrument in Europa's wake are  $H^+$  and  $H_2^+$ . Ions corresponding to a mass of 16-19 amu were observed as well, but it could not be distinguished if these were  $H_2O^+$ ,  $H_3O^+$ ,  $OH^+$  or  $O^+$  ions. From Galileo's PWS (Plasma wave instrumentation, Gurnett et al. [1992]) instrument  $O_2^+$ ,  $Na^+$  and/or  $M^+$ ,  $Ca^+$  and/or  $K^+$ ,  $Cl^+$  and  $Cl^-$  have been inferred [Volwerk et al., 2001; Johnson et al., 2009].

Near Europa  $O^+$  and  $O^{++}$  are the dominant ions.  $S^+$ ,  $S^{++}$  and  $S^{+++}$  are present as well, these three occur in roughly similar quantities. The cold thermal component (plasma in thermal equilibrium) is the dominating factor in the ion number density, while the nonthermal (not in thermal equilibrium) hot component forms a minor contribution. This should be contrasted with the plasma ion energy density that is dominated by the energetic nonthermal component [Paterson et al., 1999; Johnson et al., 2009].

The conductivity of the region surrounding Europa diverts the incoming plasma flow, such that only part of the plasma hits the surface [Kivelson et al., 2009]. In the model by Saur et al. [1998], only 20% of the plasma hits Europa. The rest flows around Europa, carrying the frozen-in magnetic field. This is illustrated in Figure 2-11. The upstream flow

*Kivelson et al.* [1999] states that the ion pick-up rate varies periodically and depends on Europa's position relative to the plasma sheet. At the point of the plasma sheet crossing, pick-up is higher. Also the strongest field aligned currents linking Europa with Jupiter's magnetosphere are expected at this point.

It has been suggested by *Intriligator et al.* [1982]; *Russell et al.*, [1998] and *Eviatar et al.* [2005] that Europa is trailed by a plume of plasma.

## 2.4 EUROPA'S WATER VAPOUR PLUMES

### 2.4.1 DISCOVERY OF THE WATER VAPOUR PLUMES



**Figure 2-12:** Europa plume, artist impression. [NASA/ESA/K. Retherford/SWRI]

The existence of water vapour plumes above Europa's south pole, has been suggested from observations made in December 2012 [*Roth et al.*, 2014a]. The discovery was made by studying Europa's ultraviolet emissions with the Space Telescope Imaging Spectrograph (STIS) on-board the Hubble Space Telescope. Hubble observed surpluses of hydrogen and oxygen emissions in aurora above the South Pole (see Figure 2-13). Plumes were not observed during previous Hubble observations (November 2012 and 1999 [*Roth et al.* [2014a]]) or results were ambiguous (June 2008 [*Saur et al.*, 2011]). Plume activity was observed for seven hours around the south pole in December 2012, when Europa was at its apocenter. The observations from November 2012 and 1999 were obtained when Europa was closer to its pericenter. This suggests plume activity might be initiated by tidal activity [*Roth et al.*, 2014a]. The inconclusive observations from June 2008 were also made when Europa was at its apocenter [*Roth et al.*, 2014a].

The plume activity observed by *Roth et al.* [2014a] is consistent with models of two 200 km high plumes of water vapour with a line-of-sight column density of approximately  $10^{20} \text{ m}^{-2}$ . An eruption velocity of 700 m/s was suggested. However, an uncertainty in height (approximately 100 km) and radial profile exists. The high velocity and relatively low number density correspond to vapour emission from narrow fractures. In *Roth et al.* [2014], supplementary] a mass flux of 7000 kg/s is suggested. Europa's escape velocity is approximately 2 km/s (see Table 2-1), therefore it is expected almost none of the water vapour escapes Europa's gravity, it falls back after  $10^3$  seconds.

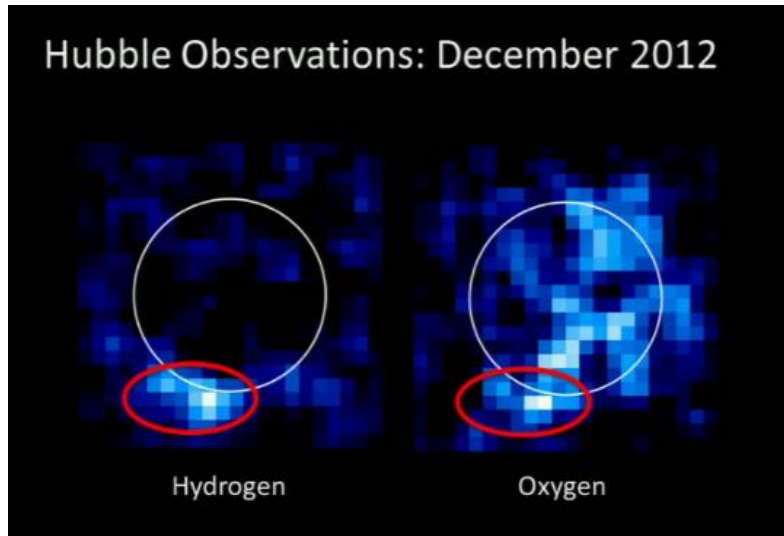


**Figure 2-13:** Hydrogen and oxygen emissions in the Europa aurora. The plume, a surplus of oxygen and hydrogen is visible at the south pole (indicated by red circle). [AGU fall conference 2013, screenshot from press release <https://www.youtube.com/watch?v=ni61Ph1layY>]

#### 2.4.2 FINDINGS SINCE THE FIRST DISCOVERY OF THE WATER VAPOUR PLUMES

On the 2<sup>nd</sup> and 3<sup>rd</sup> of June, 2014, NASA's Europa Science Definition Team (SDT) held its final meeting. Europa's water vapour plume was a central topic at this meeting. The experts at the meeting reached consensus on several key findings [Findings from the Europa Science Definition Team Plume Advisory Meeting. June 2014. [https://solarsystem.nasa.gov/europa/docs/SDTFinding\\_v7.1\\_6-27-14.pdf](https://solarsystem.nasa.gov/europa/docs/SDTFinding_v7.1_6-27-14.pdf)]. Key statements on Europa's water vapour plumes, relevant to this project are:

- *“Evidence for Europa eruptive plumes is intriguing but not definitive. Plumes have exciting science potential in exposing subsurface material but today remain unconfirmed; moreover their source is unconstrained.”* It is stated follow-on observations from ground or spaces still have to confirm the existence of water vapour plumes. The existence of plumes is a possibility but other hypotheses are viable.
- *“Plumes are currently unpredictable and, if they exist, could have spatial or temporal variability that is plausibly cyclical, episodic, or sporadic on uncertain time scales and with uncertain location; this range of possibilities should be considered when developing potential observation strategies, using the payload ultimately selected by NASA.”*  
Anomalies previously detected in Europa's tenuous atmosphere might be linked to plumes, but also suggest plume activity might not be persistent as it is on Enceladus.

A repetition of the successful HST water vapour plume observations in January and February 2014 failed to detect the plumes. Europa was close to its apocenter during these observations; this indicates the orbital position might be a requirement for plume activity, but not the only one. Possibly the plumes are non-periodic or secondary tidal effects are of importance. The non-observation does not exclude that smaller and less dense plumes are present [Roth et al., 2014b].

*Rhoden et al.* [2015] investigated the link between the plumes and Europa's tidal cycle. They did this by modelling the location and orientation of tidally-driven fractures and determining which ones match the temporal variability of the plumes best. They concluded that a tidal stress solely driven by eccentricity cannot explain the temporal variability. Introducing tidal forces caused by an oblique rotation axis and related spin pole precession can explain faults that are in tension during the observation and not during the non-observations. They stated plumes can best be observed earlier in the orbit than the apocenter, at 120 degree true anomaly. Tensile stress on the candidate fractures is maximal at that point. Furthermore they stated that a large number of faults are in tension during observations during which no plumes were detected. This suggests tidal forces are not the only mechanism controlling plume activity. This could mean that water sources are rare. Either few cracks penetrate to the sub-surface ocean, or shallow water reservoirs are needed as a source of water.

A new Hubble observation campaign to detect the plume has started in late 2014 and will last till May 2015 [Personal communication with L. Roth, February 2014].

### 2.4.3 EXISTENCE OF PLUMES SUGGESTED IN LITERATURE

The existence of plumes on Europa has been suggested earlier, associated with:

- Explosive venting caused by diurnal tides [*Hoppa et al.*, 1999]
- Low-albedo margins of triple bands and dark haloes around elliptical lenticulae caused by explosive venting of volatile-bearing water from the sub-surface [*Fagents et al.*, 2000]. In Figure 2-14 dark margins at the edge Rhadamanthys Linea are shown.
- Based on indications of a spatially non-uniform atmosphere *Nimmo et al.* [2007] predicted that the production rate of vapour from the shear heating areas is approximately 1 kg/s per km of shearing surface. The exit velocity would be approximately 450 m/s, much less than is needed to escape the surface of Europa. This implies that the bulk of the vapour will impact back on the surface of Europa. The length of such a plume is predicted to be approximately 70 km.
- Cryovolanic activities. *Quick et al.* [2013] proposed the existence of continuous eruptions resulting in 26 kilometre high plumes.

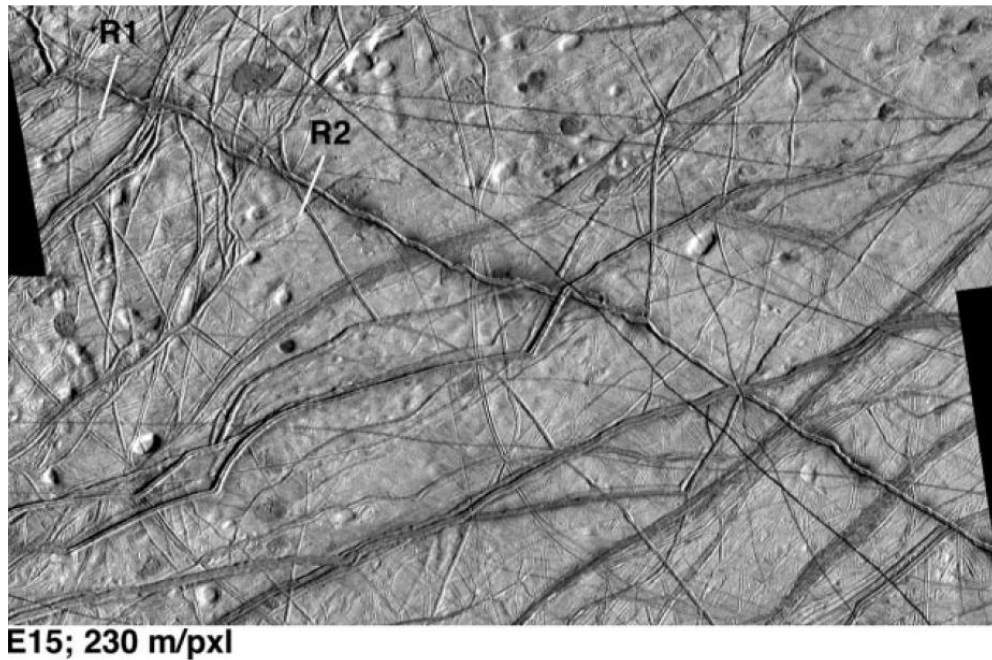


**Figure 2-14:** Segment of Rhadamanthys Linea(Galileo E15 flyby). Dark margins are visible next to the linea [*Fagents et al.*, 2000].

#### 2.4.4 PREVIOUS UNSUCCESSFUL OBSERVATIONS

*Hoppa et al.* [1999] proposed to detect Europa plumes optically during the Galileo E19 flyby, however no plumes were observed [*Hurford et al.*, 2007]. *Roth et al.* [2014a] states that plumes have not been observed in high phase angle (angle between incident light and reflected light) images of Europa both from Galileo (5/6 October 1997) and New Horizons (2 March 2007). Europa was respectively 10-40° and 92° away from pericenter.

#### 2.4.5 Conclusion and open questions

The discovery of water vapour plumes is a significant discovery. Such plumes could potentially enable the direct investigation of the composition of Europa's sub-surface environment. However, only one observation has been reported and many open questions remain, such as:

- Where exactly on Europa do the vapour plumes originate?
- Are plumes periodic, sporadic or catastrophic?
- Which process causes the water vapour plumes?
- Are the plumes linked directly to the sub-surface ocean?
- Do the plumes contain information of the composition of the sub-surface ocean?

Related to the thesis project description the following open questions can be formulated:

- What are the physical characteristics of the plumes?
- What is the contribution of the vapour plumes to the neutral particle environment of Europa?

- What is the contribution of the vapour plumes to the plasma particle environment of Europa?
- Which of these contributions can be observed by the JDC and NIM sensors of the PEP instrument on-board of JUICE?
  - o Can the composition of the plume (and possibly the sub-surface ocean) be constrained by such observations?

## 2.5 JUICE EUROPA FLYBYS OVERVIEW

Jupiter ICy moons Explorer (JUICE) is an ESA mission to characterise the Jupiter system with a particular focus on the environment of the icy moons. JUICE was selected by ESA in May 2012 to be the first Large Class mission within the Cosmic Vision Program 2015–2025. Within this program JUICE addresses four fundamental science questions [*Grasset et al., 2013*]:

- What are the conditions the formation of planets and the emergence of life?
- How does the Solar System work?
- What are the fundamental physical laws of the Universe?
- How did the Universe originate and what is it made of?

Launch is scheduled for 2022. Two flybys of Europa will be performed in February-March 2031, according to the current plan. Figure 2-15 shows the altitude during the flybys and the projection of the ground track on the surface. It is also indicated when and which instruments will operate during the flyby according to the current preliminary plan. The minimal altitude to be achieved is approximately 400 km. In-situ instruments (plasma spectrometers and magnetometer) will operate during the entire flyby [*Grasset et al., 2013*].

The Europa flybys are achieved using gravity assists from Callisto, general geometry of the flybys is shown in Figure 2-16 [*JUICE Yellow book, 2012*]. JUICE will encounter Europa at the perijove of Europa's orbit around Jupiter [*Grasset et al., 2013*]. Figure 2-17 gives a 3D overview of the flybys.

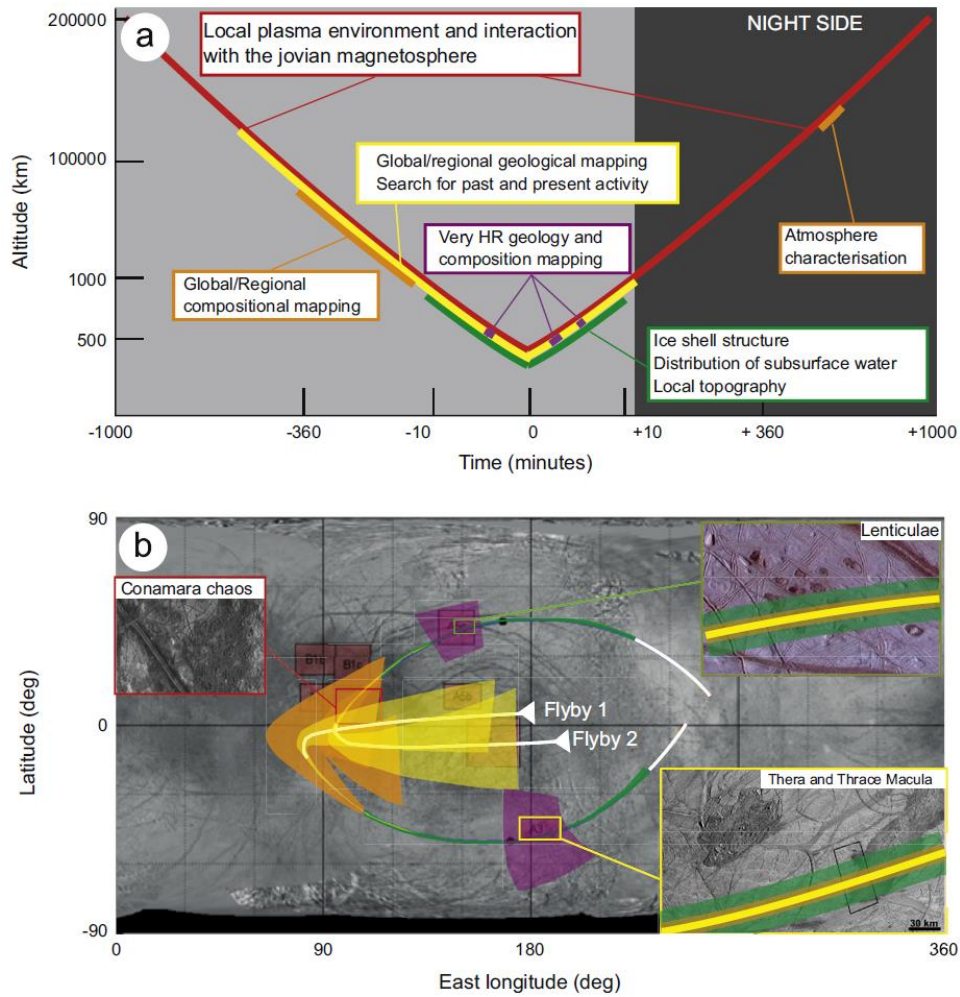


**Figure 2-15:** Overview of two Europa flybys, including (a) altitude profile and instrument operation sequence, and (b) groundtrack visualization including indication of areas of interest. Indicated on the groundtrack is the field of view of the instruments with different color codes. Yellow: narrow angle camera. Orange: spectro-imagers. Green: radar sounding experiment. Purple: wide angle camera. In-situ instruments (plasma and neutral gas package, plasma wave instrument and magnetometer) will operate throughout the entire flyby, indicated by the red curve in panel (a). Not shown for clarity: global mapping during approach and departure. [Grasset *et al.*, 2013]

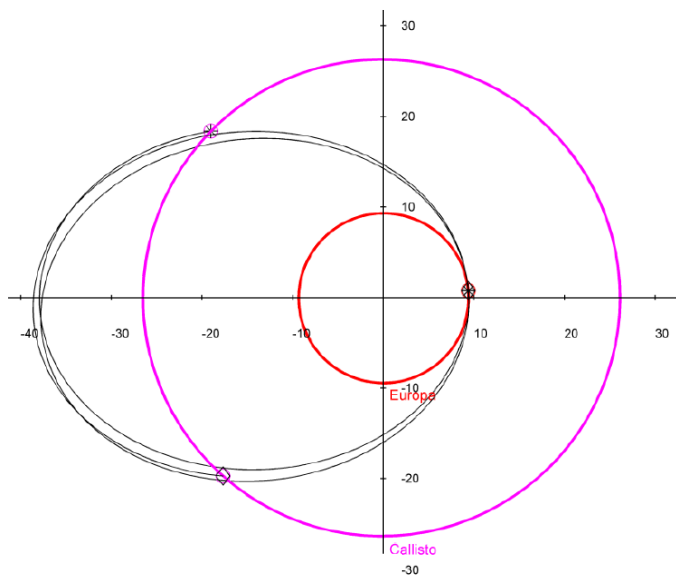


**Figure 2-16:** JUICE Europa flyby geometry. Indicated are the orbit of Callisto (in purple), Europa's orbit (in red) and the spacecraft orbit (in black). The encounters of JUICE with the moons are indicated with symbols. Reference frame: Jupiter Solar Orbital coordinate frame (JSO). The x-axis is pointing in the direction of the sun. The z-axis is perpendicular to the plane formed by the orbital velocity vector and the x-axis. The Z-axis is perpendicular to Jupiter's orbital plane. [JUICE Yellow book, 2012]

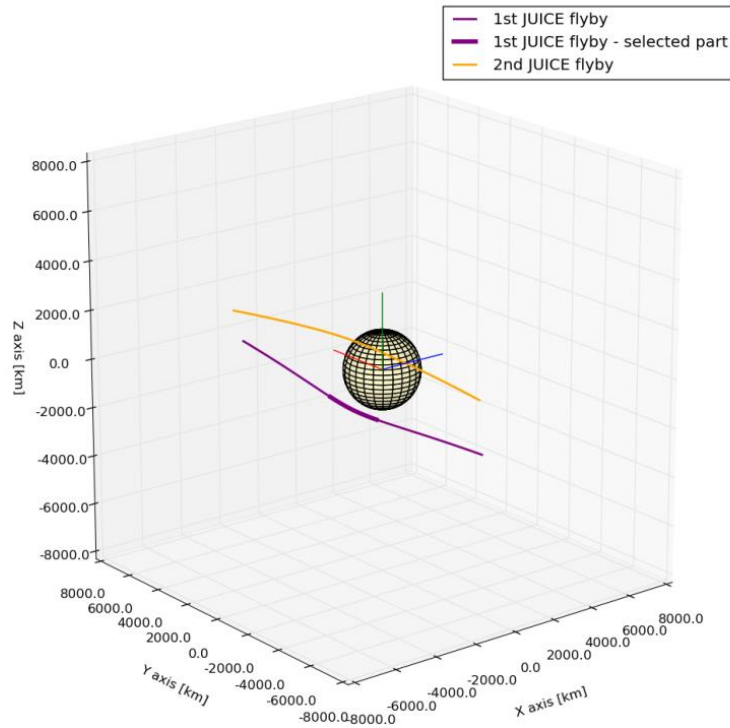


**Figure 2-17:** First (purple) and second (yellow) JUICE flyby of Europa. Also indicated (thick purple line) is the part of the JUICE flyby that will be considered in our simulations. IAU (International Astronomical Union) Europa reference frame: z-axis is perpendicular to the mean orbital plane of Europa. The positive x-axis is pointing in the direction of Jupiter and the y-axis completes the right hand system [Archinal *et al.*, 2010].

## 2.6 PEP: PARTICLE ENVIRONMENT PACKAGE ON-BOARD JUICE

PEP (Particle Environment Package) is selected to fly on board ESA's JUICE mission to Jupiter in 2022 and is under development now at IRF-Kiruna. PEP is a six sensor suite to characterize the plasma and neutral gas environment in the Jovian system. PEP will measure positive and negative ions, electrons, exospheric neutral gas, thermal plasma and energetic neutral atoms in the energy rang from  $< 0.001$  eV to  $> 1$  MeV with full angular coverage. JDC (Jovian plasma Dynamics and Composition analyser) provides distribution functions of the main ion species in the hot plasma energy range (eVs – keVs). NIM (Neutral gas and Ion Mass Spectrometer) is a high mass resolution spectrometer for exosphere and neutral gas composition measurements; it can also measure the ion component up to 10 eV. An overview of the PEP sensors and their location on the JUICE spacecraft is shown in Figure 2-18 .

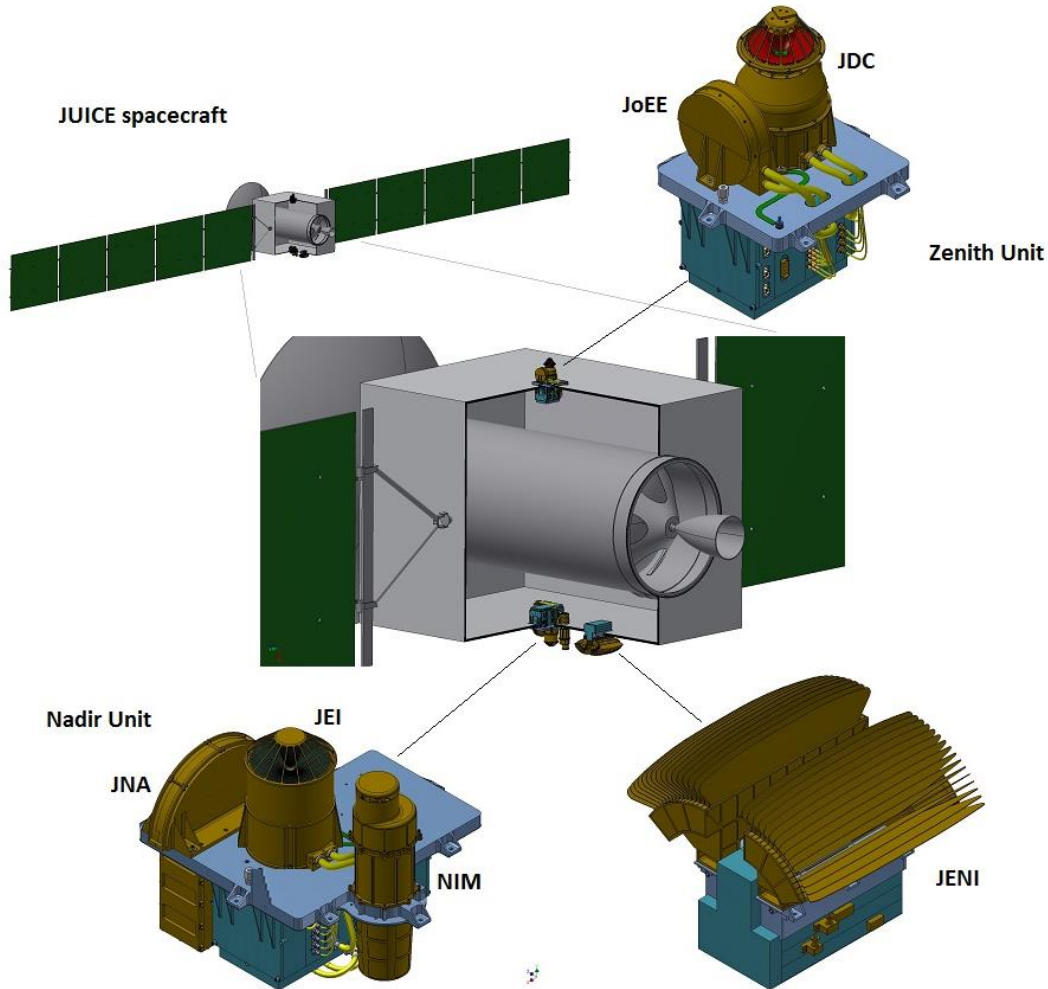


**Figure 2-18:** The PEP sensors and their location on the JUICE spacecraft. [IRF]

### 2.6.1 JOVIAN PLASMA DYNAMICS AND COMPOSITION ANALYSER (JDC)

JDC is an ion mass spectrometer covering the energy range 1 eV – 41 keV with mass resolution up to 30. Mass resolution ( $M/dM$ ) or resolving power is defined as: the mass ( $M$ ) to be resolved, divided by the capability of mass separation ( $dM$ ) between the particles. JDC provides a 3D distribution function of positive and negative ions. It also has the capability to measure charge state and electrons, though it is optimized for positive ions. [PEP Scientific and Technical Plan] A cross section of JDC is shown in Figure 2-19.

Particles entering JDC pass through an elevation scanning system before they pass the toroidal-like Electrostatic Analyser (ESA) that determines  $E/Q$  (energy per charge). The ESA consists out of two curved plates with a voltage applied over the gap between them. Only particles that have the right energy over unit charge ratio ( $E/Q$ ) can pass through the gap between the plates without colliding with the plates [Brandt 2002]. After this particles will pass a time-of-flight reflectron system [PEP Scientific and Technical Plan]. Such a system measures the time of flight of a particle in the linear

electric field. The time-of-flight depends only on the particle mass per charge and is not sensitive (with reliable limits) to the variation of entrance energy and direction [Brandt 2002].

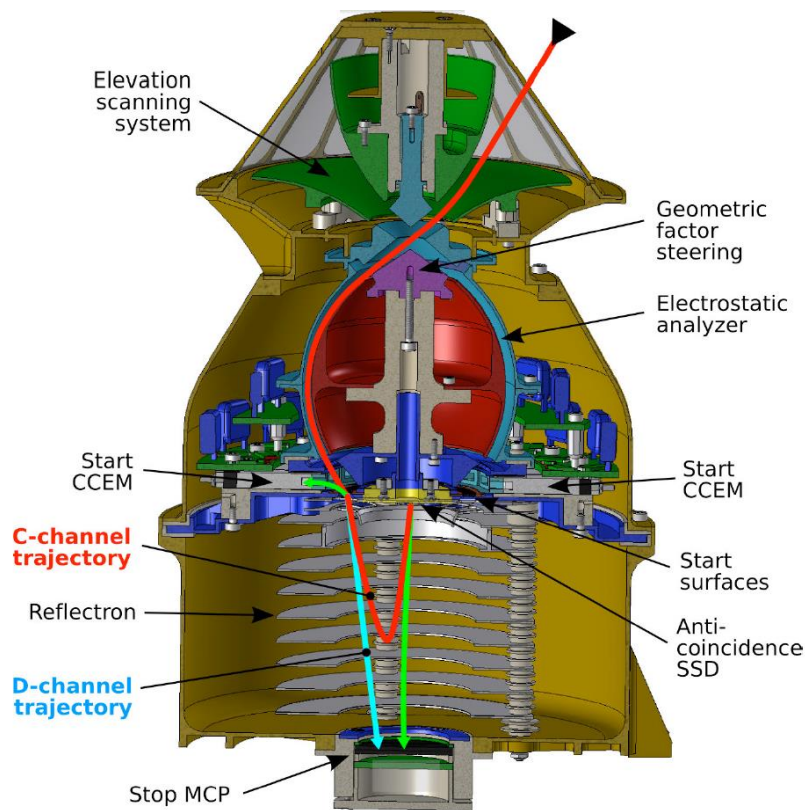


**Figure 2-19:** JDC cross section, without shielding. Red line: positive ion trajectory (C-channel). Blue line: neutral particle trajectory (D-channel). Green line: electron trajectory. CCEM = Ceramic CEM. [PEP Science and Technology Plan]

created by applying a potential difference between the entrance and exit of the tube [Eklund 2002].

When hitting the start surface, the initial charge state is lost. Particles that have a neutral or negative state after passing through the start surface travel through the reflectron directly to the stop detector. The stop detector for these particles is a micro-channel plate (MCP) [PEP Scientific and Technical Plan]. An MCP is a planar particle detector that is composed of parallel electron multiplier tubes (micro-channels). The micro-channels are inclined relative to the surface of the MCP to guarantee entering particles hit the wall of the micro-channel. Particles leaving the start surface as positive ions are reflected by a linear electric field to a different stop surface (this explains the origin of the name reflectron). At this point these particles will generate secondary electrons that are accelerated and focused on the stop MCP, but on a different area [PEP Scientific and Technical Plan]. From the particle TOF in the reflectron the  $M/Q$  ratio can be determined. From the TOF of flight of particles hitting the stop MCP directly the particle velocity can be determined and thus the mass ( $M/Q$ ), but with higher sensitivity. This works as follows:  $E/Q$  is determined by

In the JDC ToF reflectron system, the start signal is obtained when the ion hits the 'start surface' which will generate secondary electrons that will be detected by Channel Electron Multipliers (CEMs) to give a start pulse.

Channel electron multipliers consist out of a tube with a coating that has a high probability of giving secondary electron emissions. When an electron enters the tube and hits the wall of the tube, secondary electron emission occurs. The secondary electrons are accelerated by the electric field inside the tube to the energy that is sufficient to

produce even more secondary electrons, this is referred to as an 'avalanche' effect. The electric field in the tube is

the ESA, it depends on  $M/Q$  and  $v$  (particle velocity) as is expressed by Equation (2-1). This Equation can be rewritten in terms of  $M/Q$ , as is shown in Equation (2-2).

$$\frac{E}{Q} = \frac{1}{2} \left( \frac{M}{Q} \right) v^2 \quad (2-1)$$

$$\frac{M}{Q} = \frac{2 \left( \frac{E}{Q} \right)}{v^2} \quad (2-2)$$

JDC also includes functionality to estimate the original charge state  $Q$  of the major ions species [PEP Instrument Engineering Plan].

## 2.6.2 NEUTRAL GAS AND IONS MASS SPECTROMETER (NIM)

NIM (Neutrals gas and Ions Mass spectrometer) is a high mass resolution ( $M/dM > 1100$ ) mass spectrometer for the exospheric measurements. It investigates both neutral particles and thermal plasma [PEP Scientific and Technical Plan]. Figure 2-20 shows an overview of the NIM sensor.

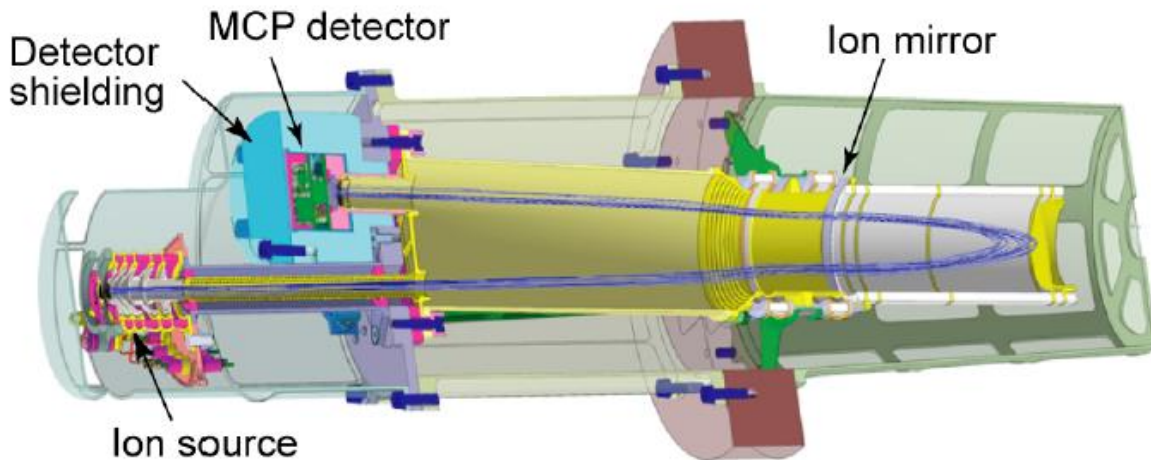


**Figure 2-20:** Design drawing of the NIM sensor [PEP Scientific and Technical Plan]

NIM is a ToF mass spectrometer with a ToF reflectron. NIM can work in two modes: neutral mode and ion mode. In the ion mode NIM collects ions from the ambient plasma. In the neutral mode ambient neutral gas entering the instrument is ionized by electron impact and the resulting ions are stored. The stored ions are extracted into an acceleration region in the form of packages of ions by a pulsing extraction voltage. Then the ions pass through the reflectron. Depending on their mass the ions in the package get separated. Detection of particles is performed by MCPs after the ions travelled through the reflectron [PEP Instrument Engineering Plan]. The spectrum of the ToF, the arrival time to the detector relative to the extraction pulse, gives the ion mass distribution. The beauty of a reflectron is that TOF depends only on mass ( $M/Q$ ) and the electric field (see Equation (2-1)). The well-optimized design of the NIM reflectron provides very high precision ( $M/dM > 1100$ ).

A ToF mass spectrometer can record a complete mass spectrum at once without having to scan over a mass range. Such as is the case for scanning mass instruments, for example quadrupole mass spectrometers. This gives ToF mass spectrometers a clear advantage over such instruments. This functionality is particularly helpful for making measurements during flybys, such as for Europa [*PEP Scientific and Technical Plan*].



### 3 PROJECT PLAN, RESEARCH QUESTIONS AND METHOD

The focus of the thesis project is on the recently described water vapour plumes and how their contribution to neutral and plasma particle environment will be observed by PEP (as was discussed in Section 2.4.5). The observations of these plumes could be of significant scientific importance, because they can potentially allow for the direct sampling of Europa's (potentially habitable) sub-surface ocean environment, without the need of an expensive landing or ice-penetrating mission.

Though the water vapour plumes contain neutral matter, it is likely that a part of the particles will become ionized. Once ionized, the charged particles can be accelerated and transported by the background electromagnetic force. Measuring those charged particles allows for indirect observations of the plumes. To determine the feasibility of this approach, it is of strong importance to determine the trajectories of ionized and neutral particles (atoms, molecules and their respective ions) from the water vapour plume in the Europa environment and to evaluate how these particles can be detected and characterized by the PEP sensors.

In *Roth et al.* [2014] it is noted that a local density enhancement (such as the water vapour plumes) would substantially alter the plasma environment. Multiple photo- and electron impact reactions that can break down water molecules and create an increased electron and ion density, are possible at Europa [*Johnson et al.*, 2009].

#### 3.1 RESEARCH QUESTION, RESEARCH OBJECTIVES AND SUB-GOALS

The main research question of the thesis project is formulated as follows:

*“Can PEP measure and characterize in-situ particles from the water vapour plume during the JUICE flyby of Europa?”*

From this the research objective of the project is formulated:

*“Determine if PEP (specifically the JDC and NIM sensors) can observe Europa's water vapour plume by modelling: (a) the trajectories of neutral and ionized particles from Europa's water vapour plumes with test-particle simulations and (b) the respective instrument observation.”*

The following sub-questions are formulated:

Q1: What is the distribution of neutral gas in the water vapour plume?

Q2: What are the electric and magnetic fields at Europa?

Q3: How do the plume particles propagate through their environment?

Q4: What will PEP measure during the JUICE flyby of Europa in the case a water vapour plume is present?

To answer these sub-questions the following sub-goals are formulated:

Q1, SG1: model the neutral gas distribution in the water vapour plume by developing a model based on vapour plume observations

Q2, SG2: model electric and magnetic fields at Europa by implementing analytical models

Q3, SG3.1: model the propagation of neutral plume particles, by means of test-particle simulations

Q3, SG3.2: model the ionization of neutral plume particles

Q3, SG3.3: model the propagation of ionized plume particles, by means of test-particle simulations

Q4, SG4: investigate the PEP instrument response (specifically JDC and NIM sensors) to plume particles (different constituents will be considered) by modelling the instrument observation

## 3.2 THEORETICAL CONTENT AND METHODOLOGY

The main hypotheses to be tested are:

- Particles of Europa's water vapour plume are observable by PEP because they are transported away from Europa as neutral particles
- Particles of Europa's water vapour plume are observable by PEP because they are transported away from Europa as ionized particles

The main method that will be used to test these hypotheses is the 'test-particle method' (sub-goal 3.1 & 3.3). This is a well described method to investigate particle motion in different environments (for a description, see for example *Ledvina et al.* [2008]). In this method the trajectories of particles through background, gravity, electric and magnetic fields (sub-goal 2) are calculated by treating particles (ions or electrons) as isolated test particles, of which the trajectory is determined by the equations of motion. Some typical applications of this method are: the study of ion pickup near planets or moons (for example: *Fatemi et al.* [2009] or *Futaana et al.* [2010]), ion deposition in planetary atmospheres, ion-neutral interaction in atmospheres and instrument response simulations [*Ledvina et al.*, 2008].

The influence of currents generated by particle motions on the fields is disregarded in the test-particle method. The background fields can be obtained from analytical functions, from MHD simulations or from hybrid simulations. In MHD theory the ionized gas is treated as a fluid and modelled by mechanical laws that are complemented to take into account electromagnetic properties [*Kivelson* 1995]. In a hybrid model ions are modelled with kinetic theory (where the motion of individual particles is considered) while electrons are treated as a massless fluid [*Fatemi* 2014]. Although MHD or hybrid simulation may provide self-consistent fields considering plasma dynamics, we decide to use analytical models as a first step in this project considering the relatively short time scale of the project.

By calculating the particle trajectories for numerous particles the density and velocity of plume particles can be estimated. To evaluate the feasibility of plume observations, a model of the instrument observation will also be implemented (sub-goal 4). From the density and velocity of the plume particles and the instrument observation model it can be derived if the PEP instrument will or will not be able to observe the water vapour plumes.

The test particle method will have to be supplemented with another model for the water vapour plumes that will provide probabilities (distribution function) of the initial states of the neutral plume particles (sub-goal 1), and a model to simulate the ionization of these neutral particles (sub-goal 3.2).

The test particle simulation of neutral plume particles is discussed in detail in Section 4.1, the test particle simulation of ionized plume particles in Section 5.1.



## 4 NEUTRAL PLUME PARTICLE SIMULATIONS

To determine if in-situ observations of Europa's water vapour plumes can be made with PEP, first only the neutral plume particles are considered. The trajectories of these particles are modelled and it is investigated if the resulting density of neutral particles during the JUICE flyby is sufficiently high to make observations with the NIM sensor. The contents of this chapter link with sub-goal 1, 3.1 and 4 from the project plan (Chapter 3).

### 4.1 METHOD

#### 4.1.1 OVERVIEW OF THE MODEL

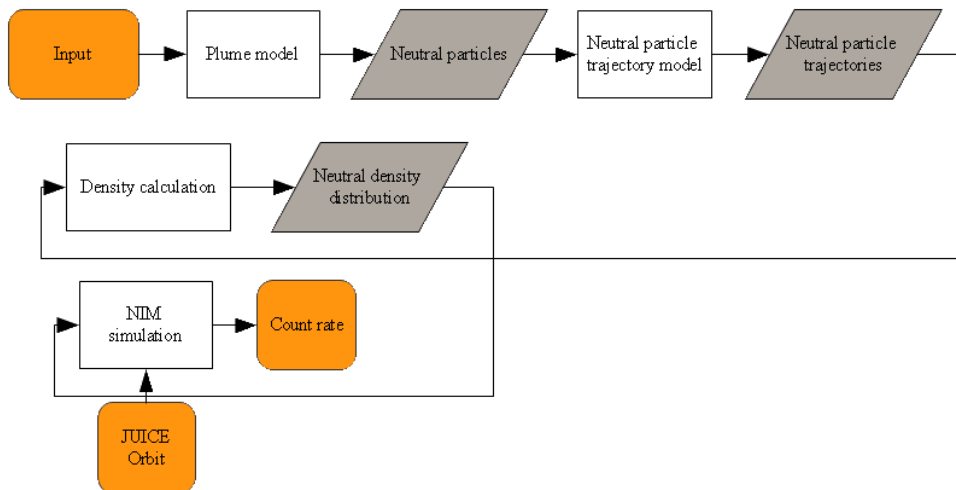


**Figure 4-1:** Schematic overview of the neutral plume particle simulation

Figure 4-1 shows a schematic overview of the neutral plume particle simulation. First plume particles with a certain velocity are generated by an assumed plume model (see Section 4.1.2). Subsequently the trajectories of these neutral particles are calculated under the influence of Europa's gravity field (see Section 4.1.4 to 4.1.6). Then, from the state of all particles at a certain time step, the particle density is calculated (see Section 4.1.9). The simulation is a type of Monte Carlo simulation because it depends on the repetition of certain calculations for a range of input values generated according to a certain probability. Density is the quantity that is observed by NIM. The density along the planned JUICE trajectories that is derived in the model is converted into a count rate, which is what the instrument actually reports.

### 4.1.2 PLUME SOURCE MODEL

In this study a simple model of the plume is employed. Neutral particles are launched from a single point source at the surface (or a series of point sources representing a crack), with a Maxwellian velocity distribution that depends on the temperature of the expelled material at the source (through the thermal velocity) and an assumed bulk velocity. We assume all the particles are water molecules (the program could be extended to different compositions by making the bulk velocity composition dependent). The physical process that lies at the origin of the plume and gives the plume particles their initial velocity is not modelled, since no observations have been made of this process.

The Maxwellian velocity distribution gives a velocity distribution of particles in a gas that is in thermodynamic equilibrium. The Maxwellian velocity distribution has the same shape as a normal distribution (see Equation (4-1)) of which the mean and the standard deviation are replaced by the bulk ( $v_{bulk}$ ) and thermal velocity ( $v_{th}$ ), respectively. The thermal velocity is determined by the temperature of the gas (T), the mass of the particles (m) and the Boltzmann constant ( $K = 1.3806488 \times 10^{-23} \text{ J/K}$ ), as is shown in Equation (4-2). It is clear from Equation (11-2) that the velocity spread becomes higher for higher temperatures for the same mass, and lower for heavier particles for the same temperature. The Maxwellian velocity distribution is visualized in Figure 4-2. The thermal velocity in this figure corresponds to the thermal velocity of a set of water molecules with mass  $2.987 \times 10^{-26} \text{ kg}$  per molecule and temperature of the gas of 230 K. The bulk velocity is chosen to be equal to the thermal velocity (460 m/s).

$$f(v, v_{bulk}, v_{th}) = \frac{1}{v_{th} \sqrt{2\pi}} e^{-\frac{(v-v_{bulk})^2}{2v_{th}^2}} \quad (4-1)$$

$$v_{th} = \sqrt{\frac{2KT}{m}} \quad (4-2)$$

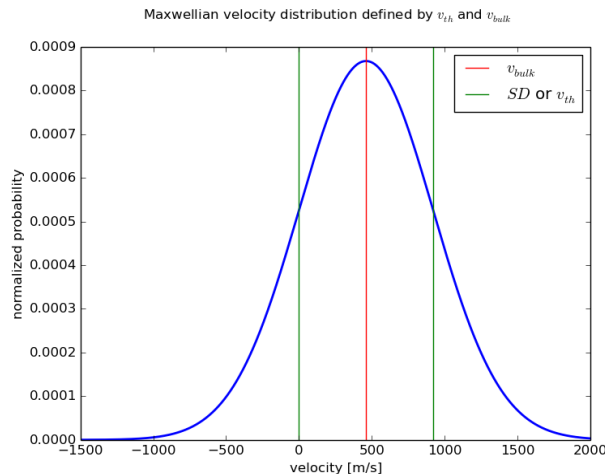


**Figure 4-2:** Maxwellian velocity distribution for 460 m/s thermal velocity and bulk velocity.

Particles are launched with a certain initial velocity of which the velocity distribution of each velocity component (in x, y and z direction) is initially given by a Maxwellian distribution. To the velocity of the z-component a constant bulk velocity is also assigned, this bulk velocity is assumed to be perpendicular to the surface at the plume source and pointing away from the surface. Particles with a velocity that would imply the particles collide with Europa immediately after launch are discarded; a new particle is generated instead. The velocity component because of Europa's rotation about its axis of rotation is not taken into account in the particle velocity.

From *Roth et al.* [2014a] it can be concluded that the plume is not originating from a single plume point source, but from a larger active area. Therefore we will also simulate a crack on the surface of Europa by placing several plume sources next to each other.

#### 4.1.3 NON-COLLISIONAL

We assume particles launched from the plume source do not interact with each other after launch. The same assumption has been made to model Enceladus plumes, for example in *Tenishev et al.* [2010], *Smith et al.* [2010] and *Dong et al.* [2011]. We will derive a range for which mass flux our model is applicable (see Section 4.5.2). The mass flux is the mass per second that is released by the plume source (whether it is a point source or an area). The density distribution of our model will scale linearly with the mass flux, so the results will be easily scalable for the applicable range.

#### 4.1.4 SUPERPARTICLES

In a test particle simulation, particles do not represent single molecules or atoms. To simulate a plume with a large mass flux unpractically high numbers of particles would be required. So, instead of launching the actual number of particles per time step a limited number of 'super' particles are launched. Each super particle represents a number of 'real' particles that are travelling together. The mass of such a super particle is then simply given by Equation (4-3) .

$$m_{super} = \frac{\dot{m} dt}{n_{super}} \quad (4-3)$$

Here  $m_{super}$  corresponds to the mass per super particle in kg,  $\dot{m}$  to the mass flux of the plume source in kg/s,  $dt$  to the time step size in seconds and  $n_{super}$  to the number of super particles.

#### 4.1.5 PARTICLE TRAJECTORIES

We assume that the only force that acts on the particles is Europa's gravity. We disregard Jupiter's gravity. This is justified by calculating the Hill sphere of Europa with relation to Jupiter. The Hill sphere indicates in which region the gravity of Europa dominates over that of Jupiter. The Hill sphere is calculated with Equation (4-4).

$$r \approx a(1 - e) \sqrt[3]{\frac{m}{3M}} \quad (4-4)$$

In this equation  $a$  is the semi-major axis of Europa's orbit about Jupiter (670900 km),  $e$  is the eccentricity of Europa's orbit (0.0101),  $m$  is the mass of Europa ( $4.79982 \times 10^{22}$  kg) and  $M$  is the mass of Jupiter ( $1.8986 \times 10^{27}$  kg). The resulting Hill sphere radius is  $1.35 \times 10^4$  km. We will consider plume simulations that are well within this sphere (i.e. the radial position of the particles with respect to Europa is one order of magnitude smaller than the Hill sphere radius).

In the simulation Europa is assumed to be a sphere with a diameter of 1562.09 km, with a homogeneous distribution of mass. The force on a particle is obtained from Newton's law of gravitation. The acceleration caused by gravity is expressed by Equation (4-5). In this equation  $\frac{d\vec{v}}{dt}$  is the acceleration vector of the particle,  $G$  is the constant of gravity ( $6.674 \times 10^{-11}$  N m<sup>2</sup> /kg<sup>2</sup>),  $M$  is the mass of Europa,  $r$  is the distance between the particle and the centre of Europa and  $\hat{r}$  is the unit vector along this distance.

$$\frac{d\vec{v}}{dt} = -\frac{GM}{r^2} \hat{r} \quad (4-5)$$

Trajectories are obtained by numerical integration. The method of integration is the 'leap frog' method. This integration method is explained in the following section.

#### 4.1.6 LEAP FROG INTEGRATION

Equations (4-6) and (4-7) express how the position and velocity of a particle can be progressed from time step  $i$  to time step  $i+1$ . First, the particle position is progressed with Equation (4-6). For the progression of position the velocity at step  $i+1/2$  is needed. For the very first progression of position (namely, from  $i = 0$  to  $i = 1/2$ ) the velocity at  $i+1/2$  is calculated with Equation (4-7), by calculating the force at  $i+1/2$  using the position at step  $i$  and using half a time step (one time step is  $\Delta t$ ). Equation (4-5) is used for calculating the force. For subsequent time steps velocity can be progressed from  $v$  at  $i+1/2$  to  $v$  at  $i+3/2$  with Equation (4-7) and using the normal time step size  $\Delta t$ .

$$\vec{x}_{i+1} = \vec{x}_i + \vec{v}_{i+1/2} \Delta t \quad (4-6)$$

$$\vec{v}_{i+1} = \vec{v}_i + \vec{f}_{i+1/2} \Delta t \quad (4-7)$$

#### 4.1.7 FROM TRAJECTORIES TO DENSITY

Then the density at a certain location is calculated from the super particle trajectories. First the space of interest around the plume is divided in a 3D grid of grid cells. From the location of all super particles at a certain time step the density in each grid cell is determined. This is done by simply calculating for each super particle to which grid cell it belongs and counting the super particles per

grid cell. Super particle density can then easily be converted in to real particle density by multiplying with the factor  $n_{super}$  as expressed in Equation (4-3).

As soon as particles collide with Europa they will no longer contribute to the density calculation. Particles that leave the grid will still contribute to the density, for those positions where they are contained in the grid.

The density contribution of a super particle is weighted over surrounding cells. We assume the size of a super particle is equal to the size of a grid cell and that mass is distributed homogeneously in the particle. Based on this we divide the density contribution over the maximum of eight cells it can be contained in. The contribution of to each cell is weighted with the volume of the super particle that is contained in that cell. Super particles that have their centre outside of the grid are not counted in any case, including when there is still some overlap with the grid.

#### 4.1.8 NOT GENERATING NEW PARTICLES AT EACH TIME STEP

Instead of launching a new set of unique super particles at each time step, only the trajectories of a limited set of particles are calculated for the required number of time steps. The state of the plume at the final time is then created by combining the positions of all particles at each previous time step. For a small number of super particles this will result in coarse density distributions. The trajectories of single particles will stand out. With large number of particles the density will smooth out and individual superparticle trajectories will no longer be distinguishable. With this technique the total number of particles in the simulation will be reduced, downsizing the required computer resources (memory and CPU time).

The total number of individual superparticles launched is  $10^6$ . For each of these particles the complete trajectory for the considered time frame will be determined.

#### 4.1.9 FROM DENSITY TO NIM COUNT RATE

Particle density is then converted to count rate with Equation (4-8). Count rate is the quantity that NIM reports. This equation applies to 5 seconds accumulation time [Personal communication with P. Wurz, University of Bern, scientist responsible for NIM development].

$$1 \text{ particle/cm}^{-3} = 5 \text{ counts} \quad (4-8)$$

This relation does not represent 1 to 1 the number of ions registered by the instrument, but should simply be considered as the output of the instrument. It should be noted 1 second accumulation might be used for the plume. In our simulation we assume the change in density over 5 seconds is not significant, so we simply take the density value at the data points of the JUICE trajectory.

The intrinsic instrument background noise is 5 counts (for a 5-second accumulation), which is a Poisson distributed noise. At Europa background noise from penetrating radiation adds about 30 counts, also Poisson distributed. The combined background counts are 35. To take into account variation of the noise we take into account a 1 sigma safety limit. This is limit is obtained by taking

the square root of 35, which is approximately 6. The 35 background counts will be subtracted from the signal, the 1 sigma safety limit accounts for random noise and cannot be subtracted. Our resulting noise limit for 5 seconds accumulation time is 6 counts.

## 4.2 SIMULATION INPUTS – PLUME MODEL

To constrain the properties of the plume three parameters are needed in our simulation: the temperature at the plume source, the mass flux and the bulk velocity. Estimates for the first two of these parameters can be obtained from the supplementary material to *Roth et al.* [2014a]. Here it will be briefly explained how these estimates have been obtained in *Roth et al.* [2014a].

First the neutral water density at the source of the plume was calculated. This was done by assuming a density distribution where the density changes exponentially with altitude, depending on a certain scale height. The neutral density in this model is integrated along a line of sight and this is related to auroral emission intensity, which was observed by the Hubble Space Telescope, by considering the rate of electron impact excitation. The water density at the source was then chosen such that it matches the intensity. The density obtained by *Roth et al.* [2014a] was  $\sim 10^{15} \text{ m}^{-3}$ .

They argued that if the derived source density ( $\sim 10^{15} \text{ m}^{-3}$ ) were to be explained by sublimation, a source temperature of 150K in the active area would be necessary. This was based on experimental relations between the temperature of water vapour and the pressure [*Marti and Mauersberger, 1993*]. *Roth et al.* [2014a] considers that the origin of the plume is an active area and not a single plume point source. However the thermal velocity resulting from a source temperature of 150 K would be too low to explain the altitude of the plume. To explain this contradiction they argue the source temperature and density are higher, but confined to a small fraction of the modelled area. This small area could be a group of fractures.

Then a source temperature of 230 K was assumed instead, to have a thermal velocity of the particles that was sufficiently high to explain the altitude of the plume. The source density resulting from sublimation at this temperature is  $3 \times 10^{21} \text{ m}^{-3}$  [*Roth et al., 2014a*]. The ratio of the previous source density and this estimate is  $3 \times 10^{-7}$ . This implies only that a percentage of the active area ( $500\,000 \text{ km}^2$ ) is actually emitting vapour (such that the total mass flux is conserved between the two cases). Assuming a fracture width of several centimetres, the active fractures in the active area would be  $10^3 - 10^4 \text{ km}$  long in total. Multiplying the area of the active fissures with the thermal velocity resulting from a source temperature of 230 K and the new density will give an estimate of the mass flux: 7000 kg/s. This mass flux is the same in the case where the source temperature is 150 K.

Because Europa's escape velocity is approximately 2 km/s, most particles will fall back to the surface (with a thermal velocity resulting from a source temperature of 230K, 460 m/s for water molecules). *Roth et al.* [2014a] estimated a residence time of  $10^3$  seconds (this is the residence time for a particle with an almost vertical launch velocity of 700 m/s). Considering this residence time and the estimated total water mass in the plume of  $3 \times 10^6 \text{ kg}$  (of the  $\sim 10^{32} \text{ H}_2\text{O}$  molecules) the

deposition rate will be 3000 kg/s, which is roughly similar to the mass flux estimate of 7000 kg/s. With this they consider the source temperature estimate of 230 K is justified.

## Model parameters

**Table 4-1:** Overview of used input parameters

Parameter	Value
Source temperature [K]	230
Source mass flux [kg/s]	0.7
Particles bulk velocity (perpendicular to local surface) [m/s]	460
Mass per particle (mass H <sub>2</sub> O molecule) [kg]	2.987x10 <sup>-26</sup>
Trajectories calculated for # superparticles	8x10 <sup>6</sup>
Time step size [s]	10
# of time steps	1000
Size of a grid cell [km <sup>3</sup> ]	10x10x10
Mass per superparticle [kg]	8.75x10 <sup>-7</sup>
Density in a superparticle with the size of a grid cell – lowest density possible in the model [# /cc]	29

Table 4-1 shows the model parameters that we use in our simulation. We assume a plume source temperature of 230K, the resulting thermal velocity is 460 m/s. This temperature is based on the discussion in *Roth et al.* [2014a], see previous section. The mass of a water molecule is assumed.

If it is assumed the plume particles only have a thermal velocity, the particles will spread isotropically from the plume source. Assuming the plume source is a narrow fissure, the plume can be expected to have a more narrow shape. To account for this we assume the particles not only have a thermal velocity but also a bulk velocity (perpendicular to the local surface). We assume the bulk velocity to be equal to the thermal velocity.

### 4.3 SIMULATION INPUTS – GRID PROPERTIES

The reference frame used in our simulations is the IAU Europa reference frame [*Archinal et al.*, 2010]. This is a Europa centred reference frame. In this frame the z-axis is perpendicular to the mean orbital plane of Europa. The positive x-axis is pointing in the direction of Jupiter and the y-axis completes the right hand system (it is opposite of the sense of rotation of Europa about Jupiter).

We assume grid cell dimensions of 10 by 10 by 10 km. A time step of 10 s for the calculation of the neutral particles is assumed. These parameters can capture the particle with a velocity of 0.5 km/s (approximately the assumed bulk velocity) within the same or neighbouring cell after a single time step.

We consider 1000 time steps for the calculation of the neutral particle trajectories. Together with a time step size of 10 s the state of the plume until 10000 s will be simulated. This is one order of

magnitude larger than it takes a particle with a velocity of 0.5 km/s to hit the surface again (~1000s).

The total simulation time is also constrained by the survival time of water molecules against the loss processes, such as photo- and electron impact ionizations. In Table 4-2 the different loss processes are listed. The loss rate for the electron impact reactions have to be multiplied with the electron density to obtain the loss rate per second. The typical electron density in Europa's orbit is 110 electrons per cc for an electron temperature of 100eV (Table 2-2). The values in the column of 20eV are chosen, because these are closest to 100 eV. Adding all losses together a value of  $9 \times 10^{-6}$  per second is obtained (if we choose 250 eV, the loss rate will be approximately  $1.677 \times 10^{-5}$  per second). So after 1000 seconds (typical flight time) 1% of the total number of particles has been lost (or approximately 1.7% in the 250 eV case). Therefore we neglect these losses in the neutral particle environment model.

**Table 4-2:** Photo- and electron impact reactions with water occurring at Europa [Johnson et al., 2009], based on [Itikawa et al., 2005].

<b>Photoreactions</b>		
<i>Reaction</i>	<i>Rate [<math>s^{-1}</math>]</i>	
$H_2O + hv \rightarrow OH + H$	$3.8 \times 10^{-7}$	
$H_2O + hv \rightarrow H_2 + O$	$2.2 \times 10^{-8}$	
$H_2O + hv \rightarrow H + H + O$	$2.8 \times 10^{-8}$	
$H_2O + hv \rightarrow H_2O^+ + e$	$1.2 \times 10^{-8}$	
$H_2O + hv \rightarrow H + OH^+ + e$	$2.0 \times 10^{-9}$	
$H_2O + hv \rightarrow OH + H^+ + e$	$4.8 \times 10^{-10}$	
<b>Electron impact reactions</b>		
<i>Reaction</i>	<i>at 20 eV [<math>cm^3 s^{-1}</math>]</i>	<i>at 250 eV [<math>cm^3 s^{-1}</math>]</i>
$H_2O + e \rightarrow OH + H + e$	$3.8 \times 10^{-8}$	/
$H_2O + e \rightarrow H_2 + O + e$	Unknown	Unknown
$H_2O + e \rightarrow H_2O^+ + 2e$	$2.3 \times 10^{-8}$	$8 \times 10^{-8}$
$H_2O + e \rightarrow H + OH^+ + 2e$	$5.8 \times 10^{-9}$	$2.6 \times 10^{-8}$
$H_2O + e \rightarrow OH + H^+ + 2e$	$3.3 \times 10^{-9}$	$2.3 \times 10^{-8}$

Also during 10000 seconds (3.2% of Europa's orbital period) Europa will have rotated approximately 11.5 degrees. At 400 km this results in a deviation of approximately 70 km w.r.t. to horizontal plane at the point of the plume source.

## 4.4 RESULTS

In this section the results of the neutral plume particle simulations are shown. The input parameters that have been used to obtain these results can be seen in Table 4-1.

### 4.4.1 DENSITY IN XY PLANE AND XZ PLANE

In Figure 4-3 the density (water particles per cubic centimetre) can be seen in a plane of 1000 by 1000 km. The plane is parallel to the x and y axis and located 400 kilometres below the plume source that is exactly at Europa's south pole.

The colourbar indicates particle density (water particles per cubic centimetre) in a logarithmic scale. Figure 4-4 shows a cut through this plane to indicate the density versus horizontal distance from the plume source at one altitude.

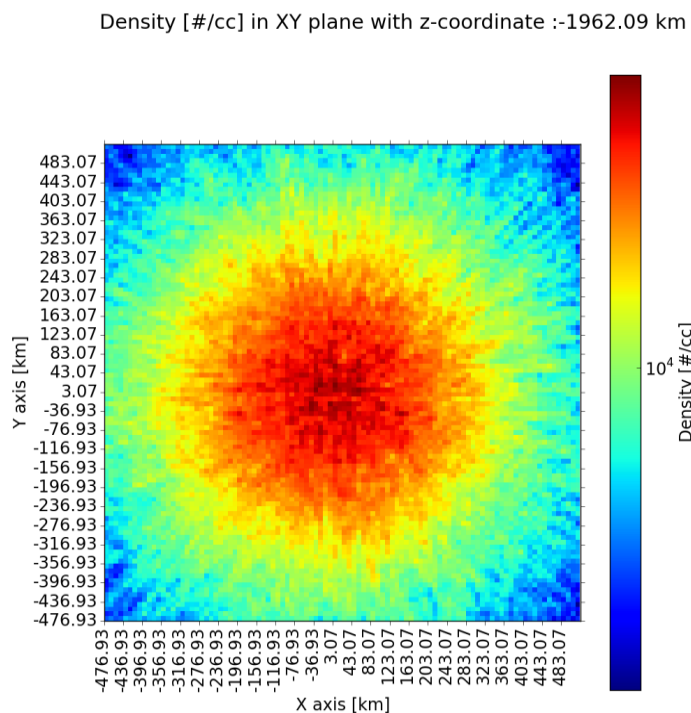


**Figure 4-3:** Density in a plane parallel to the xy axis, 400 kilometres below the plume source (located exactly at Europa's south pole)

Density [#/cc] horizontal profile in XY plane with z-coordinate :-1962.09 km

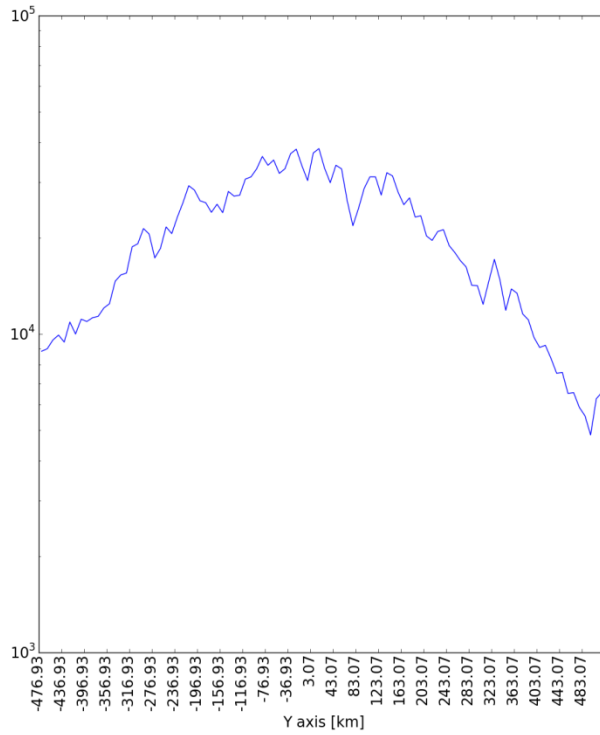


Figure 4-4: Cut through the xy plane shown in Figure 4-3, at x=0.

Density [#/cc] in XZ plane with y-coordinate :0.0 km

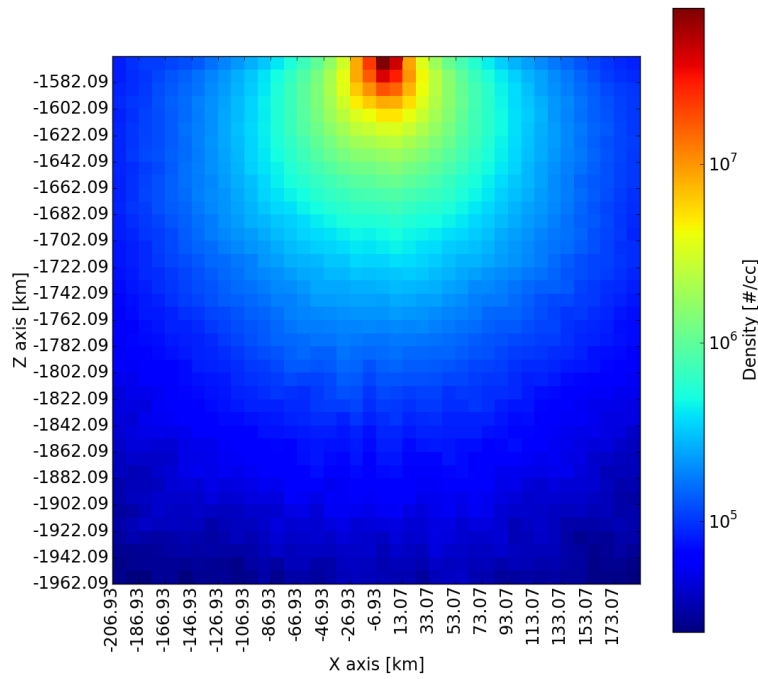
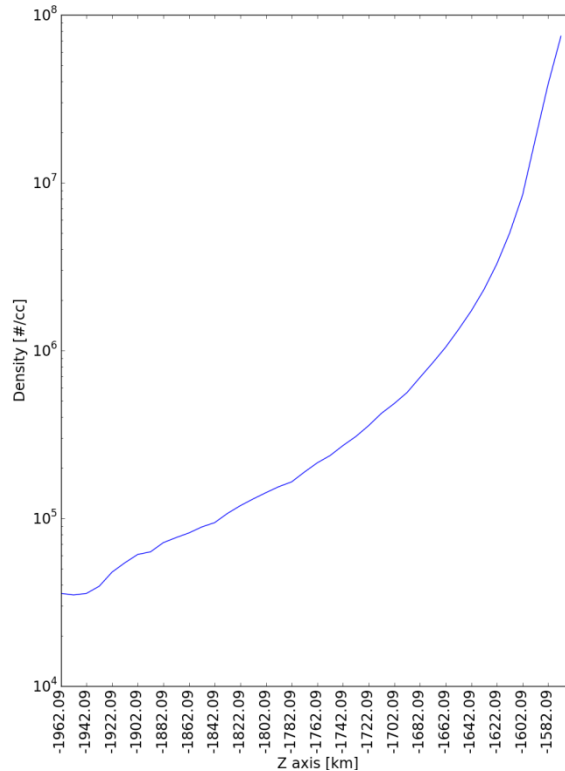


Figure 4-5: Density in a xz plane, spanning from the south pole of Europa to 400 kilometres below the pole.

Density [#/cc] vertical profile in XZ plane with y-coordinate :0.0 km



**Figure 4-6:** Density in a cut through the xz plane shown in Figure 4-5, at x =0.

In Figure 4-5 the density can be seen in a plane of 400 by 400 kilometres. The plane is parallel to the x and z axis and located at y= 0 km.

The plume is located exactly at Europa's south pole. The colourbar indicates particle density in a logarithmic scale. Figure 4-6 shows a cut through this plane to show the altitude profile.

#### 4.4.2 DENSITY DISTRIBUTION ON THE SCALE OF EUROPA

In Figure 4-7 and Figure 4-8 it can be seen how the neutral particle density in our model varies on the scale of Europa.

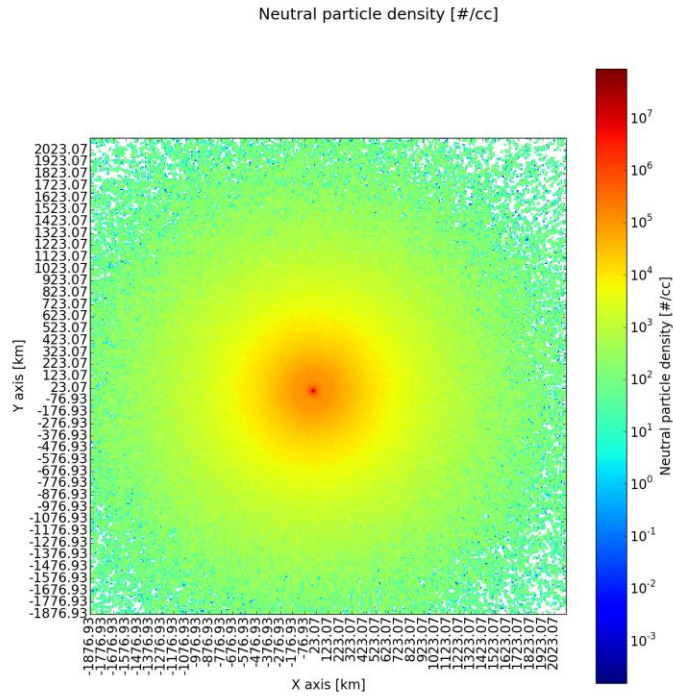


**Figure 4-7:** Neutral particle density in a xy plane, 50 km below the plume source (located at the south pole)

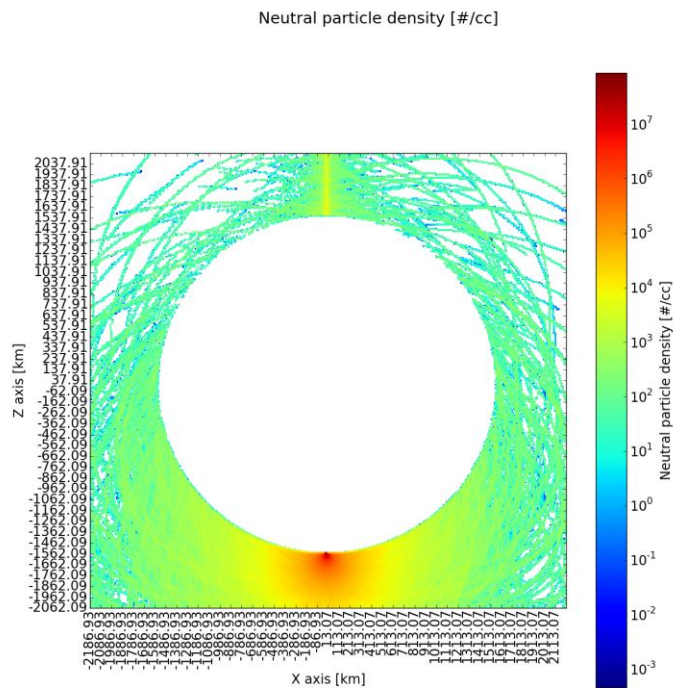


**Figure 4-8:** Neutral particle density in a xz plane at  $y = 0$ , the white disk represents Europa. The plume source is located at the south pole.

From Figure 4-7 and Figure 4-8 it can be deduced that the particles of the plume spread over a large area on the scale of Europa. Especially in the northern hemisphere we notice individual particle trajectories in the density. The density here is limited to the density contribution of individual super particles. For our analysis we focus on the areas close to the plume, where the density is not limited by the density contribution of individual superparticles.

#### 4.4.3 DENSITY DURING FLYBYS

Figure 4-9 shows the density variation during the first JUICE flyby, for the case where a plume is located directly under the point of closest approach. At the outer most trajectory data points the density approaches the minimum density value the simulation can resolve, but is still higher than the density contribution of a single super particle. The geometry of the part of the flyby considered for this simulation can be seen in Figure 2-17.

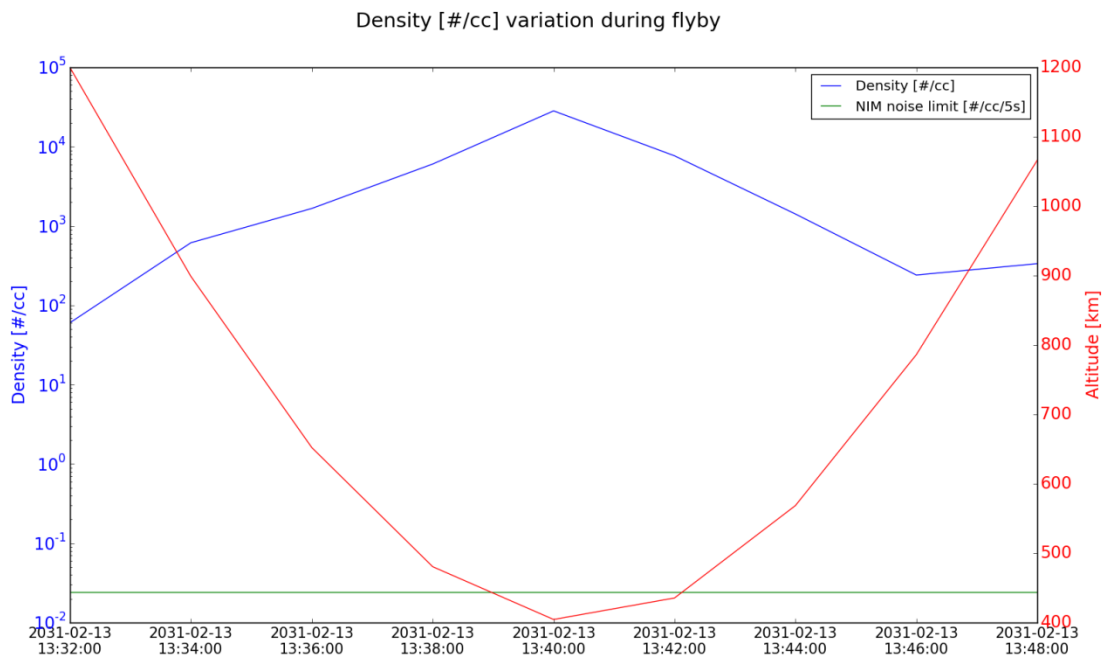


**Figure 4-9:** Density variation (blue line) during the first JUICE flyby, for a plume that is located directly under the point of the closest approach. The green line indicates the NIM count rate noise limit (6 counts per s for 5 seconds accumulation) converted into density.

#### 4.4.4 DENSITY VARIATION FOR DIFFERENT PLUME POSITIONS

In Figure 4-10 it is shown how the count rate at the closest approach (CA) varies for different plume positions. In the middle of the plot the count rate is shown for a plume that is directly under the CA. Each grid cell up, down, left or right corresponds to moving the plume one degree north, south, west or east. The noise limit (6 counts per second) is not reached in this figure.

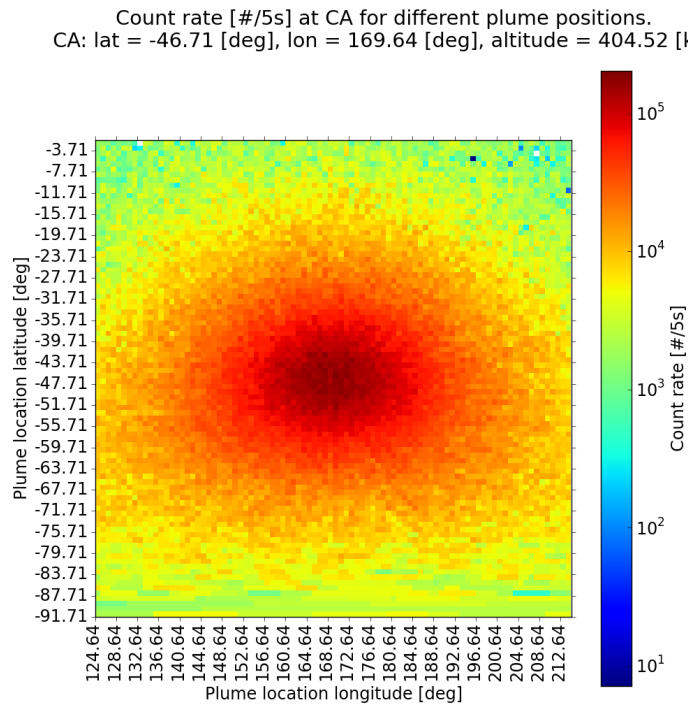


**Figure 4-10:** Density during the closest approach (CA) of the first JUICE flyby, for different positions of the plume with respect to the point of closest approach.

#### 4.4.5 RESULTS: PLUMES SOURCES ALONG A CRACK

In this section it is shown how the neutral plume particle density changes when multiple plume sources are located along a single crack. In this case we assume a crack of 1000 km is located at Europa's south pole, the crack is roughly aligned with the x axis.

To achieve this result the density distribution of one single plume source as stored in a 3D grid was rotated multiple times over the surface and positioned along the crack, and subsequently re-binned to a grid with the same size as the original. We divided the crack in 200 source plumes. The density distribution of each plume source was divided by 200, to keep the total mass flux constant.

It can be seen by comparing Figure 4-5 and Figure 4-11 to Figure 4-13 that even though the single sources along the crack have only 1/200<sup>th</sup> of the mass flux as the single plume in Figure 4-8, the maximum neutral density is only roughly one order of magnitude smaller in the crack case, than the single source case.

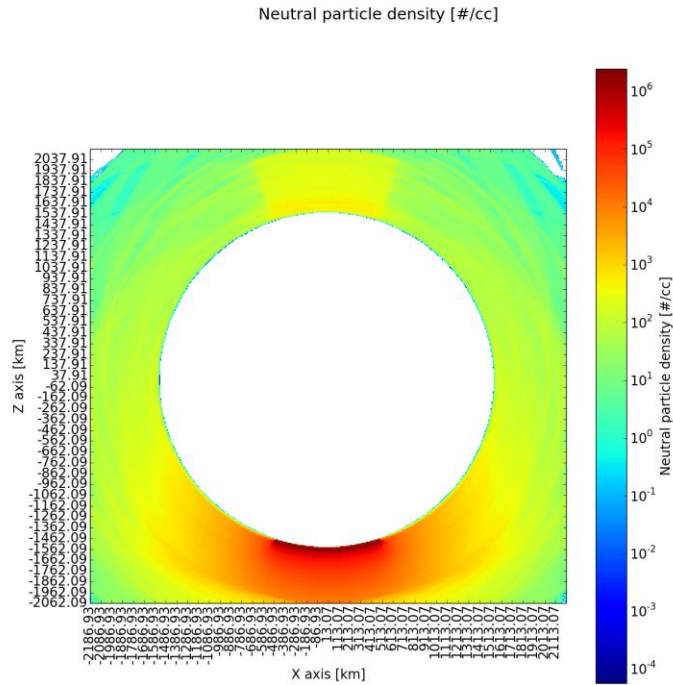


Figure 4-11: xz cross section of the grid. A 1000 km long crack is located at Europa's south pole along the x-axis.

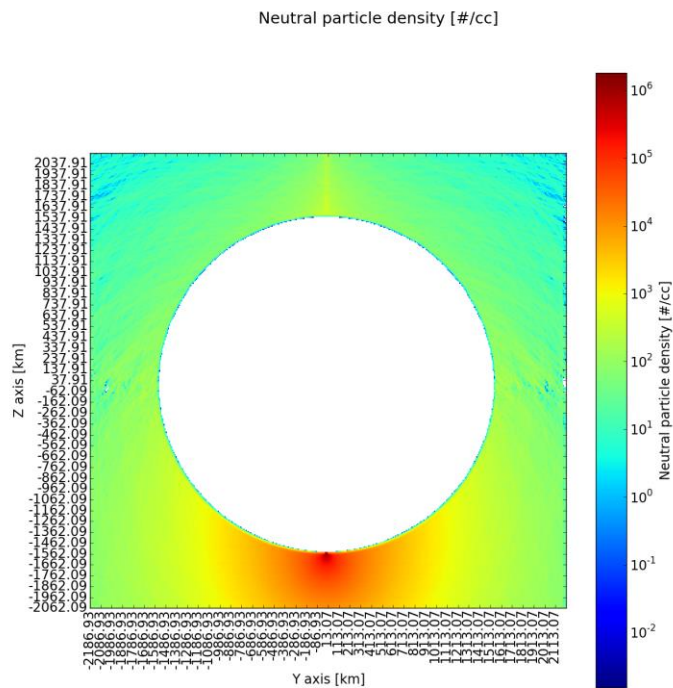
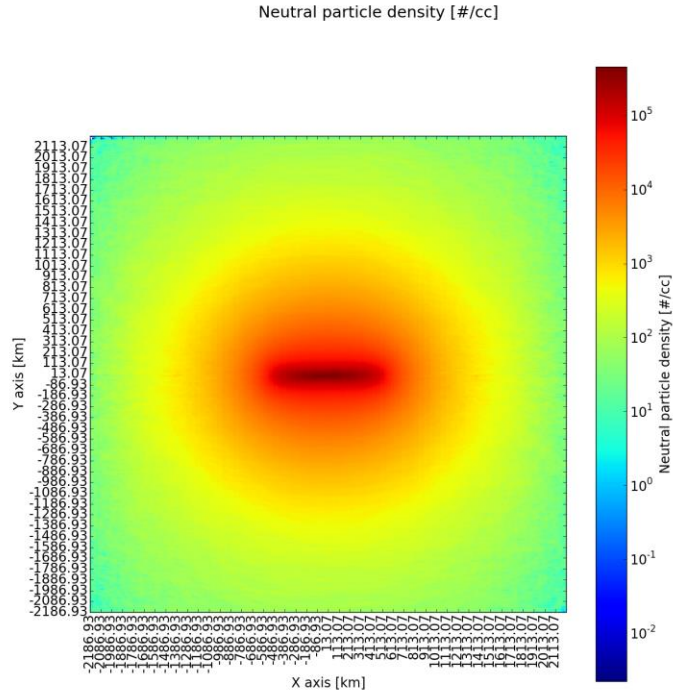


Figure 4-12: yz cross section of the grid. A 1000 km long crack is located at Europa's south pole, along the x-axis.



**Figure 4-13:** xy cross section of the grid 50 km below Europa’s south pole. A 1000 km crack is located along the X axis.

## 4.5 DISCUSSION

In this section we discuss the results of the neutral particle simulation and the NIM plume observation simulation.

### 4.5.1 FLUX CONSERVATION

A simple verification test to check the density at 400 km altitude above a plume source is done by assuming conservation of the particle flux (particles/s) between the plume source and half a spherical surface with a radius of 400 km. From the conservation of flux the density at 400 km altitude can be estimated. This is shown in Equation (4-9). In this equation  $flux_{source}$  is the flux of particles at the source (particles/s),  $A$  is the surface of half a sphere with radius 400 km (see Equation (4-10)) and  $v$  is the velocity of the particles (assumed to be 0.5 km/s). The flux at the source is calculated by dividing the mass flux (7000 kg/s) by the mass per water molecule.

$$\rho_{400\text{ km}} = \frac{flux_{source}}{Av} \quad (4-9)$$

$$A = \frac{1}{2} 4\pi(400 \times 10^3)^2 [m^2] \quad (4-10)$$

The simple approximation gives  $0.5 \times 10^9$  particles per cc for the density at 400 km altitude. The particle density at 400 km resulting from similar input in the simulation is approximately  $10^9$  particles per cc.

#### 4.5.2 NON-COLLISIONAL

To justify the assumption that the plume particles are non-collisional in our model we determine the mean free path of the particles. This distance expresses the mean distance a particle travels before colliding with another particle. The mean free path of the particle should be larger than the length scale of the area of interest to justify our assumption. The mean free path is calculated with Equation (4-11). Here  $\sigma$  is the collisional cross sectional area of a particle and  $n$  is the number density (particles per volume).

$$l = \frac{1}{\sigma n} \quad (4-11)$$

The cross sectional area is a quantity with unit  $\text{cm}^2$  that describes the likelihood of collisions between particles. The cross sectional area for the collisions between water molecules can be assumed to be the circular area resulting from a radius that is equal to the sum of the radius of two water molecules. The cross section area of a single molecule is assumed to be approximately equal to the cross sectional area of the molecule. We are focusing on water particles, so we will calculate the cross sectional area of a water molecule. The spacing between hydrogen and oxygen atoms is approximately  $10^{-8}$  cm. For a circular cross section the resulting surface is  $3.14 \times 10^{-16} \text{cm}^2$ . The collision cross section area between two water molecules is approximately four times as big (by taking the radius of a circular cross sectional area as twice the radius of one molecule). The resulting collisional cross sectional area is approximately  $10^{-15} \text{cm}^2$ . [University of Virginia, Properties of water]

In Figure 4-5 it can be seen the densest part of the plume ( $10^8$  particles per cc) extends at most 50 km from the source. From this number density and the collisional cross-section area of water molecules a mean free path of 100 km is derived (from Equation (4-11)). This length is significantly larger than the scale to which it applies. We could interpret this as an indication that the non-collisional assumption is reasonable.

A different approach is to treat the gas environment created by plume as an atmosphere and calculate the corresponding exobase. The advantage of this approach is that it does not depend on the density decay obtained from the model. The exobase is the boundary in the atmosphere, above which the atmosphere is non-collisional, below it is collisional. We use the standard method to obtain the exobase (see for example in described in *Shizgal and Arkos* [1996]). This method assumes the atmosphere is in hydrostatic equilibrium (this means there is a balance between gravity and pressure). Treating the plume particle environment as an atmosphere in hydrostatic equilibrium is an approximation, the condition of hydrostatic equilibrium is not met for the plume particles, since most of are falling back to the surface because of gravity.

The standard definition of the exobase states that the mean free path, defined by Equation (4-11), is approximately equal to the scale height  $H$ , as is shown in Equation (4-12) .

$$H \approx l = \frac{1}{\sigma n} \quad (4-12)$$

The scale height is the height for which the density varies a factor  $e$ . The scale height  $H$  is expressed in Equation (4-13), in which  $k$  is the Boltzmann constant,  $T$  is the temperature,  $M$  is the average molecular mass and  $g$  is the gravitational acceleration. For a temperature of 230 K, the molecular mass of water  $2.987 \times 10^{-26}$  kg, and a gravitational acceleration of  $1.315 \text{ m/s}^2$  for Europa, the scale height becomes 80 km.

$$H = \frac{kT}{Mg} \quad (4-13)$$

In Equation (4-12) the number density  $n$  is expressed by Equation (4-14).

$$n(z) = n_0 e^{\frac{-z}{H}} \quad (4-14)$$

In this equation the number density  $n$  is expressed as an exponential function of altitude  $z$ . The decay of density is determined by the scale height  $H$ . By substituting Equation (4-14) in Equation (4-12) we obtain Equation (4-15) that expresses the altitude of the exobase.

$$z_{exobase} = H \ln(n_0 \sigma H) \quad (4-15)$$

The exobase for a scale height of 80 km, a collisional cross section of  $10^{-15} \text{ cm}^2$  and a density of  $10^8$  particles per cc at the surface (obtained from our model) does not exist. The result of Equation is negative (-17 km), which means the condition where the probability of collisions on average is 1 is met nowhere above the surface. The atmosphere is fully non-collisional. Increasing the density at the surface to  $10^9$  particles per cc will create the exobase at 168 km. According to this method the density of  $10^8$  is approximately the maximum density for which no collisions will occur at all. The peak density in our model for a plume with a mass flux of 7000 kg/s is  $10^{12}$  this will result in an exobase of 726 km. This indicates that for densities that correspond to the mass flux reported in *Roth et al.* [2014a] a large collisional zone will occur.

From the two methods we assume that our non-collisional model is applicable for mass fluxes up to 0.7 kg/s. Note that the mass flux influences the results (the densities) linearly, as long as the environment is collisionless. For example, if twice the mass flux is assumed, the calculated neutral and plasma densities becomes also twice the value, without variations of their spatial distributions relatively. The existence of less dense plumes at Europa has been suggested in the past [*Nimmo et al.*, 2007].

In summary, the mass flux reported by *Roth et al.* [2014] is extremely high, and cannot be represented by a test particle model. The assumption that the particles are non-collisional cannot be satisfied in this case. This mass flux is bigger than the mass flux escaping from Io's atmosphere (approximately 1000 kg/s) (*Bagenal et al.* [2014]) or bigger than the mass of water coming from the Enceladus plumes (>150 kg) (*Hansen et al.* [2006]). Modelling a plume with a mass flux of 7000 kg/s would require more complex simulation methods that are more computationally expensive.

#### 4.5.3 ROTATION OF EUROPA

In Section 4.3 it was stated that during the computation time Europa would rotate about 11.5 degrees, resulting in a horizontal offset of approximately 70 km. As is shown in Figure 4-3 to Figure 4-6, an offset of 70 km (approximately 7 grid cells) does not significantly alter the resulting density of the plume at 400 km. This confirms neglecting the rotation of Europa acceptable for our purposes. Also, most particles will fall back within 1000 seconds, which is one order of magnitude shorter than the simulation time. Rotation effects can be ignored for most particles because of this reason.

#### 4.5.4 FEASIBILITY OF PLUME OBSERVATIONS BY NIM

We assumed a plume with a low mass flux: 0.7 kg/s. This is substantially lower than what was predicted by *Roth et al.* [2014a]: 7000 kg/s. Even in this low mass flux case, plume observations should be possible from 400 km altitude. The plumes in *Roth et al.* [2014a] are located on the antiojovian meridian (180 degree longitude in the IAU Europa reference frame) at 55 and 75 degrees south latitude. The projection of the point of closest approach of the first JUICE flyby is located at 170 degree longitude and 47 degrees south latitude.

From Figure 4-10 we can conclude that NIM should be able to observe plumes located at those positions during the closest approach of the flyby, even in the very low mass flux case we assumed. It is possible to lower the mass flux four orders of magnitude before the observed signal becomes close to the NIM noise limit (the corresponding mass flux is  $7 \times 10^{-5}$  kg/s, for the case when a single plume point source is located directly below the closest approach).

We conclude that even if the mass flux presented in *Roth et al.* [2014a] is overestimated by several orders of magnitude we can still expect the neutral particle density to be sufficiently high to make observations possible. The plume does not have to be directly under the point of closest approach for observations for this to be possible.

An obvious precondition is that the plume should be presented at the time of the flyby. The time particles stay in the environment is a limiting factor. As was already indicated in *Roth et al.* [2014a] neutral particles are expected to fall back quickly to Europa's surface ( $10^3$  seconds for a particle with an initial velocity of 700 m/s, almost perpendicular to the local surface).

#### 4.5.5 PLUME SOURCE: CRACK INSTEAD OF POINT

*Roth et al.* [2014a] argued that the plume does not have a single point source, but could be coming from a long (series of) cracks. If this is true, the peak density of the water molecules will be lower. We expect this effect to lower the density not more than one order of magnitude for a single crack of 1000 km length (see Section 4.4.5), bringing the NIM observational limit to the source mass flux of  $7 \times 10^{-4}$  kg/s. The area where the plume is observable will be wider than for the case of a single plume source point. Because the density in the environment is lowered by one order of magnitude, the model is applicable for mass fluxes up to 7 kg/s (one order of magnitude more than the single plume point source case).

To simulate the crack we assumed it can be represented by combining different plume point sources that are independent of each other. This will only be the case if the environment is non-collisional, this method cannot be employed for collisional plumes. The method employed here only considers a single crack, in future work this could be expanded to an active area with multiple cracks.

#### 4.5.6 BACKGROUND SIGNALS

A 1-D model calculation of Europa's exosphere has been performed by the group at University of Bern developing NIM [*Wurz et al.*, 2014]. This model is based on *Smyth et al.* [2006] and *Shematovich et al.* [2005]. The model gives the densities of established exospheric components versus altitude. The results are shown in Figure 4-14. In this figure the range of possible measurements by the NIM sensor is also shown. The signal of water at 400 km altitude is approximately  $10^5$  particles per cc for sputtered water and  $2 \times 10^2$  particles per cc for the sublimation component.

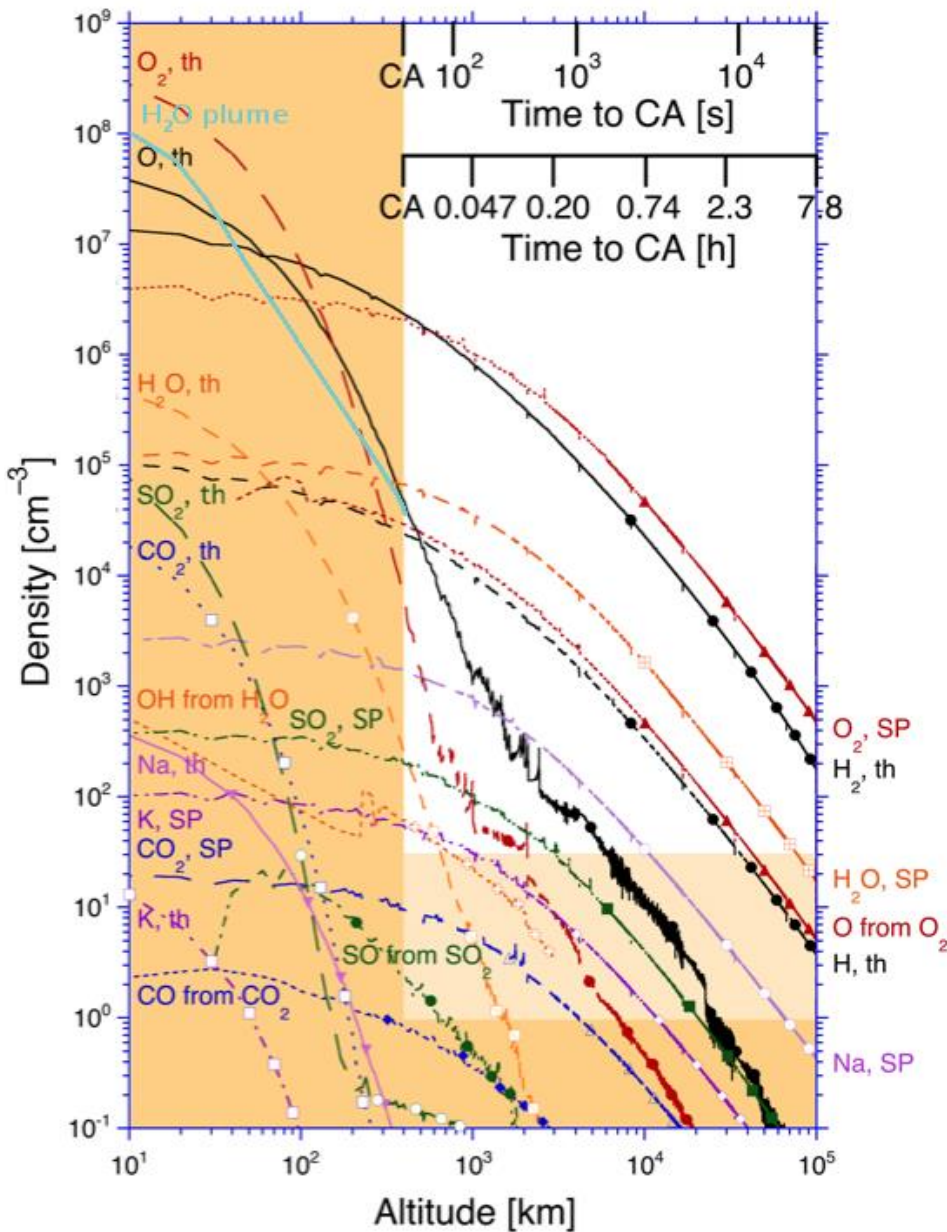


**Figure 4-14:** Density versus altitude for the constituents of Europa's exosphere, at the dayside. Both components due to sputtering (SP) and sublimation (th) are shown. The coloured boundary at the left side indicates the minimum altitude achieved by JUICE during its flybys of Europa (400 km). The white and light coloured area indicate the range of possible measurements of NIM. The white colour indicates the end of life sensitivity of NIM. On top the time to closest approach (CA) of the JUICE flyby is shown. [Wurz *et al.*, 2014]

Added in light blue is the density profile of water from the plume model (identical to the profile in Figure 4-6).

When we compare the density in our model (Figure 4-6) with the expected other water components in Europa's exosphere it can be concluded that the density in our model at 400 km ( $3 \times 10^4$  per cc) is two orders of magnitude larger than the sublimated water component. The sputtered water component and the plume signal are comparable. By increasing the mass flux to the level predicted in Roth *et al.* [2014a] we expect the density at 400 km altitude to increase as well, making the signal of the plume more recognizable. In addition the sputtering yield is expected to be lower on the plasma wake side of Europa, such that the sputtered water component is also expected to be lower. Furthermore the JNA sensor (Jovian Neutrals Analyser), also part of PEP,

could be used to constrain the precipitating flux of plasma and thus the resulting sputtered component at Europa [Wieser *et al.*, 2009].

#### 4.5.7 GRAVITY FOCUS EFFECT

In Figure 4-8 that shows the water density on the scale of Europa, it can be seen that there is a local increase in the density on the north pole of Europa (exactly opposite to the plume source). This is a gravitational lensing effect. A gravitational lens has no single focal point, but instead has a focal line. This is what we see in the simulation results. Flying through the focal line of the gravitation lens gives the best opportunity to observe a plume, when the plume is located at the other side of Europa that is observed during a flyby.

## 5 IONIZED PLUME PARTICLE SIMULATIONS

To determine if in-situ observations of Europa's water vapour plumes can be made with PEP, not only the neutral plume particles should be investigated, but also the ionized plume particles. The contents of this chapter link with sub-goal 2, 3.2, 3.3 and 4 from the project plan (Chapter 3).

The trajectories of these particles are modelled. It is investigated if they can be observed during the JUICE flyby with the JDC sensor. JDC is an ion mass spectrometer, it does not simply respond to density but it counts the number of particles per direction, per energy, per second. So for the JDC simulation from the particle trajectories not only density should be obtained but also the energy and directional distribution of the particles.

### 5.1 IONIZED PLUME PARTICLE MODEL

#### 5.1.1 Overview

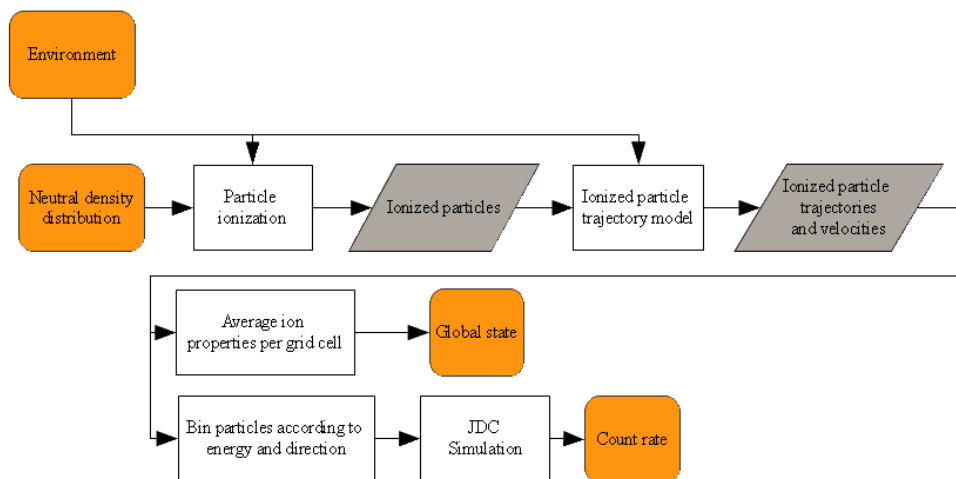


**Figure 5-1:** Schematic overview of the ionized plume particle simulation

The ion particle simulation accepts as input the density of the neutral plume stored in a 3D grid. This density represents the steady state density of the plume. By multiplying the neutral particle density with the ionization probability per time step one ionized superparticle is created in each grid cell. The trajectories of those particles as determined by electric and magnetic fields are tracked. From the particle trajectories and velocities the average properties of ions per grid cell can be determined (density, thermal speed, bulk speed and average flux). By binning the particles according to energy and direction along the JUICE trajectory, the count rate given by JDC can be simulated. This simulation is implemented using Python.

### 5.1.2 IONIZATION OF NEUTRAL PARTICLES

The ion particle simulation accepts as input the density of the neutral plume stored in a 3D grid. The density distribution represents the steady state density of the plume. We assume that the neutral particles have zero velocity, because their typical speed is <1 km/s, but after the ionization the plasma particles get the velocity of the order of ~100 km/s. From the centre of each grid cell an ionized super particle will be launched. The resulting trajectory will have a weight assigned to it that corresponds to the neutral density in the original grid cell multiplied with the ionization probability per time step.

Important ionization processes at Europa are photoionization and electron-impact ionization, these effects are listed in Table 4-2. We neglect photoionization completely because the resulting ionization rate is two or more orders of magnitude smaller than the ionization by electrons impact reactions, for an electron density of 110 particles per cc (the average value from Table 2-2). We focus on the ionization of H<sub>2</sub>O to H<sub>2</sub>O<sup>+</sup>. The rate of this effect is one order of magnitude larger than the other possible reactions with H<sub>2</sub>O mentioned in Table 4-2, at an electron energy of 20eV. We assume this rate because it will result in the lowest H<sub>2</sub>O<sup>+</sup> density (the worst case in terms of the instrument simulation). The ion density in our simulation scales linearly with the ionization rate, so to obtain the results for 250eV case the final results can simply be multiplied with 3.5 (the ratio between the two values). At the higher electron energy the other ionization reactions for water will have the same order of magnitude as the reaction that creates H<sub>2</sub>O<sup>+</sup>.

The ionization probability  $P$  per time step in our model is given by Equation (5-1), in this equation  $n_e$  is the electron density in particles per cc,  $k$  is the rate of electron impact ionization per s in cc/s (Table 4-2) and  $dt$  is the size of a time step (in s). For simplicity we assume the electron density is constant everywhere in our simulation and that ionizing electrons not depleted before electrons reach the densest part of the plume.

$$P = n_e k dt \quad (5-1)$$

For simplicity we assume the electron density is constant everywhere in our simulation and that ionizing electrons not depleted before electrons reach the densest part of the plume.

### 5.1.3 IONIZED PARTICLE TRAJECTORIES

#### 5.1.3.1 Charged particle motion: basic theory

When the neutral plume particles become ionized, their trajectories will be influenced by electric and magnetic fields. Particle motion as determined by electric and magnetic fields is described by the equations of motion of a charged particle, shown in Equations (5-2) and (5-3).

$$m \frac{d\vec{v}}{dt} = q(\vec{E} + \vec{v} \times \vec{B}) \quad (5-2)$$

$$\frac{d\vec{x}}{dt} = \vec{v} \quad (5-3)$$

In these equations  $m$  is the mass of the ion,  $\vec{v}$  the velocity of the particle,  $t$  the time,  $q$  the charge of the particle,  $\vec{E}$  the electric field,  $\vec{B}$  the magnetic field and  $\vec{x}$  the particle's position. The right hand side of Equation (5-2) is the Lorentz force which expresses the force acting on a charged particle in electric and magnetic fields [Kivelson 1995].

### **Influence of the magnetic field on charged particle motion**

Because of their newly acquired charged state, the ionized particles will start gyrating about magnetic field lines. This can be understood by considering a simplified situation. We set the electric field in Equation (5-2) to zero and assume  $B$  only has a constant component in the  $z$  direction, we then obtain Equation (5-4). This equation can be rewritten as given in Equation (5-5) to show the components of the velocity along the  $x$ ,  $y$  and  $z$ -direction ( $\hat{x}$ ,  $\hat{y}$  and  $\hat{z}$  are the unit vectors along the positive  $x$ ,  $y$  and  $z$  direction).

$$m \frac{d\vec{v}}{dt} = q(\vec{v} \times \vec{B}) \quad (5-4)$$

$$\frac{d(v_x \hat{x} + v_y \hat{y} + v_z \hat{z})}{dt} = \frac{q}{m} \left( (v_x \hat{x} + v_y \hat{y} + v_z \hat{z}) \times B_z \hat{z} \right) \quad (5-5)$$

From Equation (5-5) we can obtain the accelerations on the particle in  $x$ ,  $y$  and  $z$  direction, as given by Equations (5-6) to (5-8).

$$\frac{dv_x}{dt} = \frac{qv_y B_z}{m} \quad (5-6)$$

$$\frac{dv_y}{dt} = -\frac{qv_x B_z}{m} \quad (5-7)$$

$$\frac{dv_z}{dt} = 0 \quad (5-8)$$

Equations (5-6) to (5-8) show that there is no force acting on the particle in the direction along the magnetic field. The motion caused by the magnetic field is only in the plane perpendicular to the magnetic field.

By taking the derivative of Equations (5-6) and (5-7) we obtain Equations (5-9) and (5-10).

$$\frac{d^2v_x}{dt^2} = \frac{qB_z}{m} \frac{dv_y}{dt} \quad (5-9)$$

$$\frac{d^2v_y}{dt^2} = -\frac{qB_z}{m} \frac{dv_x}{dt} \quad (5-10)$$

In these Equations we can substitute Equations (5-6) and (5-7) to obtain Equations (5-11) and (5-12).

$$\frac{d^2v_x}{dt^2} = \left(\frac{qB_z}{m}\right)^2 v_y \quad (5-11)$$

$$\frac{d^2v_y}{dt^2} = -\left(\frac{qB_z}{m}\right)^2 v_x \quad (5-12)$$

These equations are 2<sup>nd</sup> order ordinary differential equations, in fact harmonic oscillators. The solutions of these take the form of cosine function as shown in Equation (5-13) and (5-14), in which the frequency  $\Omega$  is given by Equation (5-12),  $\delta$  represents the initial phase and  $\pm$  the sign of the charge  $q$ . The velocity  $v_0$  and initial phase  $\delta$  can be derived from the initial conditions.

$$v_x = v_0 \cos(\Omega t + \delta) \quad (5-13)$$

$$v_y = \pm v_0 \sin(\Omega t + \delta) \quad (5-14)$$

$$\Omega = \frac{qB_z}{m} \quad (5-15)$$

The motion of the particle about the magnetic field line is circular and is referred to as gyromotion or cyclotron motion. The corresponding frequency is referred to as gyrofrequency or cyclotron frequency. The motion is in the clockwise direction about the B-field if  $q > 0$  and right counter clockwise direction if  $q < 0$ . The radius of the circle (gyroradius) is described by Equation (5-16) in which  $v_0$  is the velocity perpendicular to the magnetic field.

$$\rho_c = \frac{v_0}{\Omega} = \frac{mv_0}{qB_z} \quad (5-16)$$

In conclusion, under the influence of only a homogeneous magnetic field the charged particle will describe a circular motion about the magnetic field lines in the plane perpendicular to the field line. [Kivelson 1995; Cravens 1997]

### Influence of the electrical field on charged particle motion

By setting the magnetic field in Equation (5-2) to zero we can investigate the contribution of the electric field to the motion of charged particles; the result is given in Equation (5-17). This equation shows us the particle will receive a constant acceleration along the direction of the electric field [Kivelson 1995].

$$\frac{d\vec{v}}{dt} = \frac{q}{m} (\vec{E}) \quad (5-17)$$

### Particle motion by a uniform magnetic field and a uniform external force

In this section we derive the equation of motion for a charged particle as influenced by a uniform magnetic field and a uniform external force, such as a the force caused by a uniform electric field. The external force can be split up in two components, one parallel to the magnetic field and one perpendicular to the magnetic field, as is shown in Equation (5-18).

$$\vec{F} = \vec{F}_{\parallel} + \vec{F}_{\perp} \quad (5-18)$$

The equation of motion in the direction parallel to the magnetic field is simply expressed by Equation (5-19).

$$\frac{dv_{\parallel}}{dt} = \frac{F_{\parallel}}{m} \quad (5-19)$$

As was discussed in the previous section the charged particle will not experience any acceleration in the direction along the magnetic field. After integration we obtain Equation (5-20), in which  $v_{\parallel 0}$  is the initial velocity parallel to the B-field.

$$v_{\parallel}(t) = v_{\parallel 0} + \left(\frac{F_{\parallel}}{m}\right)t \quad (5-20)$$

The equation of motion in the direction perpendicular to the magnetic field, without an external force, is given in Equation (5-21). We obtain the right side by considering Equation (5-15) and that  $\vec{B}$  and  $\vec{\Omega}$  are parallel. Equation (5-21) is now expanded by introducing a force in the direction perpendicular to the magnetic field; the result is shown in Equation (5-22).

$$\frac{d\vec{v}_{\perp}}{dt} = q(\vec{v}_{\perp} \times \vec{B}) = m\vec{v}_{\perp} \times \vec{\Omega} \quad (5-21)$$

$$\frac{d\vec{v}_\perp}{dt} = m\vec{v}_\perp \times \vec{\Omega} + \frac{1}{m}\vec{F}_\perp \quad (5-22)$$

Next the velocity  $\vec{v}_\perp$  is split up in a gyrating component  $\vec{v}_c(t)$  and a uniform component  $\vec{v}_F$ , as is shown in Equation (5-23). The components of the gyrating component are expressed by Equation (5-13) and (5-14).  $\vec{v}_F$  is uniform so  $d\vec{v}_F/dt = 0$ .

$$\vec{v}_\perp(t) = \vec{v}_c(t) + \vec{v}_F \quad (5-23)$$

The derivative of the gyrating component can be expressed as Equation (5-24), this is obtained by from Equation (5-11) and (5-7).

$$\frac{d(\vec{v}_c)}{dt} = \vec{v}_c \times \vec{\Omega} \quad (5-24)$$

Next by substituting Equation (5-23) in Equation (5-22), considering the relation given in Equation (5-24) and assuming  $d\vec{v}_F/dt = 0$ , we obtain Equation (5-25).

$$0 = \vec{v}_F \times \vec{\Omega} + \frac{1}{m}\vec{F}_\perp \quad (5-25)$$

Because  $\vec{v}_F$  and orthogonal to  $\vec{\Omega}$  we can express  $\vec{v}_F$  by Equation (5-26).

$$\vec{v}_F = -(\vec{v}_F \times \vec{\Omega}) \times \frac{\vec{\Omega}}{\Omega^2} \quad (5-26)$$

Subsequently by using Equation (5-25)  $\vec{v}_F \times \vec{\Omega}$  in Equation (5-26) can be substituted for  $-\vec{F}_\perp/m$  to obtain Equation (5-27). We obtain the right side by considering Equation (5-15) and that  $\vec{B}$  and  $\vec{\Omega}$  are in the same direction.  $\vec{F}_\perp$  can be replaced by  $\vec{F}$ , since the cross product of the component of the force parallel to the magnetic field is zero.

$$\vec{v}_F = \frac{\vec{F}_\perp \times \vec{\Omega}}{m\Omega^2} = \frac{\vec{F} \times \vec{B}}{qB^2} \quad (5-27)$$

If the force  $\vec{F}$  is replaced by the force created by a uniform electric field ( $\vec{F} = q\vec{E}$ ), Equation (5-27) becomes Equation (5-28). This equation expresses the drift motion, the motion the charged particle experiences in the direction perpendicular to the magnetic field. This motion is referred to as ExB drift.

$$\vec{v}_E = \frac{\vec{E} \times \vec{B}}{B^2} \quad (5-28)$$

The drift is always in the  $\mathbf{E} \times \mathbf{B}$  direction and is independent of the particle charge. The drift velocity is independent of charge and mass, and will be the same for all particles. If it would differ, particles could become separated according to charge and new currents would be introduced. [Cravens 1997]

**Special case: uniform and perpendicular E- and B-fields, no velocity parallel to B-field**

In the special case where a perpendicular homogeneous magnetic and electric field occur and the particle has no velocity perpendicular to the B-field, the charged particle motion will consist of a gyrating component about the magnetic field line and a drift motion in the direction perpendicular to the electric and magnetic field. The magnetic field will not cause any acceleration along the magnetic field and the drift velocity will be strictly in the direction perpendicular to the electric and magnetic field (as follows from Equation (5-28)). The resulting movement is shown in Figure 5-2.

This motion can be explained by a varying 'local' gyroradius. The particle is gyrating in the same plane as the electric field is located (since the E- and B-field are perpendicular). Because of the gyromotion the particle will have acceleration in the direction of the E-field, half of the gyroperiod. In this situation the particle will be accelerated and the gyroradius increases as the velocity perpendicular to the B-field increases, as is shown in Equation (5-16). When the gyromotion changes direction the particle will be decelerated along the E-field direction, the total velocity perpendicular to the B-field will decrease and the gyroradius will become smaller. During the time when the gyroradius is largest, the particle will cover a larger net distance. When the gyroradius is smallest the net distance is smaller. This explains the  $\mathbf{E} \times \mathbf{B}$  drift [Kivelson 1995, Cravens 1997],

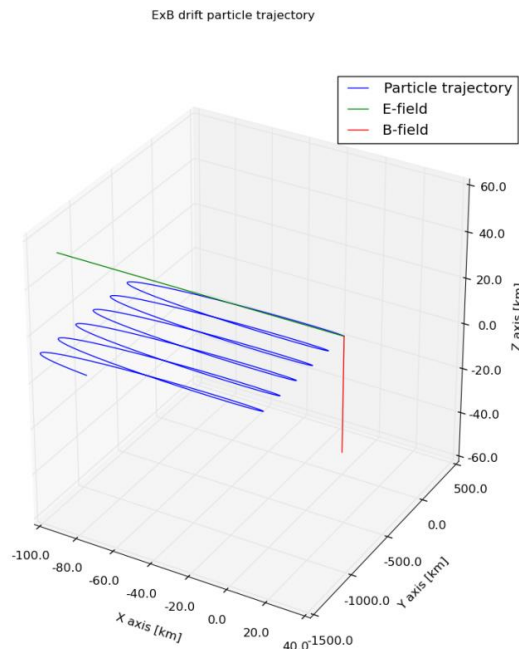


**Figure 5-2:** ExB drift trajectory of a  $\text{H}_2\text{O}^+$  particle.  $B = -414$  nT along the z-axis,  $E$  is  $-0.0315$  V/m along the x-axis, the initial position is at the origin of the three axes and the initial velocity is  $50$  km/s along positive y-axis. Note that the scale of the x and y axis is not the same.

### Special case: uniform and perpendicular E- and B-fields, zero initial velocity

Here we derive the equations of motion for a positively charged ion in the special case that there are a perpendicular uniform magnetic and electric field and the initial particle velocity is zero. The drift velocity can be expressed as given in Equation (5-29).

$$\vec{v}_E = \frac{\vec{E} \times \vec{B}}{B^2} = \frac{E}{B} \hat{x} \quad (5-29)$$

The gyromotion that is in the plane perpendicular to the B-field is given in Equation (5-30) (based on Equation (5-13) and (5-14)).  $\Omega$  is equal to  $|qB/m|$ .

$$\vec{v}_c(t) = v_0(\cos(\Omega t + \delta) \hat{x} - \sin(\Omega t + \delta) \hat{y}) \quad (5-30)$$

The total velocity experienced by the particle is the result of the gyromotion and the drift motion; it is expressed by Equation (5-31).

$$\vec{v}(t) = \vec{v}_c(t) + \vec{v}_E = (v_0 \cos(\Omega t + \delta) + \frac{E}{B})\hat{x} - v_0 \sin(\Omega t + \delta) \hat{y} \quad (5-31)$$

By setting the initial conditions  $v = 0$  at  $t = 0$ , the amplitude  $v_0$  is found to be  $E/B$  and the phase  $\delta$  is  $\pi$  rad. The particle will gyrate with the same speed as the drift speed because  $v_0 = E/B$ . The total velocity will be zero for every time instant that corresponds to an integer multiple of the gyroperiod. The trajectory of the particle is expressed by Equation (5-32) and

$$\vec{x}(t) = \left(\frac{E}{B}\right) \left[t - \frac{1}{\Omega} \sin(\Omega t)\right] \quad (5-32)$$

$$\vec{y}(t) = \left(\frac{E}{\Omega B}\right) [1 - \cos(\Omega t)] \quad (5-33)$$

(5-33). These equations are obtained by integrating the equations for the velocity and assuming the initial position is zero. The gyroradius (Equation (5-34)) is obtained from the gyration velocity  $v_0$  and the gyrofrequency  $\Omega$ .

$$\rho_c = \frac{v_0}{\Omega} = \frac{E}{B\Omega} \quad (5-34)$$

The resulting motion is shown in Figure 5-3. A neutral particle that becomes ionized and starts experiencing this motion is referred to as a 'pick-up' ion. The motion can be understood as follows: the particle with zero initial velocity will be accelerated in the direction of the E-field. As soon as the particle has a non-zero velocity the gyromotion will start, which has an acceleration component in the same direction as the velocity of the particle. Subsequently this acceleration will reverse direction and the particle will be decelerated till its velocity is zero again. From that point the process will repeat.

At Europa's orbit in Jupiter's magnetosphere the electric field is created by the movement of magnetized plasma at velocity  $\vec{u}$ . The field can be derived from the Lorentz force, when no force is working on the particles in the plasma rest frame:  $\vec{E} = \vec{u} \times \vec{B}$ . The electric field is referred to as the convectional electric field.

The velocity of the particle will vary between 0 in the cusps and  $2\vec{u}$  at the peaks of the cycloid, with respect to the centre of gyration. The centre of gyration moves at velocity  $\vec{u}$  along the ExB direction. The centre of gyration will move  $2\pi\rho_c$  gyroradii in one gyroperiod in the ExB direction [Luhmann 1995; Cravens 1997].

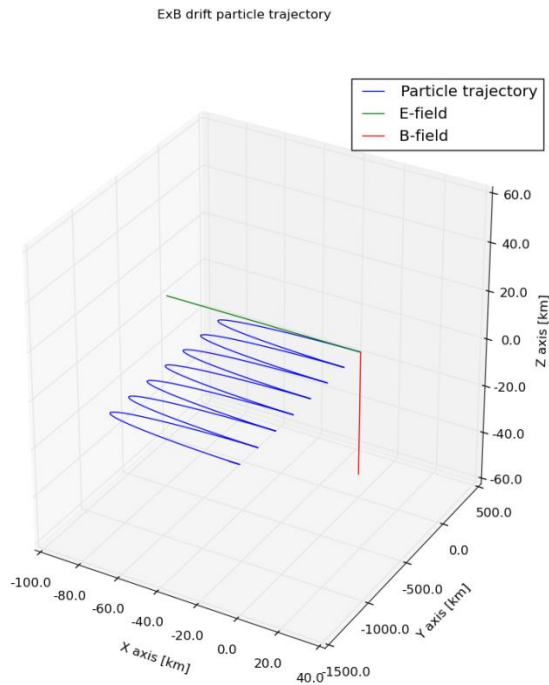


**Figure 5-3:** ExB drift trajectory of a  $\text{H}_2\text{O}^+$  particle.  $B = -414$  nT along the z-axis and  $E$  is  $-0.0315$  V/m along the x-axis, the initial velocity is zero and the initial position is at the origin of the three axes.

### 5.1.3.2 Charged particle motion in our model: theory

In our model we assume a homogeneous magnetic field. We assume the only electric field is the convectional electric field produced by the corotational plasma. The direction of this E-field in the IAU reference frame is along the negative x axis (as shown in Figure 5-3). We assume a magnetic field that is parallel to the z axis (also shown in Figure 5-3). The particles will get an ExB drift in the negative y direction (also shown in Figure 5-3).

According to the results of the neutral simulation (Section 4.1.2), the neutral particles have a velocity between 0 and 1 km/s (approximately thermal velocity + bulk velocity). Thus, we can assume that the initial velocity of the charged particles right after the ionization is significantly

lower than the velocity after the pick-up. Therefore, we neglect the initial velocity of the pick-up ions in this simulation. The trajectory of a pick-up ion with non-zero initial velocity will behave exactly as shown in Figure 5-3.

$\vec{E}$ , the convective electric field, can be expressed by Equation (5-35). In this equation  $\vec{v}_b$  is the bulk velocity of charged particles expressed by Equation (5-36). Here we only consider plume ions and plasma sheet ions.

$$\vec{E} = -\vec{v}_b \times \vec{B} \quad (5-35)$$

$$\vec{v}_b = \frac{n_{cp} \vec{v}_{b\ cp} + n_{plume} \vec{v}_{b\ plume}}{n_{cp} + n_{plume}} \quad (5-36)$$

Equation (5-36) shows that  $\vec{v}_b$  (the bulk velocity of charged particles) will approach the bulk velocity of the corotational plasma ions ( $\vec{v}_{b\ cp}$ ), when the number of corotational plasma ions ( $n_{cp}$ ) is higher than the number of ionized plume particles ( $n_{plume}$ ). If the plume ion density becomes higher than the corotational plasma ion density,  $\vec{v}_b$  will approach the bulk velocity of the ionized plume particles ( $\vec{v}_{b\ plume}$ ). Those particles have initially a velocity of approximately 0.5 km/s (the bulk velocity of the neutral particles), which is small compared to the velocity of the corotational plasma ions (approximately 70 km/s relative to Europa). In the second case the particle trajectories can't be assumed to be dominated by ExB drift. The ion density in our model should be lower than the ion density reported at Europa in Table 2-2, such that the ion bulk velocity is approximately that of the corotational plasma.

We neglect the effect of Europa's gravity on the ionized plume particles. The acceleration experienced by the particles due to the Lorentz force is significantly higher than the acceleration because of gravity. The gravitational acceleration on the surface of Europa is 1.315 m/s<sup>2</sup>. The acceleration experienced by the corotational electric field is 1.7x10<sup>5</sup> m/s<sup>2</sup>. This value is obtained by considering that the acceleration  $a = F/m = qE/m$ , q is 1.60217657x10<sup>-19</sup> coulomb, m is the mass of a water molecule 2.98x10<sup>-26</sup> kg. The field strength is obtained from Equation (5-35), by taking the corotational velocity as 76 km/s (from Table 2-2) and the magnetic field strength 415 nT (average from Table 2-2). The acceleration of the magnetic field varies from 0 at the cusps to decelerate the acceleration caused by the electric field completely. The velocity obtained by gravity will be close to the corotational velocity after 5x10<sup>5</sup> seconds. We will only consider the particle trajectories in time frames that are much shorter than this period. We only consider the trajectories well within the Hill sphere of Europa, so the effect of Jupiter's gravity on the trajectories can also be ignored. This was earlier discussed in Section 4.1.5.

### 5.1.3.3 Fields in our model

We assume the magnetic field in our model is in the negative z-direction of the IAU Europa frame, and the electric field is in the negative x-direction of the IAU Europa frame.

Figure 5-4 shows that the magnetic field imposed on Europa also has components in the x and y direction, for a reference frame where the x axis points in the direction of the plasma co-rotation, y points towards Jupiter and z is along the spin axis of Europa. Europa experiences a time varying magnetic field because the rotation axis of Jupiter and the magnetic field are tilted approximately 10 degree. Europa rotates in the plane spanned by Jupiter's spin equator [Khurana *et al.*, 1998]. We assume the magnetic fields is parallel to the z-axis in the IAU Europa frame, this corresponds closest to the situation where  $B_y$  is zero and  $B_x$  approximately 40-80 nT (this corresponds to the position where Europa passes the magnetic equator). This extra magnetic field component has 10-20% of the field strength of the main component we assume parallel to the z-axis (415 nT the average from Table 2-2). The extra magnetic field component means that the field will be tilted in the direction of the corotational flow. The picked up plume ions will move in the direction of the component of the plasma flow direction that is perpendicular to the B-field. In the case that there is some tilt in the direction of the plasma flow, the direction of the particles will change. The trajectories will be tilted relative to the XY plane in our simulation. The perpendicular component of the field that determines properties like the gyroradius and gyrofrequency will also change compared to the case when there is no other component but the z-component. We choose to neglect these changes in this work.

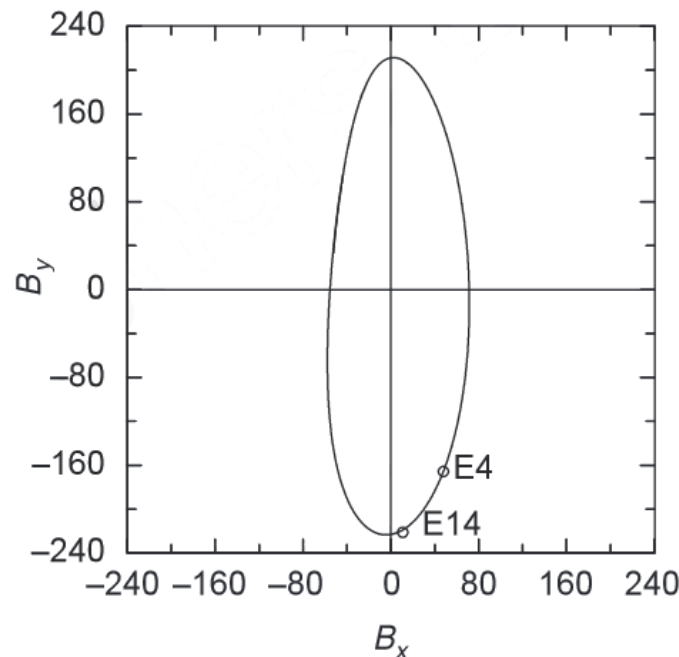


**Figure 5-4:** Modelled varying magnetic field experienced by Europa, in nT. The x axis is along the direction of plasma co-rotation, the y axis is orientated towards Jupiter, and the z axis is along the spin axis of the moon, the z component remains approximately constant. E4 and E14 indicate the observations made during two Galileo flybys [Khurana *et al.*, 1998].

The induced magnetic field of Europa is created by the time varying x and y components of the magnetic field shown in Figure 5-4. At its strongest the induced field can be up to 250 nT near the surface [Khurana *et al.*, 2009]. The strength of the field decreases with  $1/r^3$  (in which r is the radial position). But at the plume source that is located on the surface, the influence of the plume source can be significant. The induced magnetic field is at its weakest when Europa crosses the plasma sheet (the time varying components are at their weakest at this point). Assuming the imposed field is converted to the induced field strength without losses, the field strength at the surface is equal to the maximum  $B_x$  in Figure 5-4 (approximately 80 nT) at the plasma sheet crossing. The induced magnetic field will locally make the field inhomogeneous and introduce complexity in the particle trajectories. The ExB component caused by the z-aligned field and x aligned corotational flow will still be the dominating factor. At the altitude of 400 km, the field strength will have reduced to 40 nT (assuming 80 nT at the surface decays with  $1/r^3$ ). For simplicity we assume in this work that there is no induced magnetic field present. We also neglect the influence of the Alfvén wings (see Section 2.3) on the magnetic field lines close to Europa. The angle introduced in the magnetic field because of the Alfvén wings is in the range of 4.5 to 30 degrees [Kivelson *et al.*, 2004].

The electric field near Europa is dominated by the field imposed by the corotational plasma, as stated in the discussion in the previous section. We assume the plasma stream is homogeneous and that therefore the electric field is homogeneous too. In reality, close to Europa deviations in the electric field will occur, as is shown in Figure 2-11 . For simplicity we neglect these effects in this work.

#### 5.1.3.4 Charged particle motion in our model: implementation

Because we neglect the initial velocity of particles and gravity, and assume homogeneous fields, all ionized water plume molecules will essentially follow the same trajectory but from a different start position. Therefore we are allowed to calculate only a single ion trajectory and translate it to each grid cell of the store neutral density grid. Each trajectory will be assigned a weight that corresponds to the number of ionized neutral particles inside the original cell. The result of aforementioned assumptions is that massive savings in computation time can be made

The position and velocity of the original particle are calculated using the following integration scheme of the equations of motion given in Equations (5-2) and (5-3). This integration scheme is similar to the leap frog integration described in Section 4.1.6, to go from step  $i-1$  to  $i+1$  the state at step  $i$  is calculated first and used for integration. At the first step (step  $i$ ) position and velocity are obtained from the initial state at  $t=0$  using forward difference as is shown in (5-37) and (5-38).

$$\vec{x}(1) = \vec{x}(0) + \vec{v}(0)dt \quad (5-37)$$

$$\vec{v}(1) = \frac{q}{m} (\vec{E} + \vec{v}(0) \times \vec{B})dt \quad (5-38)$$

Subsequently position and velocity are updated to step  $i+1$  using Equation (5-39) and (5-40).

$$\vec{x}(i+1) = \vec{x}(i-1) + \vec{v}(i)2dt \quad (5-39)$$

$$\vec{v}(i+1) = \frac{q}{m}(\vec{E} + \vec{v}(i) \times \vec{B})2dt + v(i-1) \quad (5-40)$$

Similarly as in the neutral particle simulation we do not launch new particles at each time step, but calculate only the trajectories of all the initial particles and combine the positions of all time steps before the step of interest to get the state of the system.

### 5.1.3.5 Ion collisions

We assume ion particle collisions do not occur. The mean free path for the neutral particles is assumed to be non-collisional, as was discussed in Section 4.1.3. The ion density will be lower, so we assume the ionized plume particles will be non-collisional too.

## 5.1.4 LARGE SCALE SIMULATION

We simulate several macro parameters of the plume plasma (ion density, bulk speed, thermal speed and average flux) for every cell of a large scale 3D grid. The methods used to calculate these parameters for a grid are discussed in this section.

### 5.1.4.1 Ion density

The space of interest around the ionized plume particles is divided in a 3D grid. In each grid cell the ion particle density is calculated. This is done by counting how many super particles are present in each grid cell. Each super particle has attached to it a certain weight that is equal to the neutral particle density in the original grid cell it was launched from multiplied with the ionization probability per time step. As soon as particles collide with Europa they will no longer contribute to the density calculation.

### 5.1.4.2 Ion bulk velocity

The bulk velocity (or the mean velocity) is calculated as follows.

$$\bar{v}_j = \frac{\sum_{i=1}^n v_{js_i} w_{s_i}}{\sum_{i=1}^n w_{s_i}} \quad (5-41)$$

Here,  $\bar{v}_j$  the average of each velocity component of all particles in the grid cell of interest is calculated using Equation (5-41). In this equation  $v_{js_i}$  represents the velocity of a super particle in x, y or z direction and  $w_{s_i}$  represents the weight of each superparticle. The sums  $\sum_{i=1}^n v_{s_i} w_{s_i}$  and

$\sum_{i=1}^n w_{s_i}$  can be calculated in our simulation, without having to store the velocities of all the particles in the memory, this way the calculation can be made significantly less computationally intensive. From these values the bulk speed (magnitude of the bulk velocity) in each grid cell can be calculated using Equation (5-42).

$$\bar{v}_{bulk} = \sqrt{\bar{v}_x^2 + \bar{v}_y^2 + \bar{v}_z^2} \quad (5-42)$$

In our model we convert to  $v_{bulk}$  to the average energy per grid cell  $\bar{E}$  (in eV), this is done using Equation (5-43). In this Equation  $m_{H_2O}$  is the mass per water molecule ( $2.987 \times 10^{-26}$  kg) and  $q_e$  is used to convert the system of energy from Joule to electronvolt ( $q_e = 1.602176565 \times 10^{-19}$  J/eV).

$$\bar{E} = \frac{1}{2} m_{H_2O} \bar{v}_{bulk}^2 \frac{1}{q_e} \quad (5-43)$$

### 5.1.4.3 Thermal speed

The thermal speed in each grid cell is also calculated. Thermal speed (which in mathematics is the standard deviation of the speed of the superparticles) is given by:

$$SD = \sqrt{\frac{1}{\sum_{i=1}^n w_{s_i}} \sum_{i=1}^n (\bar{v}_i - \bar{v}_{bulk})^2} \quad (5-44)$$

In which  $\bar{v}_i$  is the velocity vector of a single particle and  $\bar{v}_{bulk}$  the bulk speed in a grid cell. Equation (5-44) can be expanded to Equation (5-45) and subsequently into Equation (5-46) taking into account the sum of the velocity vectors of all particles ( $\sum_{i=1}^n \bar{v}_i$ ) is the sum of all the velocity vectors of all superparticles multiplied with their respective weight ( $\sum_{i=1}^n \bar{v}_{s_i} w_{s_i}$ ).

$$SD = \sqrt{\frac{1}{\sum_{i=1}^n w_{s_i}} \sum_{i=1}^n (\bar{v}_i^2 - 2\bar{v}_i \bar{v}_{bulk} + \bar{v}_{bulk}^2)} \quad (5-45)$$

$$SD = \sqrt{\frac{1}{\sum_{i=1}^n w_{s_i}} \left( \sum_{i=1}^n (w_{s_i} \bar{v}_{s_i})^2 - 2\bar{v}_{bulk} \sum_{i=1}^n \bar{v}_{s_i} w_{s_i} + \bar{v}_{bulk}^2 \sum_{i=1}^n w_{s_i} \right)} \quad (5-46)$$

In Equation (5-46) the sums  $\sum_{i=1}^n (w_{si} \bar{v}_{si})^2$ ,  $\sum_{i=1}^n \bar{v}_{si} w_{si}$  and  $\sum_{i=1}^n w_{si}$ , and the bulk speed  $\bar{v}_{bulk}$  can be calculated independently, without having to store all velocity components of all particles, resulting in a significant reduction of computer resources.

#### 5.1.4.4 Average flux

The average flux (particles per cm<sup>2</sup> per s) is calculated by multiplying the bulk speed with the ion density in each grid cell.

## 5.2 FEASIBILITY OF DETECTING THE PLUME WITH JDC

We calculate the count rate of the JDC sensor along the JUICE trajectory. For the JDC feasibility study, the differential flux of the water ions (in the unit of particles/(cm<sup>2</sup> sr s eV)) are to be determined from the simulation of the Europa plume. This differential flux is the particle number flux (in the unit of particles /cm<sup>2</sup> s) per solid angle (in the unit of steradian) per energy (in the unit of eV). It is a function of direction and energy. This differential flux can be converted to count rate, which is what the instruments actually reports. Details of JDC sensor are summarized in Section 5.3.3.

### 5.2.1.1 Differential flux

To determine the differential flux first the particles in a certain spatial grid cell are binned according to energy, azimuth and elevation angles of the velocity vector. The available range and number of bins of each of these parameters depends on the instrument. In our simulation the binned particles are stored in a 3D grid, in which the axes correspond to the energy E and two directions (azimuth  $\varphi$  and elevation  $\theta$ ) bins.

The azimuth angle is defined as the clockwise angle about the z-axis in the xy plane of the IAU Europa frame. Zero azimuth corresponds to the x-axis. Azimuth ranges from -180 to 180 degree. Elevation in our simulation is defined as the angle about the y-axis with relation to the xy plane. Zero elevation corresponds to the xy plane, 90 degree corresponds to a vector parallel and in the direction of the z axis, -90 degree corresponds to the vector parallel to the z axis and in the negative z direction. We simply translate this reference system to every location for which we do the JDC feasibility study, without rotating the frame.

To calculate the elevation  $\theta$  and azimuth  $\varphi$  we first need to calculate the velocity per superparticle, which is given by Equation (5-47). Azimuth is given by Equation (5-48) and elevation by Equation (5-49).

$$v_i = \sqrt{v_{ix}^2 + v_{iy}^2 + v_{iz}^2} \quad (5-47)$$

$$\theta_i = \arcsin\left(\frac{v_z}{v_i}\right) \quad (5-48)$$

$$\varphi_i = \arctan2(v_y, v_x) \quad (5-49)$$

To obtain the differential flux of the given energy and angular bin we first calculated the particle flux in the bin,  $flux(x, y, z; E, \theta, \varphi)$ .

$$flux(x, y, z; E, \theta, \varphi) = \rho v = \frac{1}{vol} \sum_{i=1}^n w_{si} v_{si} \quad (5-50)$$

Here  $i$  represents each superparticle in the in the specific energy and angular bin. The flux is in the unit of  $cm^{-2}s^{-1}$ . Here  $vol$  is the volume of the spatial grid cell for which the plasma simulation is done. To convert the flux into differential flux  $j(x, y, z; E, \theta, \varphi)$  we divide the flux in each energy and direction bin by the width of the bin in energy ( $\Delta E$  in eV) and the solid angle defined by elevation and azimuth of the bin ( $\Delta\Omega$  in steradian), this is shown in Equation (5-51).

$$j(x, y, z; E, \theta, \varphi) = \frac{flux(x,y,z;E,\theta,\varphi)}{\Delta E \Delta\Omega} \quad (5-51)$$

The solid angle of the bin is calculated using Equation (5-52), in which the index 1 and 2 indicate the lower and upper limit of the bin. In our simulation particles will only be in the XY plane, where the elevation angles  $\theta$  are small. Therefore we simplify Equation (5-52), assuming  $\sin(\theta) = \theta$ , to Equation (5-53). The factor  $\frac{\pi^2}{180}$  is needed for the conversion from degree squared to steradian.

$$\Delta\Omega = (\sin(\theta_2) - \sin(\theta_1))(\varphi_2 - \varphi_1) \frac{\pi^2}{180} \quad (5-52)$$

$$\Delta\Omega \cong (\theta_2 - \theta_1)(\varphi_2 - \varphi_1) \frac{\pi^2}{180} \quad (5-53)$$

### 5.2.1.2 From differential flux to count rate

To convert the simulated differential flux (in  $\# cm^{-2} sr^{-1} s^{-1} eV^{-1}$ ) to counts for the specific instrument bin (direction (elevation/azimuth) and energy), the differential flux is multiplied with the geometric factor  $G$  (in  $cm^2 sr eV/eV$ ), the energy at the middle of the energy bin  $E$ , the time step size  $\Delta t$  and an additional efficiency  $\varepsilon$ . This is shown in Equation (5-54).

$$counts(E, \Omega) = j(E, \Omega) G E \Delta t \varepsilon \quad (5-54)$$

The geometric factor is a factor that combines all the efficiencies (that do not change in time) of the instrument in one factor. The additional efficiency accounts for efficiency that will decrease during the instrument's lifetime.

### 5.3 SIMULATION INPUTS: PHYSICAL PARAMETERS

In this section the different physical model parameters are discussed.

#### 5.3.1 NEUTRAL DENSITY GRID

We consider three neutral plume cases to which the ion particle simulation will be applied, in each of these cases the mass flux is 0.7 kg/s:

- A single plume point source at Europa's south pole (the case discussed in Section 4.4).
- A 1000 kilometre crack consisting of 200 individual independent plume sources located at Europa's south pole (identical to the case discussed in Section 4.5.5).
- A 1000 kilometre crack consisting of 200 individual plume sources located directly under the closest approach of the first JUICE flyby of Europa. All crack plume sources are located at the same latitude. The middle of the crack is directly under the projection of the closest approach on the surface of Europa.

#### 5.3.2 ENVIRONMENT PARAMETERS

In Table 5-1 the physical environment input parameters used for our simulations are shown. The properties of the ion trajectories that result from these parameters are shown in Table 5-2.

**Table 5-1:** Physical input parameters ionized plume particle simulation

Parameter	Value	Source
Ionization rate of H <sub>2</sub> O into H <sub>2</sub> O <sup>+</sup> [cc s <sup>-1</sup> ]	2.3x10 <sup>-8</sup>	Ionization rate at electron energy 20 eV (from Table 4-2)
Electron density [particles/cc]	110	Average value from Table 2-2
Charge of H <sub>2</sub> O <sup>+</sup> [Coulomb]	1.602176565x10 <sup>-19</sup>	1 elementary charge
Magnetic field (B) components [Tesla]	[0, 0, -415x10 <sup>-9</sup> ]	Average value from Table 2-2
Bulk velocity corotational plasma (u) [m/s]	[0,-76x10 <sup>3</sup> ,0]	Average value from Table 2-2
Electric field E [V/m]	[-0.0315,0,0]	Negative of the cross product of u and B

**Table 5-2:** Properties of the ion trajectory resulting from the inputs given in Table 5-1

Parameter	Value
Gyroradius [km]	34.14
Gyrofrequency [cycles/s]	0.35
Gyroperiod [s]	2.82
ExB drift velocity [km/s]	76

### 5.3.3 JDC INSTRUMENT PROPERTIES

The input parameters used for the JDC instrument simulation are shown in Table 5-3.

**Table 5-3:** input parameters JDC simulation

Parameter	Value	Source
G total geometric factor [cm <sup>2</sup> sr eV/eV]	5.58x10 <sup>-4</sup>	[Personal correspondence with Martin Wieser, IRF]
Efficiency $\epsilon$	0.1	[Personal correspondence with Martin Wieser, IRF]
Maximum number of energy bins	96	
Number of azimuth bins	16	[PEP Experiment Interface Document part 2]
Maximum number of elevation bins	16	
Energy range	1 eV to 41 keV	
Azimuth range [deg]	-180 to 180	
Elevation range [deg]	-90 to 90	
Size of the spatial grid cell [km]	10x10x10	
Integration time [s]	1	

It should be noted that the number of azimuth bins is fixed because it is determined by the geometry of the instrument. The number of elevation bins and the elevation range can be altered by changing the instrument settings, these properties depend on the electric field applied at the entrance of the instrument. The number of energy bins also depends on the instrument settings. The numbers of energy and elevation bins we assume are typical for IRF ion mass spectrometers. We also assume an ideal instrument that has a full spherical field of view, because the orientation of the instrument and the spacecraft during the flyby is not fixed yet.

### 5.3.4 JUICE TRAJECTORY

We simulate the JDC observation along the part of the first JUICE flyby that is closest to Europa, as is shown in Figure 2-17. In Figure 5-5 only the geometry of the closest part of the flyby is shown, the corresponding time is also indicated. The spacecraft is coming from approximately the positive y direction and moving in the negative y direction, it is flying in the same direction as the corotational plasma flow.

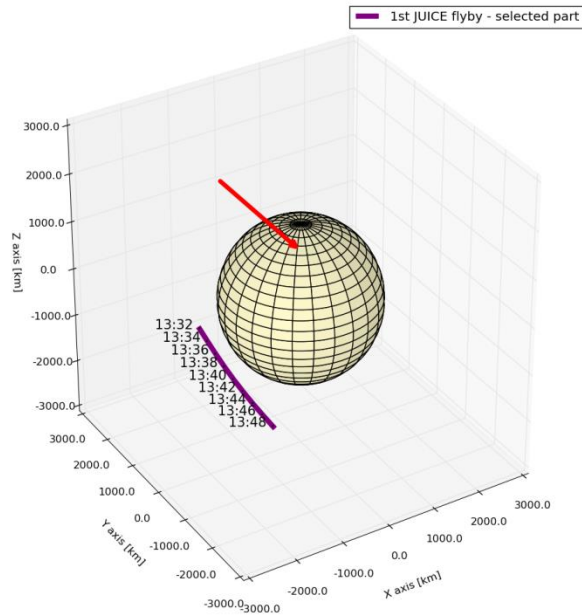


**Figure 5-5:** Part of the first JUICE flyby that is considered in our simulation (purple). The time during the flyby in hours and minutes is shown. The corresponding date is 2031-02-13. Closest approach is at 13:40. The red arrow indicates the direction of the corotational flow.

## 5.4 SIMULATION INPUTS: TECHNICAL

In this section the technical inputs of the model are discussed.

### 5.4.1 TIME STEP SIZE

The size of the time steps for the computation of the particle trajectory should be chosen such that the particle trajectory is accurately represented. Furthermore increasing the number of time steps, will increase the number of particles per grid cell, which will lower the density contribution of each superparticle. Having more particles in each grid cell will improve the quality of the plasma simulation and the statistics in the JDC observation calculation. We choose a time step size of 0.1 seconds for the simulation of the plasma macro parameters (ion density, bulk speed and thermal speed) and 0.02 seconds for the JDC observation simulations.

### 5.4.2 NUMBER OF TIME STEPS

We choose the number of time steps such that all the initial ions have travelled through the simulation box of the neutral density simulations. For the macro property simulation we select 600

time steps and for the instrument simulation 3000 steps. We assume the generation of ions in the plume is in steady state during our simulation (we previously assumed the neutral density grid represents the steady state of the neutral density). After all the particles have travelled through the grid, the system will reach steady state. All particles travel at about 76 km/s on average, as a consequence of the ExB drift. A particle that travels from the furthest edge of the grid to the other edge (~4500 km; see Figure 4-12), will take about 60 seconds. The time step size should be about 0.1 seconds, this leads to a number of time steps of about 600 for large-scale simulations. For the instrument feasibility studies we choose a time step size of 0.02 seconds, 3000 time steps are needed. Furthermore the time step size and number of time steps for the JDC observation simulation are constrained by the realistically available real time computation time (48 hours).

### *5.4.3 GRID CELL SIZE*

For the choice of the grid cell size in the large scale simulation the effect of gyration on the particle motion should be considered. If the size of the grid cell is much larger than the gyroradius, this motion will be averaged out and no effect will be seen in the properties of the ion flow. On the other hand, if the grid cell size is significantly smaller the particles might not pass through each neighbouring grid cell, but skip over some cells and the contribution of the particle to the grid will not be accurately represented.

We choose a grid cell size of 10 by 10 by 10 km. For a gyroradius of approximately 34 km, the top and the cusps of the cycloid is approximately 70 km. This implies at least seven cells exist to represent the ion trajectory in the direction of the cusps. The maximum velocity of the particle will be  $2u$  (with  $u$  the velocity of the corotational flow), so for a timestep of 0.1 seconds the particle will travel 15.2 km. This means it will be present in each neighbouring grid cell for each timestep. In the direction of the ExB drift the particle will travel 76 km/s, and travel approximately 214 km during one gyroperiod. The number of cells along this part of the motion is 21. The distance travelled during one time step is about 7.6 km, so each particle travels through each neighbouring cell without skipping over a cell.

#### 5.4.4 OVERVIEW

Table 5-4 and Table 5-5 summarize the parameters for the large-scale simulation and the JDC observation simulation, respectively.

**Table 5-4:** Technical input parameters for the large scale simulation

<b>Parameter</b>	<b>Value</b>
Time step size [s]	0.1
Number of time steps	600
Ionization rate per time step [ $s^{-1}$ ]	$2.53 \times 10^{-7}$
Grid cell size [km]	10x10x10
Size of the grid [grid cells along x, y and z axis]	200x200x1

**Table 5-5:** Technical input parameters for the JDC observation simulation

<b>Parameter</b>	<b>Value</b>
Time step size [s]	0.02
Number of time steps	3000
Ionization rate per time step [ $s^{-1}$ ]	$5.06 \times 10^{-8}$
Grid cell size [km]	10x10x10

## 5.5 RESULTS

In this section we present the spatial variation of the following macro parameters of the plume plasma: ion density, bulk speed or average energy, thermal speed and average flux. Additionally the JDC instrument observations simulations are also shown.

### 5.5.1 SINGLE PLUME SOURCE AT THE SOUTH POLE

The ion density (Figure 5-6), bulk speed (Figure 5-8), thermal speed (Figure 5-9) and average flux (Figure 5-10) for the situation where a single plume source is located at the south pole of Europa are shown. In Figure 5-11 the simulated count rate per energy and azimuth bin observed by the JDC instrument during the moment of the closest approach during the first JUICE flyby is shown.

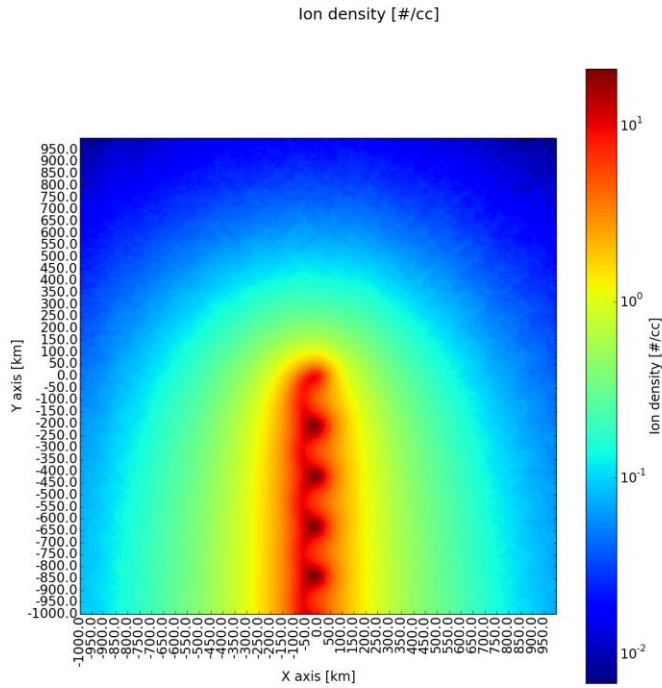


**Figure 5-6:** Ion density in the XY plane, 50 km below Europa's south pole. A single plume source is located at Europa's south pole.

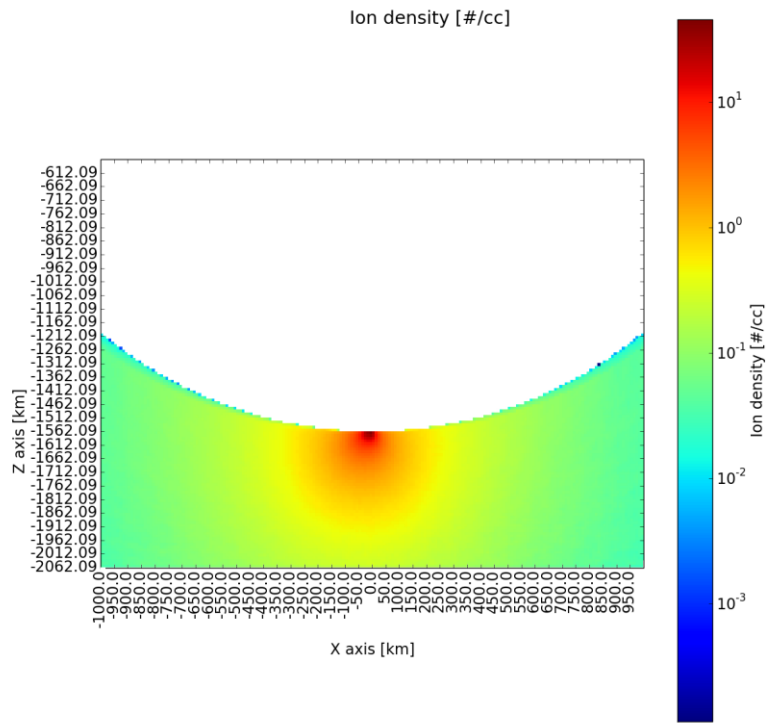


**Figure 5-7:** Ion density in the XZ plane at Y=0. A single plume source is located at Europa's south pole.

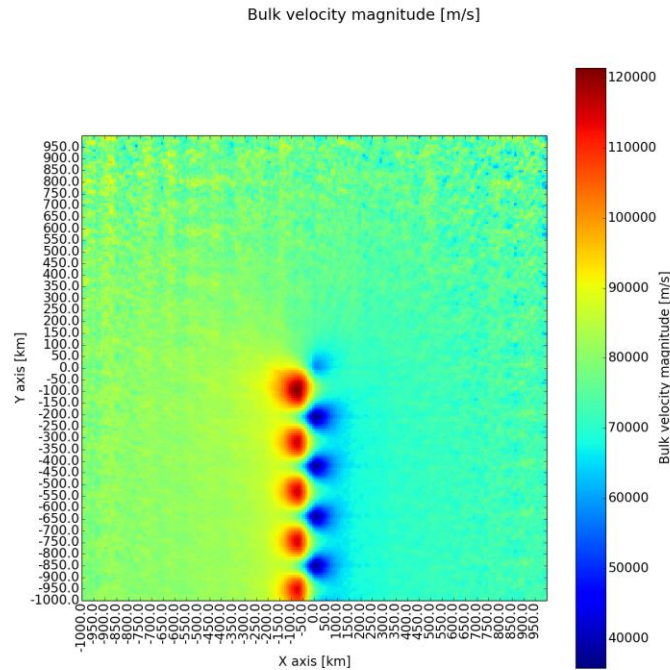


**Figure 5-8:** Bulk speed in the XY plane of grid cells, 50 km below Europa's south pole. A single plume point source is located at Europa's south pole.

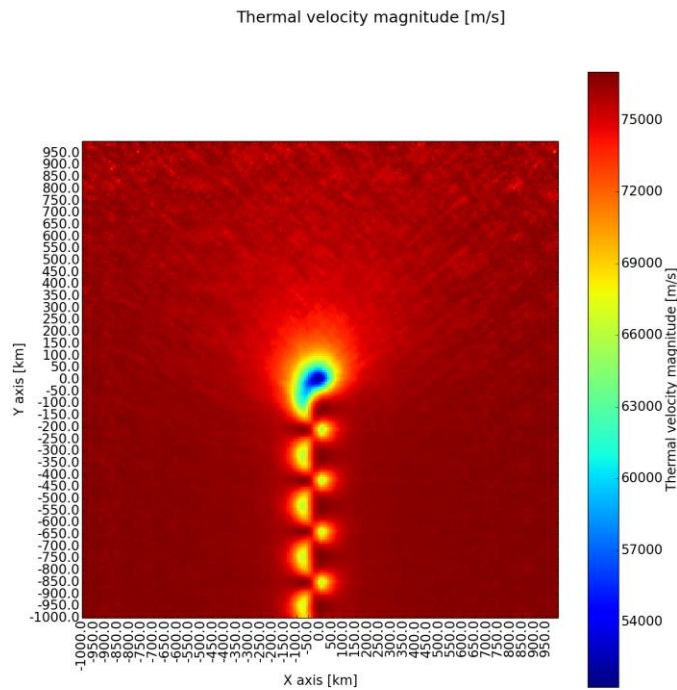


**Figure 5-9:** Thermal speed in the XY plane of grid cells, 50 km below Europa's south pole. A single plume source is located at Europa's south pole.

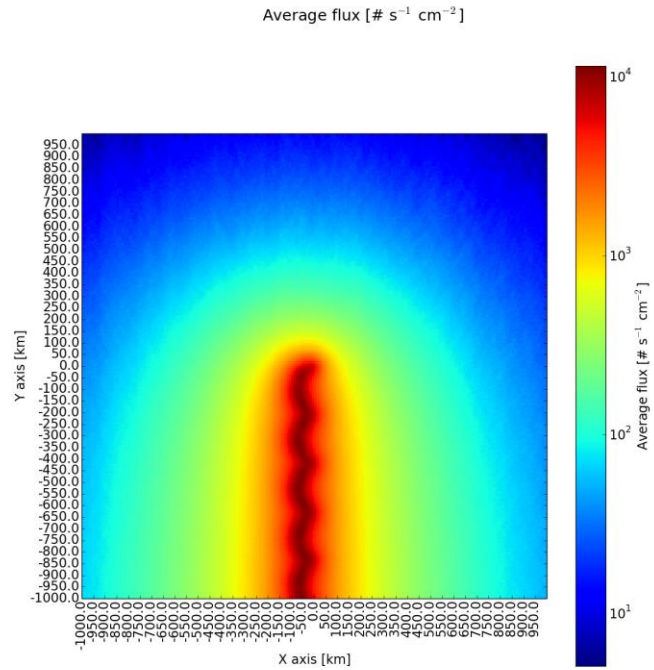


**Figure 5-10:** Average flux in the XY plane of grid cells, 50 km below Europa's south pole. A single plume source is located at Europa's south pole.

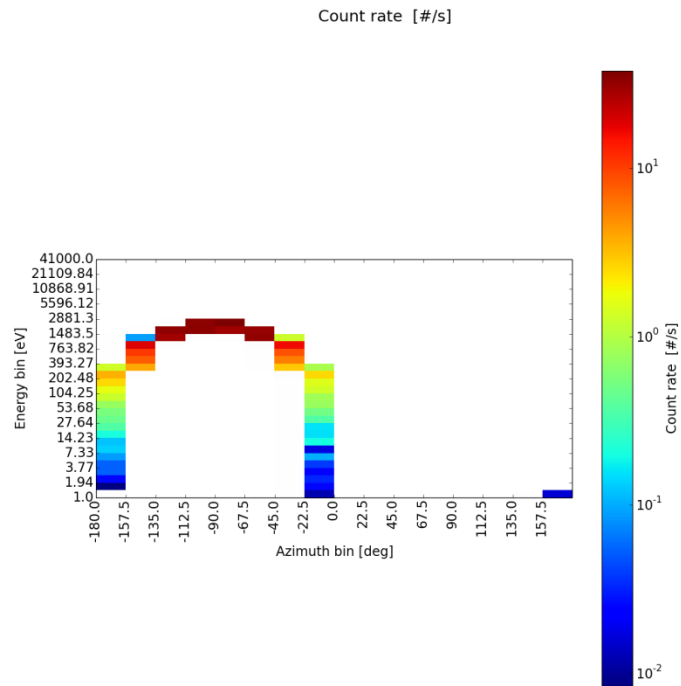


**Figure 5-11:** Count rate per energy and azimuth bin at the closest approach of the first JUICE flyby. The elevation angle of the instrument is zero degree. A plume point source is located at Europa's south pole.

### 5.5.2 A CRACK LOCATED AT EUROPA'S SOUTH POLE

The ion density (Figure 5-6), bulk speed (Figure 5-13), thermal speed (Figure 5-14) and average flux (Figure 5-15) are shown for the situation where a single plume source is located at the south pole of Europa. In Figure 5-16 the simulated count rate per energy and azimuth bin as observed by the JDC instrument during the moment of the closest approach during the first JUICE flyby is shown.

In Figure 5-17 the count rate per energy bin versus the different time steps of the first flyby trajectory are shown. These are the energy bins for the azimuth bin that has -180 degree as a lower limit. Figure 5-18 shows the same but for the bin that has -90 degree azimuth as a lower limit. The geometry of the flyby is shown in Figure 5-5, closest approach is at 13.40.

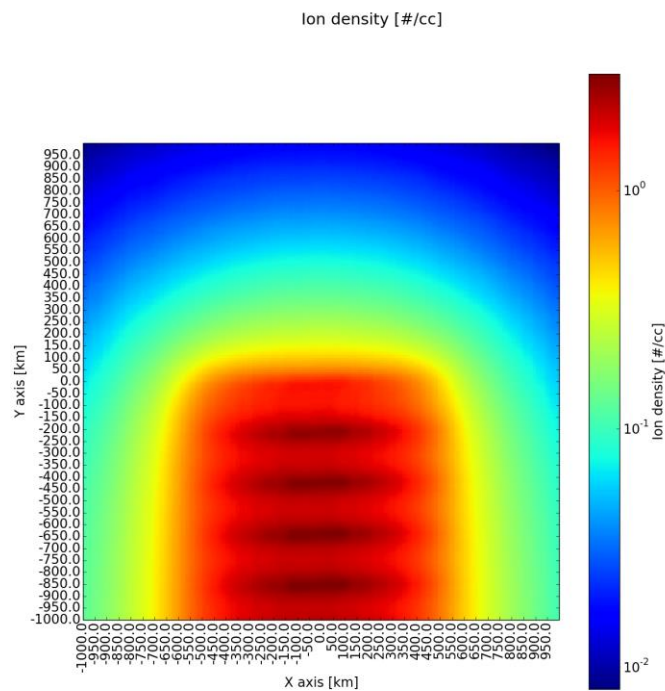


**Figure 5-12:** Ion density in particles per cc, 50 km below Europa's south pole.

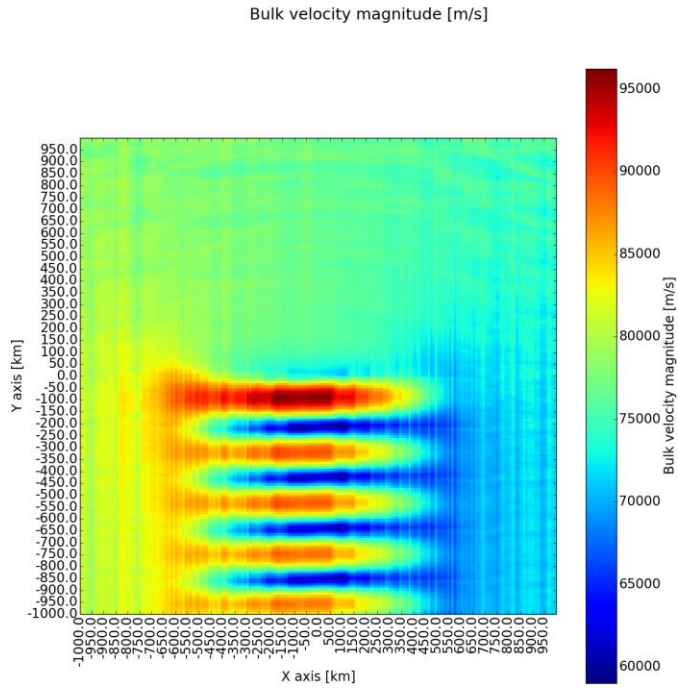


Figure 5-13: Bulk speed in each grid cell, 50 km below Europa's south pole.

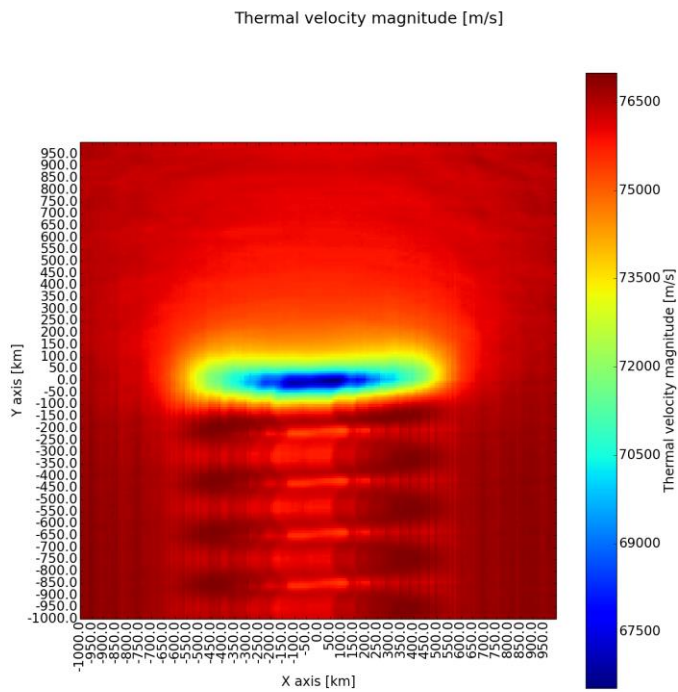
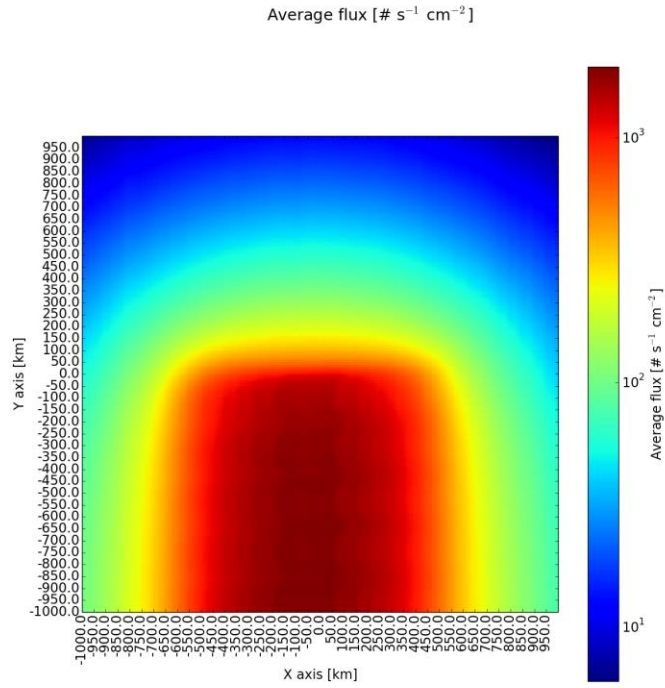
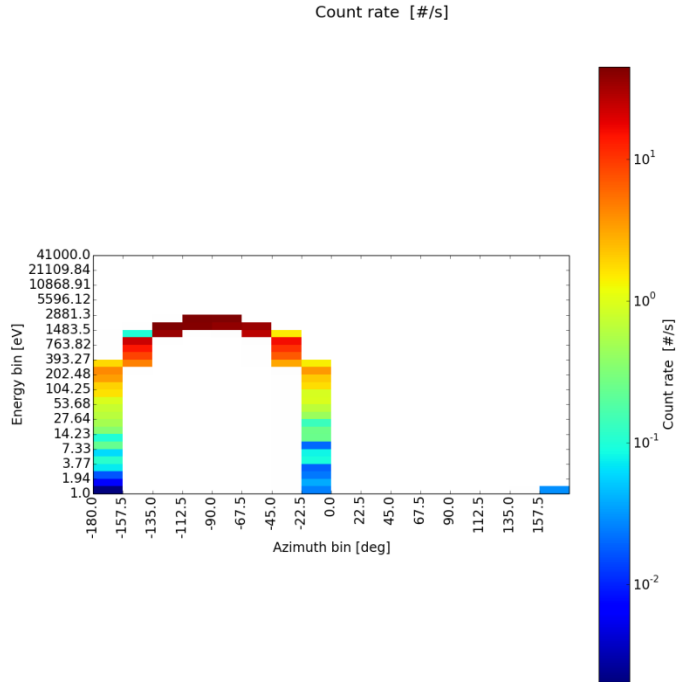


Figure 5-14: Thermal speed in each grid cell, 50 km below Europa's south pole.



**Figure 5-15:** Average flux in each grid cell, 50 km below Europa's south pole.



**Figure 5-16:** Count rate per energy and azimuth bin at the closest approach of the first JUICE flyby. The instrument elevation angle is zero.

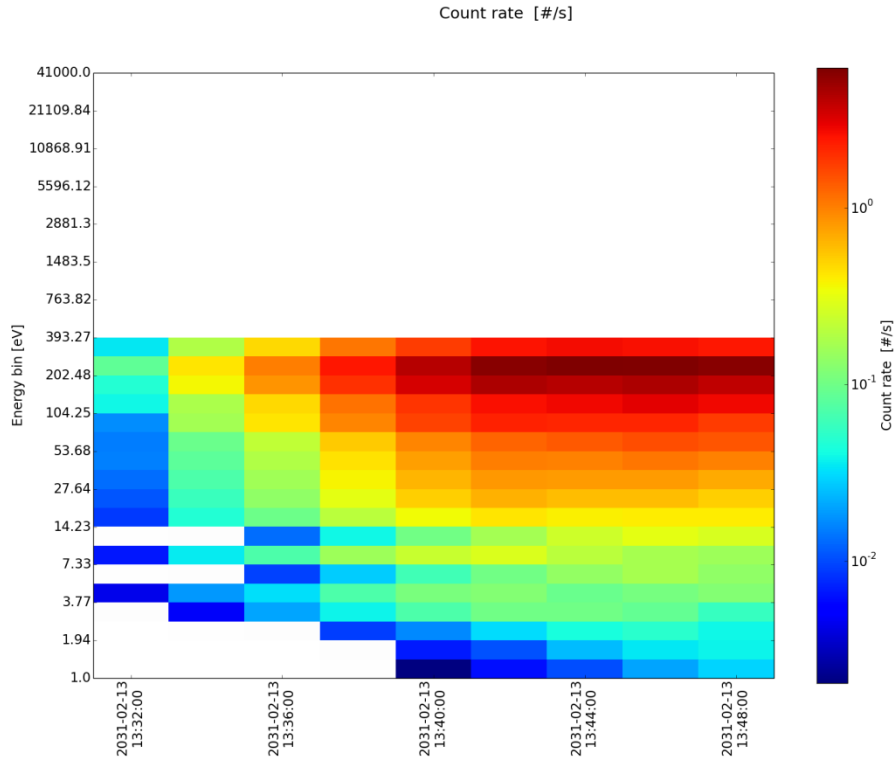


**Figure 5-17:** Count rate per energy bin during the first JUICE flyby of Europa. The elevation angle is zero. The azimuth bin is the bin that has -180 degree azimuth as lower limit. CA is at 13.40.

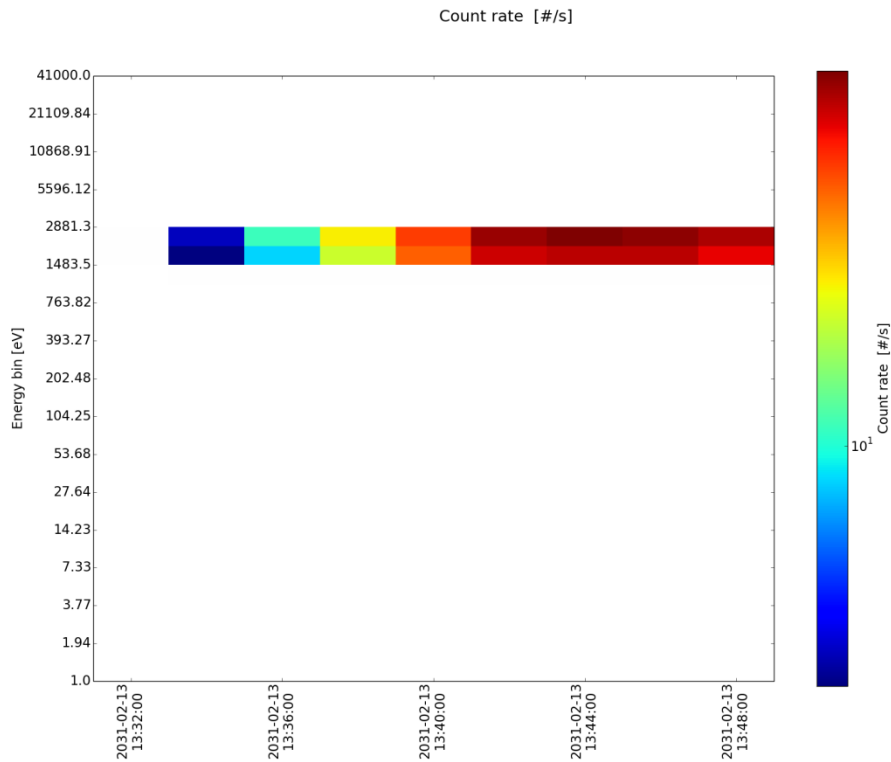


**Figure 5-18:** Count rate per energy bin during the first JUICE flyby of Europa. The elevation angle is zero. The azimuth bin is the bin that has -90 degree azimuth as a lower limit. CA is at 13.40.

### 5.5.3 A CRACK LOCATED BELOW THE CLOSEST APPROACH

In this section the results of the JDC plume observations are shown, for the case when a 1000 km crack is located below the closest approach. The crack coordinates have the same latitude. Figure 5-19 shows the count rate per energy and azimuth bin at the closest approach, for zero elevation. In Figure 5-17 the count rate per energy bin versus the different time steps of the first flyby trajectory are shown. These are the energy bins for the azimuth bin that has -180 degree as a lower limit. Figure 5-21 shows the same but for the bin that has -90 degree azimuth as a lower limit. The geometry of the flyby is shown in Figure 5-5, closest approach is at 13.40.

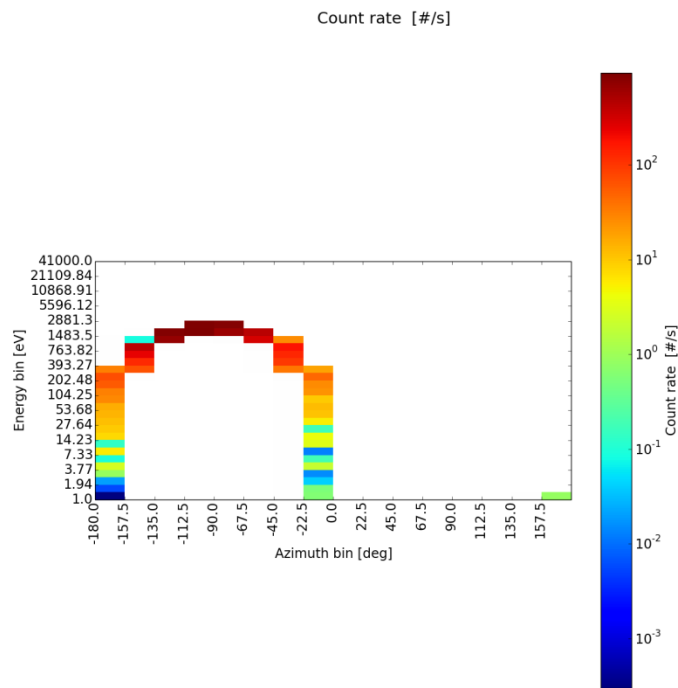


**Figure 5-19:** Count rate per energy and azimuth bin at the closest approach of the first JUICE flyby. The elevation angle is zero. CA is at 13.40.

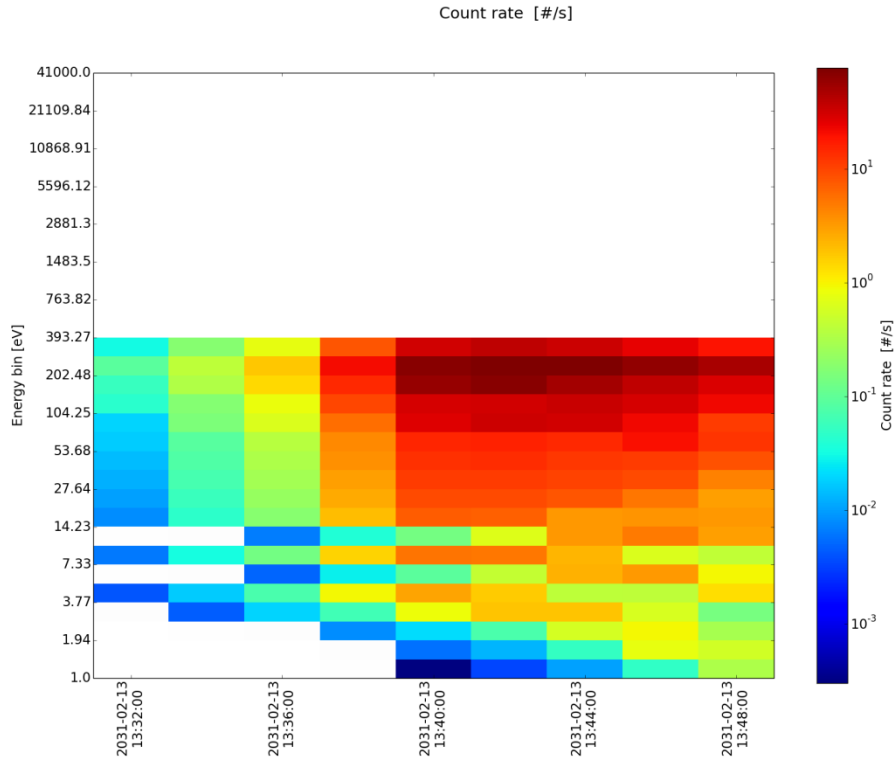


**Figure 5-20:** Count rate per energy bin during the first JUICE flyby of Europa. The elevation angle is zero. The azimuth bin is the bin that has -180 degree azimuth as a lower limit. CA is at 13.40.

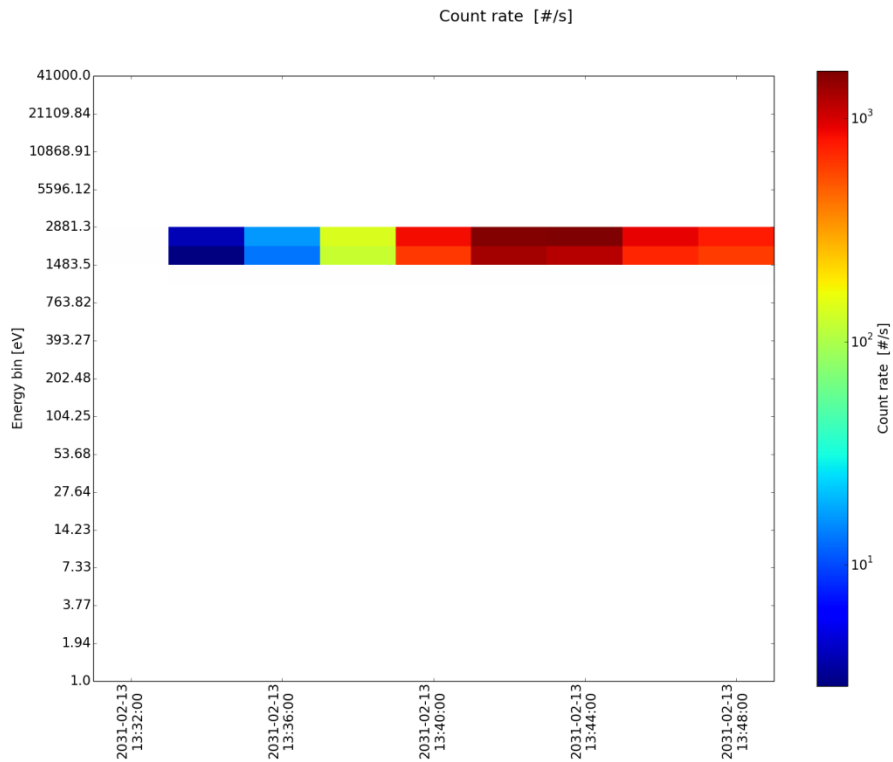


**Figure 5-21:** Count rate during the first JUICE flyby of Europa. The elevation angle is zero. The azimuth bin corresponds to the bin that has -90 degree azimuth as a lower limit. CA is at 13.40.

## 5.6 DISCUSSION

In this section the results of the plasma macro parameters and the JDC plume observation feasibility simulations are discussed.

### 5.6.1 PLUME ION DENSITY VERSUS PLASMA SHEET ION DENSITY

To be able to assume that the motion of the ionized plume particles is determined by ExB drift, the density of the ionized plume particles has to be lower than the ion density in the plasma sheet so that the bulk velocity of the ions approaches that of the background ions (as was discussed in Section 5.1.3.2). The ion plasma density at Europa typically varies between 12 – 170 particles per cc (see Table 2-2). For a single plume source with a mass flux of 0.7 kg/s the peak plume ion density approaches  $10^2$  particles per cc (see Figure 5-7), which is higher or close to the typical ion density at Europa. Therefore we select 0.07 kg/s as the limit of applicability of our model, in the case of a single plume source. For the 1000 km crack case, we consider the limit of applicability a mass flux of 0.7 kg/s. The modelled ion density will approach  $10^1$  for a mass flux of 0.7 kg/s in that case. It should be noted the ion density scales linearly with the plume source density.

### 5.6.2 SINGLE PLUME POINT SOURCE AT THE SOUTH POLE

In this case we recognize the following features in the ion density (Figure 5-6), bulk speed (Figure 5-8) and thermal speed (Figure 5-8) plots:

- The contribution of the densest part of the plume to the macro parameters is significantly larger than the rest of the particles; because of this we recognize the signature of the trajectories of the particles from close to the plume source in the ion density, bulk speed and thermal speed.
- The trajectories of particles from the densest part clearly follow the expected particle motion. The top of the cycloids is two gyroradii away from the cusps (approximately 70 km) along the x-axis. The length of each cycloid along the y-axis (the ExB direction) corresponds to two pi times the gyroradius. We can see this in the density distribution.
- We can see that at the tops of the cycloid motion the density is locally lower: this is because the particles have a higher velocity there and less of them are present at the same time in the corresponding grid cells. The density is higher in the cusps of the cycloids, this is where the particles have a lower velocity and more of them are present at the same time.
- In the bulk speed plot we can also recognize the signature of the densest part of the plume. As expected the velocity is lower at the positions that correspond to the cusps of the motion and higher at the positions that correspond to the tops of the motion.
- In the thermal speed plot we can see that the thermal speed is lowest where the trajectories coming from the densest part of the plume dominate the bulk speed distribution. Outside of the area dominated by plume source particles the thermal speed becomes higher. The lowest thermal speed is observed closest to the plume source, this area is dominated by particles starting the cycloid motion. Close to the cusps particles have a low velocity and so

the spread is smaller than on other locations. Subsequent cusps do not have such a low thermal speed because those grid cells contain both particles approaching the cusp (decelerating) and particles leaving the cusp (accelerating), thus the spread is larger. We also observe the tops of the cycloids in the thermal speed; the spread is smaller there because this area is dominated by particles that have a velocity that is close to two times the drift velocity here.

Figure 5-11 shows the result of a JDC plume observation simulation. The figure shows the simulated differential flux for every azimuth and energy bin at the closest approach of the first JUICE flyby, for the case when a single plume source is located at the south pole of Europa. The figure shows the azimuth versus energy distribution for elevation bin that has 0 degree azimuth as a lower limit. All particles in our simulations move in the plane with 0 degree elevation. In the energy versus azimuth plot we observe the following behaviour:

- We can see all particles are coming from azimuth angles between -180 and 0 degree. The azimuth angle of the particles is the azimuth angle of the velocity vector of those particles. In Figure 5-22 the range of azimuth angles a particle can have is indicated. All particle trajectories are translated copies of this one, the azimuth range will be the same for every particle.
- The count rate is higher for azimuth angles of -90 degree, this corresponds to particles that are at the top of the cycloid and have a larger velocity and thus a higher flux. The flux is lowest for particles that have an azimuth angle of -180 or 0 degrees, where the velocity of the particles is lowest.

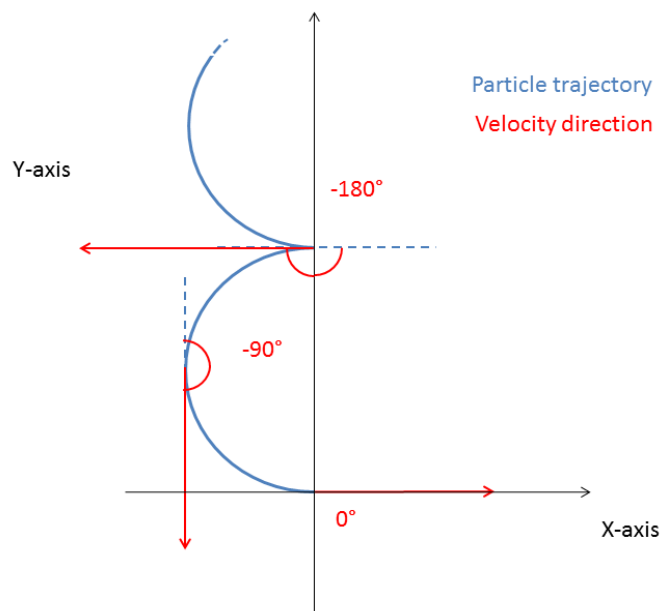


**Figure 5-22:** Range of velocity direction angles (or azimuth angles) of charged particle trajectories

### 5.6.3 A CRACK AT THE SOUTH POLE

In the results of the large scale simulation (ion density, bulk speed, thermal speed) we recognize the combined contribution of different plume point sources. The contribution to the plasma environment of one plume source was discussed in the previous section.

Table 5-6 shows the JDC background count rate at Europa. When we compare the background noise (in counts/s) and the signal of the ionized plume particles in Figure 5-11 (approaching  $10^2$  counts/s) we see that the noise rate is on the same order of magnitude or one order of magnitude larger than the signal. A constant background can be subtracted, but a background typically varies. Assuming the noise is Poisson distributed we take the square root of the noise rate to obtain the standard deviation of the noise. We assume that if the signal strength is larger than the standard deviation of the noise, we can discriminate the signal. For an integration time of 1 second the plume signal corresponds to 100 counts and the average noise to 1250 counts. The standard deviation of the average noise is approximately 35. This means the signal is larger than the varying part of the background, and it should be possible to discriminate the signal. The strength of the signal can be increased by increasing the integration time. The signal will increase linearly (if it is constant over the integration time), while the standard deviation of the noise increases with the power  $\frac{1}{2}$ . This technique can be used to increase the count rate of the looking directions other than the one corresponding to the tops of the cycloid motion.

**Table 5-6:** JDC background count rates at Europa [Private communication with Dr. Martin Wieser, IRF].

JDC background at Europa [counts/s]	500
JDC worst case background at Europa [counts/s]	$2 \times 10^3$

It should be noted that the count rates in Table 5-6 are for the current state of development. The shielding of JDC has not been optimized for Europa yet, improvements might be made in the future. Additionally the real case will be more complex, because the noise signal will be a function of the signal strength. The noise will be higher when the signal is higher.

The peak count rate at the closest approach does not vary significantly between the case where a single plume is located at the south pole (Figure 5-11) and the case where a crack is located at the south pole (Figure 5-16). This is because the density at the position of the closest approach does not change significantly between the two cases. This can be seen by comparing the density at the latitude of -45 degrees (latitude of closest approach) between Figure 4-8 and Figure 4-11. If the mass flux of the plume is set to 0.07 kg/s (one order of magnitude less than what was used to generate the results), the signal has the same order of magnitude as the noise limit (considering the direction with the highest count rate). In such a case the integration time would have to be increased to make detections possible.

In Figure 5-17 and Figure 5-18 the count rate per energy bin for two azimuth directions is shown. We can observe that the count rate increases over time. The closest approach is approximately at 13.40. After the closest approach the count rate keeps increasing. This is because the spacecraft approaches Europa from the positive y direction and continues in the negative y direction. All

plume ions move in the direction of the corotational flow (negative y direction), therefore the density of particles becomes higher after the closest approach

#### 5.6.4 A CRACK BELOW THE CA

For the case when a crack is located below the closest approach the peak count rate increases with one order of magnitude (approaching  $10^3$  counts per second). Here we also recognize that the count rate increases after the closest approach, in the direction of the corotational flow.

#### 5.6.5 COMPARISON WITH BACKGROUND SIGNAL OF WATER IONS

The density of neutral water molecules close to the source crack is  $10^6$ - $10^7$  particles per cc in our model. The atmospheric density of water molecules is up to  $3 \times 10^5$  close to the surface (see Section 4.5.6). The water molecules in the atmosphere will contribute to the plasma environment too. Assuming that the velocities of the neutral atmospheric water molecules are low compared to drift velocity, their trajectories will behave similarly as the particles in our simulation. We expect the two signals can be distinguished because their global distribution is different. Ionized plume particles form a collimated beam of ions (an 'ion plume') while the exospheric particles are more broadly distributed in velocity space. Distinguishing these signals is recommended for future study.

#### 5.6.6 DEPLETION OF ELECTRONS

In our simulation we assumed that the electron density is constant and ionizing electrons are not depleted. This way all parts of the plume are ionized equally. A similar assumption about the electron density was made by *Roth et al.* [2014a] to determine the intensity of the plume aurora as caused by electron impact ionization. If the neutral density is increased there will be a certain point for which the ion density becomes saturated, the ionizing electrons will lose so much energy that they cannot ionize any more neutrals. In such a case there will be a shell around the plume source, in which no ionization is possible because of the lack of electron impact ionization.

To estimate the importance of this effect we calculate the mean free path of electrons with respect to the water molecules. Equation (4-11) gives the mean free path. According to *Itikawa and Mason* [2005] the cross sectional area for electron collisions with water molecules varies from  $0.411 \times 10^{-16}$  to  $1.01 \times 10^{-16}$  for electron temperatures of 20eV and 250 eV respectively. For a neutral density of  $10^8$  particles per cc this would result in a mean free path of 1000 to 2000 km. This is significantly larger than the scale to which the density applies. This means that on average electrons will pass through the densest part of the plume without colliding.

If we scale the peak density ( $10^8$  particles per cc) to the mass flux of 7000 kg/s reported in *Roth et al.* [2014a] we obtain a density of  $10^{12}$  particles per cc. For such a density the mean free path will be only 0.1-0.2 km. The density in our model scales linearly as long as the particles are non-collisional, for a mass flux of 7000 kg/s this is certainly not true. However this approximation does give an indication that for high mass flux plumes, the electron density could decrease inside the plume. If this is true it would suggest that the mass flux estimated by *Roth et al.* [2014a] is in fact a lower

limit since not all neutrals in the denser parts of the plumes have become ionized and contribute to the aurora intensity.

### 5.6.7 LIFETIME OF $H_2O^+$

*Liang et al.* [2005] lists several  $H_2O^+$  recombination rates at Callisto (see Table 5-7). We use these as a first order approximation at Europa. Considering the electron- $H_2O^+$  recombination rates listed in *Liang et al.* [2005] we get a total recombination rate of  $4.26 \times 10^{-7} \text{ cm}^3\text{s}^{-1}$ . By multiplying this value with the average electron density at Europa from Table 2-2 (110 particles per cc) we obtain a rate of  $4.7 \times 10^{-5}$  per second. From this follows that after approximately 6 hours 100% of the  $H_2O^+$  ions will have recombined. The orbital period of the plasma at Europa's orbit is approximately 10 hours (the rotation period of Jupiter's magnetosphere). The plume ions will persist for a significant part of this time. We consider that this is an indication that ionized plume particles could contribute to the formation of a long plasma plume or plasma torus at Europa's orbit (described in Section 2.3.3). The  $H_2O^+$  that is neutralized again could on its turn contribute to the formation of the neutral torus described in 2.1.5.3. We recommend this subject for further investigation.

**Table 5-7:**  $H_2O^+$  electron recombination [*Liang et al.*, 2005].

Reaction	Rate [ $\text{cm}^3\text{s}^{-1}$ ]
$H_2O^+ + e^- \rightarrow O + 2 H$	$2.9 \times 10^{-7}$
$H_2O^+ + e^- \rightarrow O + H_2$	$4.7 \times 10^{-8}$
$H_2O^+ + e^- \rightarrow OH + H$	$8.9 \times 10^{-8}$



## 6 CONCLUSIONS AND RECOMMENDATIONS

### 6.1 NEUTRAL PLUME PARTICLE SIMULATION

We modelled the trajectories of neutral water particles from the plume and derived the density profile. We assumed a thermal velocity of the plume source of 460 m/s, based on observations reported in *Roth et al.* [2014]. The bulk velocity was set to the same value. Our model is applicable to the non-collisional regime. This corresponds to the total mass flux of the plume of 0.7 kg/s in the case of a single plume point source and 7 kg/s for a 1000 km crack.

The density profile derived from the model was used to simulate observations with the NIM sensor during the first JUICE flyby of Europa. The simulations show that plumes with a mass flux of 0.7 kg/s (both a single point source and 1000 km crack) are observable with NIM from the JUICE trajectory. The mass flux can be lowered several orders of magnitude before the density approaches the observational limit (to  $7 \times 10^{-5}$  kg/s in the case of a plume point source below the closest approach or  $7 \times 10^{-4}$  kg/s for a 1000 km crack below the closest approach). We have shown for which positions on Europa's surface the plume can be observed. If the plume is located more than 40 degree away from the projection of the closest approach on the surface, detection is still possible, above the noise level of NIM. Our results also indicate that because of the gravity lens effect, an intensification of plume particle density is to be expected on the opposite side of Europa than the plume is. This offers an interesting opportunity to observe plumes that are on the opposite side of Europa than the flyby. We also compared the density profile of the plume to an existing 1D exospheric model, the plume particle density and the sputtered water density are comparable at 400 km altitude (for a single plume point source with 0.7 kg/s mass flux).

### 6.2 Ionized plume particle simulation

We modelled the ExB drift trajectories of  $\text{H}_2\text{O}^+$  ions from the neutral plume we modelled. Our model is applicable for ion densities that are lower than the corotational plasma density. This corresponds to the total mass flux of the plume of 0.07 kg/s for the single plume point source and 0.7 kg/s for the 1000 km crack.

From the ionized particle trajectories the differential flux was determined. This differential flux was used to simulate the JDC plume particle observations. We have shown that observations of the plume with JDC are possible. We compared the case of a 1000 km crack located at the south pole and a 1000 km crack below the closest approach of JUICE. The corresponding total mass flux can be as low as 0.7 kg/s for the crack at the south pole and 0.07 kg/s for the crack below the CA (for 1 second integration time).

In our simulation ionized particles move purely because of the ExB drift caused by the convective electric field. This assumption only makes sense when the density of the plume plasma is lower than the density of the corotational plasma.

### 6.3 RECOMMENDATIONS FOR FUTURE WORK

Regarding the future modelling of the dynamics of neutral plume particles, we make the following recommendations:

- We have argued that to model plumes with a higher mass flux, in particular the flux reported in *Roth et al.* [2014a], particle collisions cannot be ignored (see Section 4.5.2). More complex and computationally demanding models are unavoidable.
- We have considered the case of a single plume point source and a single active crack that are active continuously. *Roth et al.* [2014a] suggests the plume originates from an active area with multiple cracks. Therefore we recommend expanding to the simulation of an active area of multiple cracks, possibly taking temporal variability into account.

To model plumes with a mass flux that is similar to what is reported in *Roth et al.* [2014a], we recommend the following:

- The influence of the plume ions on the electric fields needs to be considered (see Section 5.6.1).
- The depletion of ionizing electrons will have to be taken into account (see Section 5.6.6).
- The effect of Europa's induced magnetic field should be included (see Section 5.1.3.3).

Regarding the future modelling of PEP observations of the plumes, we recommend the following:

- The signal of the neutral plume particles should be compared with the exospheric water population produced by sputtering (see Section 4.5.6).
- The signal of ionized plume particles should be compared with the ionized population of exospheric water, originally produced by sputtering (see Section 5.6.5).

Furthermore we recognize that Europa's water vapour plumes might contribute to creation of Europa's plasma and neutral tori (see Section 5.6.7). This is a topic for further investigation.

## BIBLIOGRAPHY

- M. H. Acuna, K. Behannon, and J. E. P. Connerney. In: *Physics of the Jovian Magnetosphere*. Ed. by A. J. Dessler. Cambridge University Press, 1983. Chap. Jupiter's magnetic field and magnetosphere.
- C. Alexander, R. Carlson, G. Consolmagno, G. R., and D. Morrison. In: *Europa*. Ed. by R. T. Pappalardo, W. B. McKinnon, and K. Khurana. University of Arizona Press, 2009. Chap. The Exploration History of Europa, pp. 3–26.
- J. D. Anderson, G. Schubert, R. A. Jacobson, E. L. Lau, W. B. Moore, and W. L. Sjogren. "Europa's Differentiated Internal Structure: Inferences from Four Galileo Encounters". In: *Science* 281 (Sept. 1998), pp. 2019–2022.
- J. Anderson, E. L. Lau, G. Sjogren W. L. and Schubert, and W. B. Moore. "Europa's Differentiated Internal Structure: Inferences from Two Galileo Encounters". In: *Science* 276 (May 1997), pp. 1236–1239.
- B. A. Archinal et al. "Report of the IAU Working Group on Cartographic Coordinates and Rotational Elements: 2009". In: *Celest Mech Dyn Astr* 109.2 (2010), pp. 101–135. issn: 1572-9478. doi:10.1007/s10569-010-9320-4.
- F. Bagenal et al. "Magnetospheric Science Objectives of the Juno Mission". In: *Space Science Reviews* (Feb. 2014). issn: 1572-9672. doi: 10.1007/s11214-014-0036-8.
- F. Bagenal. "Empirical model of the Io plasma torus: Voyager measurements". In: *Journal of Geophysical Research: Space Physics* 99.A6 (1994), pp. 11043–11062. issn: 2156-2202. doi: 10.1029/93JA02908.
- F. Bagenal and J. D. Sullivan. "Direct plasma measurements in the Io torus and inner magnetosphere of Jupiter". In: *Journal of Geophysical Research: Space Physics* 86.A10 (1981), pp. 8447–8466. issn: 2156-2202. doi: 10.1029/JA086iA10p08447.
- E. Bierhaus, K. Zahnle, and C. Chapman. In: *Europa*. Ed. by R. T. Pappalardo, W. B. McKinnon, and K. Khurana. University of Arizona Press, 2009. Chap. Europa's Crater Distributions and Surface Ages, pp. 161–180.
- P. C. Brandt. In: *Sensors and Instruments for Space Exploration*. Ed. by S. H. Hymork and I. Sandahl. 3rd ed. Swedish Institute of Space Physics, 2002. Chap. Particle measurements in space plasmas.
- A. L. Broadfoot, B. R. Sandel, D. E. Shemansky, J. C. McConnell, G. R. Smith, J. B. Holberg, S. K. Atreya, T. M. Donahue, D. F. Strobel, and J. L. Bertaux. "Overview of the Voyager ultraviolet spectrometry results through Jupiter encounter". In: *Journal of Geophysical Research: Space Physics* 86.A10 (1981), pp. 8259–8284. issn: 2156-2202. doi: 10.1029/JA086iA10p08259.
- M. E. Brown. "Potassium in Europa's Atmosphere". In: *Icarus* 151.2 (2001), pp. 190–195. issn:0019-1035. doi: 10.1006/icar.2001.6612.
- D. Burgess. "Introduction to space physics". In: ed. by M. G. Kivelson and C. T. Russell. Cambridge University Press, 1995. Chap. Collisionless shocks.

- R. Carlson, W. Calvin, J. Dalton, G. Hansen, R. Hudson, R. Johnson, T. MMcCord, and M. Moore. In: Europa. Ed. by R. T. Pappalardo, W. B. McKinnon, and K. Khurana. University of Arizona Press, 2009. Chap. Europa's Surface Composition, pp. 283–328.
- F. J. Crary, F. Bagenal, L. A. Frank, and W. R. Paterson. "Galileo plasma spectrometer measurements of composition and temperature in the Io plasma torus". In: Journal of Geophysical Research: Space Physics 103.A12 (1998), pp. 29359–29370. issn: 2156-2202. doi: 10.1029/1998JA900003.
- T. E. Cravens. Physics of Solar System Plasmas. Cambridge University Press. doi: 10.1017/CBO9780511529467.
- P. A. Delamere and F. Bagenal. "Solar wind interaction with Jupiter's magnetosphere". In: Journal of Geophysical Research 115.A10 (2010). issn: 0148-0227. doi: 10.1029/2010ja015347.
- T Doggett, R. Greeley, P. H. Figueredo, and K. Tanaka. In: Europa. Ed. by R. T. Pappalardo, W.B. McKinnon, and K. Khurana. University of Arizona Press, 2009. Chap. Geologic Stratigraphy and Evolution of Europa's Surface, pp. 137–160.
- Y. Dong, T. W. Hill, B. D. Teolis, B. A. Magee, and J. H. Waite. "The water vapor plumes of Enceladus". In: Journal of Geophysical Research 116.A10 (2011). issn: 0148-0227. doi: 10.1029/2011ja016693.
- U. Eklund. In: Sensors and Instruments for Space Exploration. Ed. by S. H. Hymork and I. Sandahl. 3rd ed. Swedish Institute of Space Physics, 2002. Chap. Particle and photon detectors.
- S. A. Fagents, R. Greeley, R. J. Sullivan, R. T. Pappalardo, L. M. Prockter, and T. G. S. Team. "Cryomagmatic Mechanisms for the Formation of Rhadamanthys Linea, Triple Band Margins, and Other Low-Albedo Features on Europa". In: Icarus 144.1 (2000), pp. 54 –88. issn: 0019-1035. url:10.1006/icar.1999.6254.
- F. P. Fanale et al. "Tyre and Pwyll: Galileo orbital remote sensing of mineralogy versus morphology at two selected sites on Europa". In: Journal of Geophysical Research: Planets 105.E9 (2000), pp. 22647–22655. issn: 2156-2202. doi: 10.1029/1999JE001102.
- S. Fatemi. "Computing, visualizing and analyzing ion trajectories". MA thesis. Lulea University of Technology, 2009. url: <http://epubl.ltu.se/1653-0187/2009/043/LTU-PB-EX-09043-SE.pdf>.
- L. A. Frank and W. R. Paterson. "Return to Io by the Galileo spacecraft: Plasma observations". In: Journal of Geophysical Research: Space Physics 105.A11 (2000), pp. 25363–25378. issn: 2156-2202. doi: 10.1029/1999JA000460.
- L. A. Frank and W. R. Paterson. "Survey of thermal ions in the Io plasma torus with the Galileo spacecraft". In: Journal of Geophysical Research: Space Physics 106.A4 (2001), pp. 6131–6149. issn: 2156-2202. doi: 10.1029/2000JA000159.
- Y. Futaana, S. Barabash, M. Holmstrom, A. Fedorov, H. Nilsson, R. Lundin, E. Dubinin, and M. Franz. "Backscattered solar wind protons by Phobos". In: Journal of Geophysical Research 115.A10 (2010). issn: 0148-0227. doi: 10.1029/2010ja015486.
- O. Grasset et al. "JUper ICy moons Explorer (JUICE): An ESA mission to orbit Ganymede and to characterise the Jupiter system". In: Planetary and Space Science 78 (Apr. 2013), pp. 1–21. issn: 0032-0633. doi: 10.1016/j.pss.2012.12.002.

- R. Greeley and C. R. Chyba. In: *Jupiter: the planet, satellites and magnetosphere*. Ed. by F. Bagenal, T. E. Dowling, and W. McKinnon. Cambridge University Press, 2004. Chap. Geology of Europa.
- D. A. Gurnett, W. S. Kurth, A. Roux, S. J. Bolton, E. A. Thomsen, and J. B. Groene. "Galileo plasma wave observations near Europa". In: *Geophysical Research Letters* 25.3 (1998), pp. 237–240. issn: 1944-8007. doi: 10.1029/97GL03706.
- D. Gurnett, W. Kurth, R. Shaw, A. Roux, R. Gendrin, C. Kennel, F. Scarf, and S. Shawhan. "The Galileo Plasma wave investigation". English. In: *Space Science Reviews* 60.1-4 (1992), pp. 341–355. issn: 0038-6308. doi: 10.1007/BF00216861.
- K. Hand, C. Chyba, J. Priscu, R. Carlson, and K. Neelson. In: *Europa*. Ed. by R. T. Pappalardo, W. B. McKinnon, and K. Khurana. University of Arizona Press, 2009. Chap. Astrobiology and the Potential for Life on Europa, pp. 589–630.
- C. J. Hansen. "Enceladus' Water Vapor Plume". In: *Science* 311.5766 (Mar. 2006), pp. 1422–1425. issn: 1095-9203. doi: 10.1126/science.1121254.
- A. Hendrix, C. Barth, C. Hord, and A. Lane. "Europa: Disk-Resolved Ultraviolet Measurements Using the Galileo Ultraviolet Spectrometer". In: *Icarus* 135.1 (1998), pp. 79–94. issn: 0019-1035. doi: 10.1006/icar.1998.5983.
- T. Hill, A. Dessler, and C. Goertz. In: *Physics of the Jovian Magnetosphere*. Ed. by A. J. Dessler. Cambridge University Press, 1983. Chap. Magnetospheric models.
- G. Hoppa, R. Greenberg, B. Tufts, and P. Geissler. "Plume detection on Europa: locations of favorable tidal stress." In: *Lunar and Planetary Science XXX*. 1999. url: <http://www.lpi.usra.edu/meetings/LPSC99/pdf/1603.pdf>.
- T. A. Hurford, P. Helfenstein, G. V. Hoppa, R. Greenberg, and B. G. Bills. "Eruptions arising from tidally controlled periodic openings of rifts on Enceladus". In: *Nature* 447.7142 (May 2007), pp. 292–294. issn: 1476-4687. doi: 10.1038/nature05821.
- Y. Itikawa and N. Mason. "Cross Sections for Electron Collisions with Water Molecules". In: *Journal of Physical and Chemical Reference Data* 34.1 (2005), p. 1. issn: 0047-2689. doi: 10.1063/1.1799251.
- H. M. Jara-Orue and B. L. Vermeersen. "Effects of low-viscous layers and a non-zero obliquity on surface stresses induced by diurnal tides and non-synchronous rotation: The case of Europa". In: *Icarus* 215.1 (Sept. 2011), pp. 417–438. issn: 0019-1035. doi: 10.1016/j.icarus.2011.05.034.
- R. Johnson, M. Burger, T. Cassidy, F. Leblanc, M. Marconi, and W. H. Smyth. In: *Europa*. Ed. by R. T. Pappalardo, W. B. McKinnon, and K. Khurana. University of Arizona Press, 2009. Chap. Composition and Detection of Europa's Sputter-induced Atmosphere, pp. 507–528.
- R. E. Johnson. "Sodium at Europa". In: *Icarus* 143.2 (2000), pp. 429–433. issn: 0019-1035. doi:10.1006/icar.1999.6327.
- J. S. Kargel, J. Z. Kaye, J. W. H. III, G. M. Marion, R. Sassen, J. K. Crowley, O. P. Ballesteros, S. A. Grant, and D. L. Hogenboom. "Europa's Crust and Ocean: Origin, Composition, and the Prospects for Life". In: *Icarus* 148.1 (2000), pp. 226–265. issn: 0019-1035. doi: 10.1006/icar.2000.6471.

- S. A. Kattenhorn and L. M. Prockter. "Evidence for subduction in the ice shell of Europa". In: *Nature Geoscience* (Sept. 2014). issn: 1752-0908. doi: 10.1038/ngeo2245.
- K. Khurana, M. Kivelson, D. Stevenson, G. Schubert, C. Russell, R. J. Walker, and C. Polanskey. "Induced magnetic fields as evidence for subsurface oceans in Europa and Callisto". In: *Nature* 395 (1998), pp. 777–780. doi: 10.1038/27394.
- K. Khurana, M. Kivelson, V. Vasyliunas, N. Krupp, J. Woch, A. Lagg, B. H. Mauk, and W. Kurth. In: *Jupiter: the planet, satellites and magnetosphere*. Ed. by F. Bagenal, T. E. Dowling, and W. McKinnon. Cambridge University Press, 2004. Chap. The Configuration of Jupiter's Magnetosphere.
- K. K. Khurana. "Euler potential models of Jupiter's magnetospheric field". In: *Journal of Geophysical Research: Space Physics* 102.A6 (1997), pp. 11295–11306. issn: 2156-2202. doi: 10.1029/97JA00563.
- M. G. Kivelson, K. K. Khurana, D. J. Stevenson, L. Bennett, S. Joy, C. T. Russell, R. J. Walker, C. Zimmer, and C. Polanskey. "Europa and Callisto: Induced or intrinsic fields in a periodically varying plasma environment". In: *Journal of Geophysical Research: Space Physics* 104.A3 (1999), pp. 4609–4625. issn: 2156-2202. doi: 10.1029/1998JA900095.
- M. Kivelson. In: *Magnetospheric Current Systems*. Ed. by S.-i. Ohtani, F. Ryoichi, M. Hesse, and R. L. Lysak. Vol. 118. American Geophysical Union, 2000. Chap. Currents and Flows in Distant Magnetospheres.
- M. Kivelson. "Introduction to space physics". In: ed. by M. G. Kivelson and C. T. Russell. Cambridge University Press, 1995. Chap. Physics of space plasmas. M. Kivelson, K. Khurana, and M. Volwerk. In: *Europa*. Ed. by R. T. Pappalardo, W. B. McKinnon, and K. Khurana. University of Arizona Press, 2009. Chap. Europa's Interaction with the Jovian Magnetosphere, pp. 545–570.
- A. J. Kliore, D. P. Hinson, F. M. Flasar, A. F. Nagy, and T. E. Cravens. "The Ionosphere of Europa from Galileo Radio Occultations". In: *Science* 277.5324 (1997), pp. 355–358. doi: 10.1126/science.277.5324.355
- N. Krupp, A. Lagg, S. Livi, B. Wilken, J. Woch, E. C. Roelof, and D. J. Williams. "Global flows of energetic ions in Jupiter's equatorial plane: First-order approximation". In: *Journal of Geophysical Research: Space Physics* 106.A11 (2001), pp. 26017–26032. issn: 2156-2202. doi: 10.1029/2000JA900138.
- W. Kurth, D. Gurnett, A. Persoon, A. Roux, S. Bolton, and C. Alexander. "The plasma wave environment of Europa". In: *Planetary and Space Science* 49.3?4 (2001). Magnetospheres of the Outer Planets (Part I), pp. 345 –363. issn: 0032-0633. doi: [http://dx.doi.org/10.1016/S00320633\(00\)00156-2](http://dx.doi.org/10.1016/S00320633(00)00156-2).
- A. Lagg. "In-situ observations of a neutral gas torus at Europa". In: *Geophys. Res. Lett.* 30.11 (2003). issn: 0094-8276. doi: 10.1029/2003gl017214.
- S. Ledvina, Y.-J. Ma, and E. Kallio. "Modeling and Simulating Flowing Plasmas and Related Phenomena". English. In: *Comparative Aeronomy*. Ed. by A. Nagy, A. Balogh, T. Cravens, M. Mendillo, and I. Mueller-Wodarg. Vol. 29. Space Sciences Series of ISSI. Springer New York, 2008, pp. 143–189. isbn: 978-0-387-87824-9. doi: 10.1007/978-0-387-87825-6\_5.

- M.-C. Liang, B. F. Lane, R. Pappalardo, M. Allen, and Y. L. Yung. "Atmosphere of Callisto". In: *Journal of Geophysical Research* 110 (2005). doi: 10.1029/2004JE002322.
- J. Luhmann. "Introduction to space physics". In: ed. by M. G. Kivelson and C. T. Russell. Cambridge University Press, 1995. Chap. Ionospheres.
- J. Marti and K. Mauersberger. "A survey and New Measurements of Ice Vapor Pressure At Temperatures Between 170 and 250 K". In: *Geophys. Res. Lett.* 20.5 (Mar. 1993), pp. 363–366.
- B. H. Mauk, D. G. Mitchell, S. M. Krimigis, E. C. Roelof, and C. P. Paranicas. "Energetic neutral atoms from a trans-Europa gas torus at Jupiter". In: *Nature* 421 (2003), pp. 920–922. doi: 10.1038/nature01431.
- B. H. Mauk, D. G. Mitchell, R. W. McEntire, C. P. Paranicas, E. C. Roelof, D. J. Williams, S.M. Krimigis, and A. Lagg. "Energetic ion characteristics and neutral gas interactions in Jupiter's magnetosphere". In: *Journal of Geophysical Research: Space Physics* 109.A9 (2004). issn: 2156-2202. doi: 10.1029/2003JA010270.
- T. B. McCord et al. "Hydrated salt minerals on Europa's Surface from the Galileo near-infrared mapping spectrometer (NIMS) investigation". In: *Journal of Geophysical Research* 104 (May 1999), pp. 11827–11851.
- T. B. McCord et al. "Salts on Europa's Surface Detected by Galileo's Near Infrared Mapping Spectrometer". In: *Science* 280 (May 1998), pp. 1242–1245.
- T. B. McCord, G. B. Hansen, J.-P. Combe, and P. Hayne. "Hydrated minerals on Europa's surface: An improved look from the Galileo NIMS investigation". In: *Icarus* 209.2 (Oct. 2010), pp. 639–650. issn: 0019-1035. doi: 10.1016/j.icarus.2010.05.026.
- M. A. McGrath, C. J. Hansen, and A. Hendrix. In: *Europa*. Ed. by R. T. Pappalardo, W. B. McKinnon, and K. Khurana. University of Arizona Press, 2009. Chap. Observations of Europa's Tenuous Atmosphere, pp. 485–506.
- D. Morrison and J. Samz. *Voyage to Jupiter*. National Aeronautics and Space Administration, 1980.
- F. M. Neubauer. "Alfvén wings and electromagnetic induction in the interiors: Europa and Callisto". In: *Journal of Geophysical Research: Space Physics* 104.A12 (1999), pp. 28671–28684. issn: 2156-2202. doi: 10.1029/1999JA900217.
- F. Nimmo, R. Pappalardo, and J. Cuzzi. "Observational and Theoretical Constraints on Plume Activity at Europa". In: *AGU fall meeting*. 2007.
- G. W. Ojakangas and D. J. Stevenson. "Thermal state of an ice shell on Europa". In: *Icarus* 81.2 (1989), pp. 220–241. issn: 0019-1035. doi: 10.1016/0019-1035(89)90052-3.
- C. Paranicas, R. W. McEntire, A. F. Cheng, A. Lagg, and D. J. Williams. "Energetic charged particles near Europa". In: *Journal of Geophysical Research: Space Physics* 105.A7 (2000), pp. 16005–16015. issn: 2156-2202. doi: 10.1029/1999JA000350.
- C. Paranicas, J. M. Ratliff, B. H. Mauk, C. Cohen, and R. E. Johnson. "The ion environment near Europa and its role in surface energetics". In: *Geophysical Research Letters* 29.5 (2002), pp. 18–1–18–4. issn: 1944-8007. doi: 10.1029/2001GL014127.

- W. R. Paterson, L. A. Frank, and K. L. Ackerson. "Galileo plasma observations at Europa: Ion energy spectra and moments". In: *Journal of Geophysical Research: Space Physics* 104.A10 (1999), pp. 22779–22791. issn: 2156-2202. doi: 10.1029/1999JA900191.
- PEP Experiment Interface Document part 2. Tech. rep. Swedish Institute of Space Physics, 2012.
- PEP Instrument Engineering Plan. Tech. rep. Swedish Institute of Space Physics, 2012.
- PEP Scientific and Technical Plan. Tech. rep. Swedish Institute of Space Physics, 2012.
- L. C. Quick, O. S. Barnouin, L. M. Prockter, and G. W. Patterson. "Constraints on the detection of cryovolcanic plumes on Europa". In: *Planetary and Space Science* (2013). doi: doi:10.1016/j.pss.2013.06.028.
- A. R. Rhoden, T. A. Hurford, L. Roth, and K. Retherford. "Linking Europa's plume activity to tides, tectonics, and liquid water". In: *Icarus* 253 (2015), pp. 169–178. issn: 0019-1035. doi:10.1016/j.icarus.2015.02.023.
- L. Roth, K. D. Retherford, J. Saur, D. F. Strobel, P. D. Feldman, M. A. McGrath, and F. Nimmo. "Orbital apocenter is not a sufficient condition for HST/STIS detection of Europas water vapour aurora". In: *Proceedings of the National Academy of Sciences* (Nov. 2014), p. 201416671. issn:1091-6490. doi: 10.1073/pnas.1416671111.
- L. Roth, J. Saur, K. D. Retherford, D. F. Strobel, P. D. Feldman, M. A. McGrath, and F. Nimmo. "Transient Water Vapor at Europa's South Pole". In: *Science* 343.6167 (Jan. 2014), pp. 171–174.
- J. Saur, D. F. Strobel, and F. M. Neubauer. "Interaction of the Jovian magnetosphere with Europa: Constraints on the neutral atmosphere". In: *Journal of Geophysical Research: Planets* 103.E9 (1998), pp. 19947–19962. issn: 2156-2202. doi: 10.1029/97JE03556.
- N. Schilling, F. M. Neubauer, and J. Saur. "Influence of the internally induced magnetic field on the plasma interaction of Europa". In: *Journal of Geophysical Research* 113.A3 (2008). issn: 0148-0227. doi: 10.1029/2007ja012842.
- G. Schubert, J. Anderson, S. T., and W. B. McKinnon. In: *Jupiter: the planet, satellites and magnetosphere*. Ed. by F. Bagenal, T. E. Dowling, and W. McKinnon. Cambridge University Press, 2004. Chap. Interior Composition, Structure and Dynamics of the Galilean Satellites.
- G. Schubert, F. Sohl, and H. Hussmann. In: *Europa*. Ed. by R. T. Pappalardo, W. B. McKinnon, and K. Khurana. University of Arizona Press, 2009. Chap. Interior of Europa, pp. 353–368.
- V Shematovich, R Johnson, J Cooper, and M Wong. "Surface-bounded atmosphere of Europa". In: *Icarus* 173.2 (Feb. 2005), pp. 480–498. issn: 0019-1035. doi: 10.1016/j.icarus.2004.08.013.
- B. D. Shizgal and G. D. Arkos. "Nonthermal Escape of Atmospheres of Venus, Earth and Mars". In: *Reviews of Geophysics* 34.4 (Nov. 1996), pp. 483–505.
- K. N. Singer, W. B. McKinnon, and L. Nowicki. "Secondary craters from large impacts on Europa and Ganymede: Ejecta size-velocity distributions on icy worlds, and the scaling of ejected blocks". In: *Icarus* 226.1 (Sept. 2013), pp. 865–884. issn: 0019-1035. doi: 10.1016/j.icarus.2013.06.034.
- W. H. Smyth and M. L. Marconi. "Europa's atmosphere, gas tori, and magnetospheric implications". In: *Icarus* 181.2 (Apr. 2006), pp. 510–526. issn: 0019-1035. doi: 10.1016/j.icarus.2005.10.019.

- D. J. Southwood, M. G. Kivelson, R. J. Walker, and J. A. Slavin. "Io and its plasma environment". In: *Journal of Geophysical Research: Space Physics* 85.A11 (1980), pp. 5959–5968. issn: 2156-2202. doi: 10.1029/JA085iA11p05959.
- F. Taylor, S. K. Atreya, T. Encrenaz, D. Hunten, P. Irwin, and T. Owen. In: *Jupiter: the planet, satellites and magnetosphere*. Ed. by F. Bagenal, T. E. Dowling, and W. McKinnon. Cambridge University Press, 2004. Chap. The Composition of the Atmosphere of Jupiter.
- JUICE science study team. JUICE assessment study report (Yellow Book). Tech. rep. ESA, 2012. url: <http://sci.esa.int/juice/49837-juice-assessment-study-report-yellow-book/>.
- V. Tennishev, M. R. Combi, B. D. Teolis, and J. H. Waite. "An approach to numerical simulation of the gas distribution in the atmosphere of Enceladus". In: *Journal of Geophysical Research* 115.A9 (2010). issn: 0148-0227. doi: 10.1029/2009ja015223.
- B. Travis, J. Palguta, and G. Schubert. "A whole-moon thermal history model of Europa: Impact of hydrothermal circulation and salt transport". In: *Icarus* 218.2 (Apr. 2012), pp. 1006–1019. issn: 0019-1035. doi: 10.1016/j.icarus.2012.02.008.
- S. Vance and J. Goodman. In: *Europa*. Ed. by R. T. Pappalardo, W. B. McKinnon, and K. Khurana. University of Arizona Press, 2009. Chap. Oceanography of an Ice-Covered Moon, pp. 459–484.
- V. Vasyliunas. In: *Physics of the Jovian Magnetosphere*. Ed. by A. J. Dessler. Cambridge University Press, 1983. Chap. Plasma distribution and flow.
- University of Virginia. PHYS304: properties of water. url: <http://galileo.phys.virginia.edu/classes/304/h2o.pdf>.
- M. Volwerk, M. G. Kivelson, and K. K. Khurana. "Wave activity in Europa's wake: Implications for ion pickup". In: *Journal of Geophysical Research: Space Physics* 106.A11 (2001), pp. 26033–26048. issn: 2156-2202. doi: 10.1029/2000JA000347.
- M. Wieser, S. Barabash, Y. Futaana, M. Holmstrom, A. Bhardwaj, R. Sridharan, M. Dhanya, P. Wurz, A. Schaufelberger, and K. Asamura. "Extremely high reflection of solar wind protons as neutral hydrogen atoms from regolith in space". In: *Planetary and Space Science* 57.14-15 (2009), pp. 2132–2134. issn: 0032-0633. doi: 10.1016/j.pss.2009.09.012.
- P. Wurz, A. Vorburger, A. Galli, M. Tulej, N. Thomas, A. Yann, O. Mousis, S. Barabash, M. Wieser, and H. Lammer. "Measurement of the Exospheres of Europa, Ganymede, and Callisto". Presentation at EPSC2014.
- C. Zimmer, K. K. Khurana, and M. G. Kivelson. "Subsurface Oceans on Europa and Callisto: Constraints from Galileo Magnetometer Observations". In: *Icarus* 147.2 (2000), pp. 329 – 347. issn: 0019-1035. doi: 10.1006/icar.2000.6456.